The Development Of A Mathematical Model Of The Detached Lever Escapement

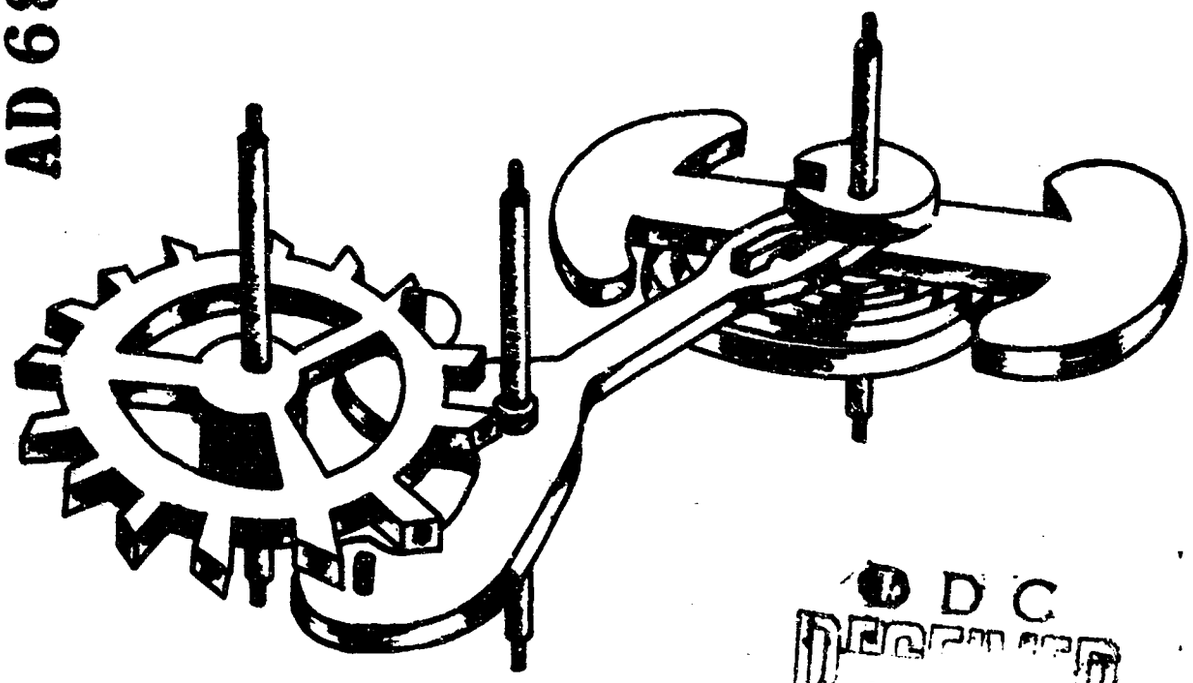

VMI RESEARCH LABORATORIES

VIRGINIA MILITARY INSTITUTE
LEXINGTON, VIRGINIA

THIS RESEARCH WAS CONDUCTED UNDER CONTRACT NO. DA-49-186-AMC-176(D) WITH THE HARRY DIAMOND LABORATORIES, BRANCH 430, WASHINGTON, D. C. 20438

THE DEVELOPMENT OF A MATHEMATICAL MODEL OF THE DETACHED LEVER ESCAPEMENT

By

RICHARD B. MINNIX

VMI RESEARCH LABORATORIES

Virginia Military Institute
Lexington, Virginia
July 1968

PREFACE

This report presents a summary of a study which was conducted in an attempt to determine sources of rate error and to facilitate design of more accurate detached lever escapements. The work was performed primarily during the summer months from 1964 to 1968 under the sponsorship of Harry Diamond Laboratories.

Unfortunately, the historical development of the detached lever escapement has proceeded almost exclusively along artistic lines with very little analytical guidance being provided. The objectives of this contract, broadly stated, were to derive general design equations that could be used with a computer to optimize the kinematics and dynamics of any detached lever escapement.

The publication of this report does not conclude the present study. Further modification of the basic model is planned as outlined in section 9. Preliminary investigations are already being conducted on an "out-of-beat" escapement. The results of any further work will be presented in a subsequent report.

Each of the computer programs discussed in this report was written for Virginia Military Institute's IBM-1620 computer. This installation is equipped with a Fortran II-D compiler with Monitor I, and two 1311 disk drive units. Its total storage capacity is 40 K. Although actual program listings are not included herein, they are available upon request from the author.

It is a pleasure to acknowledge the contributions of personnel at Harry Diamond Laboratories who assisted in various ways during the course of study. Mr. David S. Bettwy was responsible for the initiation of this

work and guided it through its early stages. Mr. William E. Ryan worked on the basic model geometry and checked most of the results. He first recognized the basic assymetric nature of the motion of the detached lever escapement. Mr. David Haley provided valuable assistance for the latter stages of the program. Above all, the contributions of Mr. David L. Overman, Technical Assistant on the contract for HDL, were truly outstanding. He provided all of the experimental measurements on the T5E1 escapement. His consultation and advice throughout the course of study were an immeasurable aid. He also read the manuscript and provided many helpful comments.

In addition to these, other contributors were Dr. Edward F. Turner,Jr., Professor of Physics at Washington and Lee University, who helped formulate the basic model geometry; and Miss Dorothy Drawbond who displayed much patience and rendered superb service as typist.

ABSTRACT

An analytical model of the detached lever escapement has been developed in an attempt to determine sources of rate error and to facilitate design of more accurate timers. The objectives of the investigation are general design equations that can be used to attain an escapement design which is less torque sensitive.

The model is analyzed both energetically and by approximate solution of the differential equations of motion. Predictions of the model, primarily the torque-amplitude relationship and beat rate error, are compared with experimental data from an actual escapement mechanism. The correlation between the theoretical and experimental performance of the escapement is used to indicate where further modification of the model is required.

Mathematical analysis of the model shows the relative importance of various energy loss mechanisms considered. The radial thrust applied to the balance staff by the hairspring is shown to be one of the major loss mechanisms. Other analysis shows that the portion of the cycle when the balance and lever are in free motion between the end of unlocking and the beginning of impulse, the "catch-up" portion of the cycle, plays a decisive role in the properties of the escapement.

TABLE OF CONTENTS

LIST OF TABLES

LIST OF FIGURES

LIST OF FIGURES (continued)

1. INTRODUCTION

In adapting the detached lever escapement to use in ordnance timing mechanisms, personnel at the Harry Diamond Laboratories discovered that the high accuracy traditionally realized in watches and clocks using this escapement could not be maintained.[1]

Some of the causes believed responsible for the degradation in accuracy were as follows:

a. elimination of costly jewelled bearings,

b. strengthening of fragile, small diameter pivots,

c. loosening of tolerances to decrease cost,

d. increased variations in input torques and output loads resulting from ordnance applications,

e. increased escapement frequency necessary for high resolution in short timing intervals,

f. operation over wide temperature extremes and after prolonged exposure to shock and vibration.

The gross effect of all these factors is to produce greater variations in the effective impulse delivered to the oscillating balance assembly. Because variations in friction and in the impulse can never be eliminated, the most desirable (accurate over all conditions) escapement is one having the least variation in frequency with changes in the effective impulse. An escapement which shows a large variation in timekeeping properties as the input torque is varied is said to be torque sensitive. Thus, the quality of a given escapement design can be assessed by determining its degree of torque sensitivity.

It is suspected that the geometry and inertia of an escapement's components, including their method of interaction, are the parameters which govern the magnitude and shape of its torque sensitivity characteristic. If these parameters could be changed to obtain a flat characteristic (no torque sensitivity) then it would be possible to achieve much more accurate timing movements with essentially no increase in cost.*

In order to bypass much of the costly empirical approach to improvement pursued in the past, a mathematical approach to achieving a less torque sensitive geometry was proposed. A mathematical model of the escapement allows more efficient investigation of parameter variations and the resulting performance changes. A program of this type has been conducted by Shinkle[2] on the two-center, cylinder-type escapement and has produced highly valuable results. Shinkle has also done a noteworthy but less detailed analysis of the detached lever escapement[3] which does not treat the detailed geometry and interactions of the escapement components. Another recent analysis[4] also neglects this area of concern.

The investigation covered by this report was begun during the summer of 1964 under Contract No. DA-49-186-AMC-176(D) with the Harry Diamond Laboratories. The major objective of the program is to provide design information which will lead to the minimization of an escapement's torque sensitivity. The initial objective is the development of a mathematical model of the T5E1 pin lever escapement and the validation of the model

---

*An alternate approach to the torque sensitivity problem is to devise a mechanism which delivers a constant impulse regardless of the input torque. Such a device is not considered in this study because of the cost and complexity it would add to the escapement.

through comparison of theoretical and experimental performance results. This report describes the progress made in these areas to date and recommends further action leading to their completion.

Geometry of the 25 Hz pin lever escapement used in the T5E1 timing movement was chosen as a starting point for the analysis because this timer had demonstrated a very low torque sensitivity in tests. The basic approach is the derivation of the differential equations governing the motion of the escapement system and the solution of these equations under steady-state operation* to yield values of the period of oscillation for given input torques. The equations include most of the essential geometric and dynamic design parameters such as shapes, center distances and inertias of the parts. Energy loss mechanisms which are influenced by the input torque, collision processes, and escape wheel lag are also considered. Operating parameters which were neglected because of certain assumptions will be discussed later.

---

*Steady-state operation is defined by a constant amplitude of oscillation for a given torque applied to the escape wheel.

2. DESCRIPTION OF ESCAPEMENT OPERATION

Before the escapement model can be defined, a graphical description of the essential parts and of the escapement action of a typical detached lever mechanism must be presented.

Basic nomenclature and geometry are shown for the 50 bps, T5E1 pin lever escapement in Figure 1. The mechanism has three main components: the balance and hairspring (hairspring not shown), the lever and pallets, and the escape wheel. The balance and hairspring form an oscillator which establishes the basic frequency of the system. The escape wheel serves as an intermediary between the balance and the escape wheel shaft whose speed of rotation is to be controlled by the escapement. The function of the lever and pallets is to serve as a two-way torque and information linkage between the balance and the escape wheel.

The sequence of events during the forward half-cycle (escape wheel acts on entrance pallet pin) is depicted in a schematic fashion in Figure 2. Each of the pallet pins and the impulse pin are shown as points; the balance and lever fork details have been omitted for clarity in illustration.

The angular displacements of the balance, lever, and escape wheel at each stage of the motion are specified by β, ρ, and ϵ, respectively. These angles are measured from reference lines drawn between centers of the balance and lever, and the lever and escape wheel as shown.

The action sequence is as follows. As the impulse pin, which is rigidly attached to the oscillating balance, starts its downward travel from maximum amplitude β_m (Figure 2a), the lever is held in just the right position for the impulse pin to miss the first tang of the lever fork but to engage the second. The lever is restrained during this downward travel

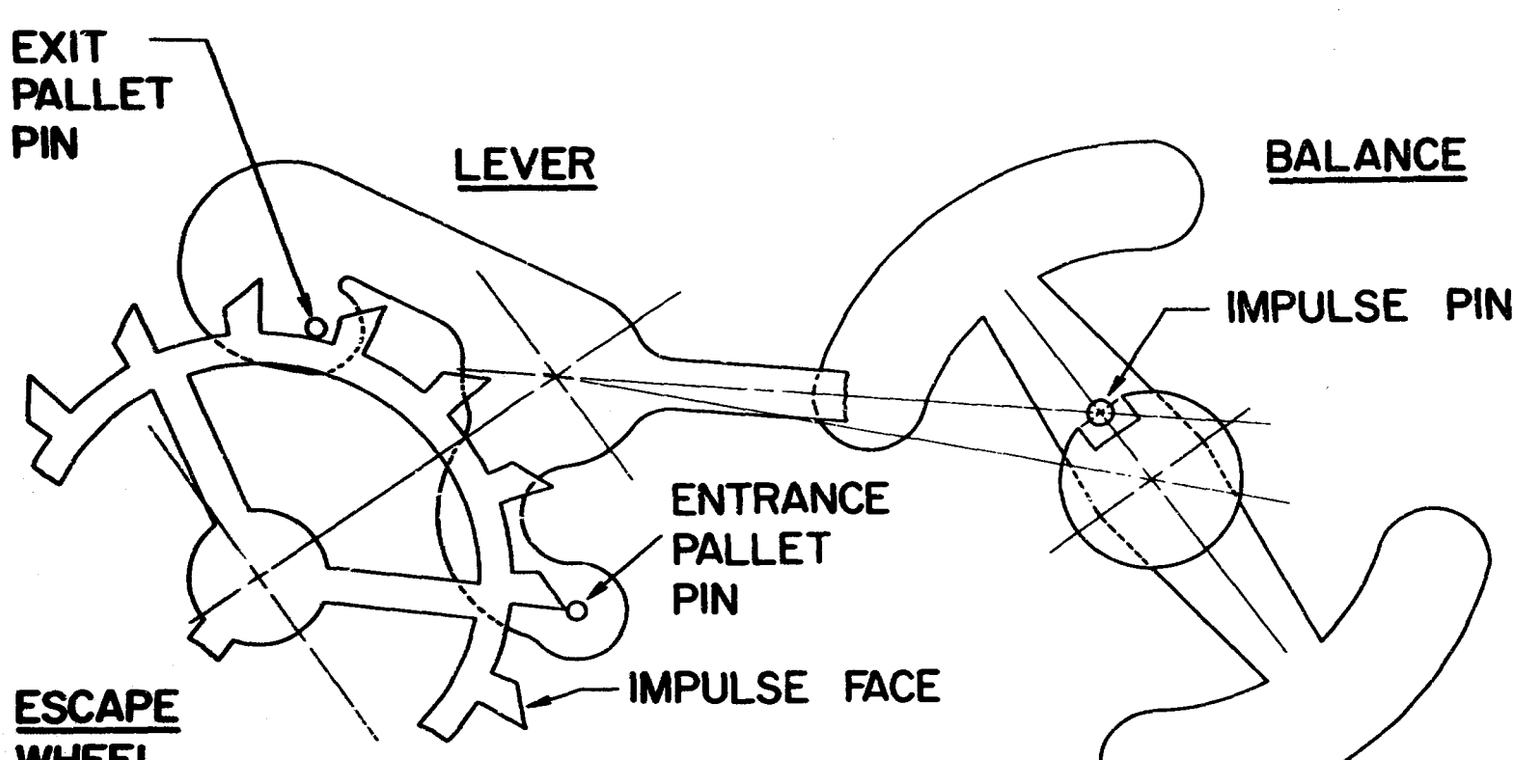

Figure 1. The T5E1 escapement.

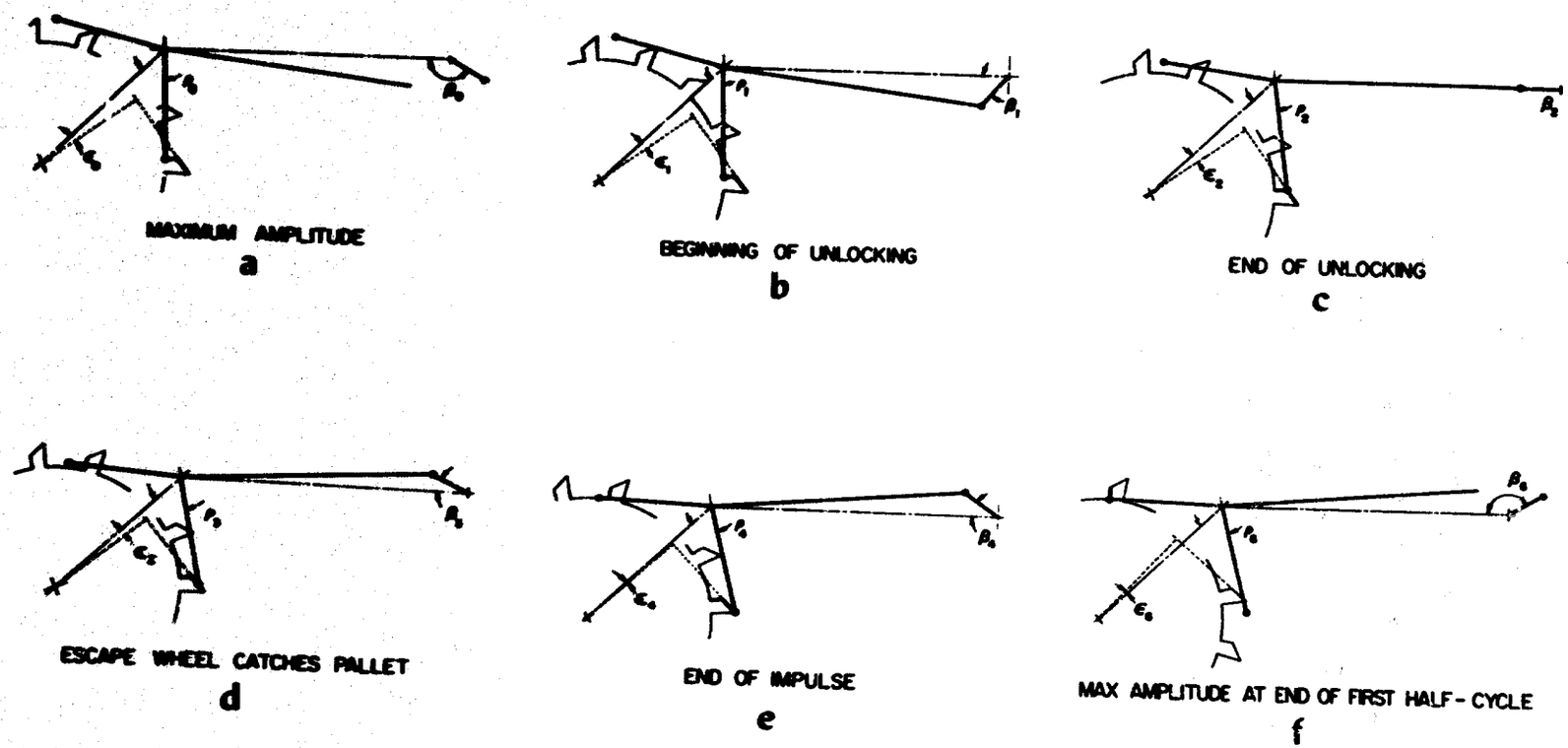

Figure 2. Events during the forward half-cycle.

of the balance by the counterclockwise torque applied to the escape wheel; the lever, in turn, locks the escape wheel preventing its rotation.

Unlocking begins when the impulse pin strikes the lever tang (Figure 2b). The balance and impulse pin drive the lever counterclockwise, which in turn causes the entrance pallet pin to move out along the locking face of the escape wheel tooth. Because of the geometrical interaction between the escape wheel tooth and the pallet pin and lever, the escape wheel is caused to move slightly during the unlocking phase of the motion.

At the instant of unlock (Figure 2c), the balance and lever have a finite velocity while the escape wheel has essentially zero velocity. The balance and lever will thus "run away" from the escape wheel and there will be a time lag before the beginning of impulse. During this time lag the escape wheel is accelerated counterclockwise by the applied torque sufficiently to catch up with the pallet (Figure 2d).

With the escape wheel now rotating and the entrance pallet pin in contact with the live face of the escape wheel tooth, an impulse is delivered by the escape wheel to the balance through the lever and impulse pin until the end of the impulse face on the escape wheel tooth is reached (Figure 2e). This impulse supplies energy to the balance to maintain its motion.

After the escape wheel rotates through a small additional displacement, it is locked by the exit pallet pin on the locking face of another escape wheel tooth. The balance, meanwhile, has been rotating freely toward the top of its swing. Its position (β_5) at the instant of relocking the escape wheel is indeterminate from geometrical considerations alone and is thus not shown in Figure 2.

As soon as the balance reaches its maximum amplitude (Figure 2f) the reverse half-cycle begins and the entire sequence of events is repeated with the escape wheel acting on the exit pallet pin.

The motion of the escapement has been broken up into twelve phases; the limits used to delineate each of the phases are defined in Table 1. A basic asymmetry is introduced into the motion of the escapement because of the requirement that the escape wheel rotate in the same sense in each half-cycle. This produces an asymmetrical interaction between the escape wheel tooth and the pallet lever and, as a result, the forward and reverse half-cycles are not identical. Analysis of an entire cycle of operation of the escapement is therefore required.

TABLE 1

PHASE END-POINTS USED TO DEFINE THE MOTION OF THE ESCAPEMENT

Balance Wheel Displacement	End-points of phases of the motion		
β_m	maximum amplitude; start	1st quarter-cycle	forward half-cycle
β_1	begin unlocking		
β_2	end unlocking		
β_3	"catch-up", impulse begins	2nd quarter-cycle	
β_4	end of impulse		
β_5	escape wheel locked		
β_6	maximum amplitude; $(\phi' - \beta_m)$		
β_6	maximum amplitude; $(\phi' - \beta_m)$	3rd quarter-cycle	reverse half-cycle
β_7	begin unlocking		
β_8	end unlocking		
β_9	"catch-up"; impulse begins; $(\phi' - \beta_3)$	4th quarter-cycle	
β_{10}	end of impulse		
β_{11}	escape wheel locked		
β_{12}	maximum amplitude $(= \beta_m)$		

3. BASIC MODEL GEOMETRY

In order to define the model escapement a detailed description of the three main components and their pertinent dimensions is necessary.

Relations Between Basic Dimensions

Dimensions R_1, R_2, R_e, W, and Q, and angles γ and Ω, as used to define the geometry of the escape wheel and teeth, are shown in Figure 3. L, Q, and Ω are related to the basic dimensions R_1, R_2, and γ by

$$W = R_2 \cos\gamma - \sqrt{R_1^2 - R_2^2 \sin^2\gamma} \tag{3.1}$$

$$Q = R_2 \sin\gamma \tag{3.2}$$

$$\Omega = \sin^{-1}(R_2 \sin\gamma / R_1) \tag{3.3}$$

The radius R_e defines the depth of locking engagement of the pallet pin.

Figure 3 also shows the dimensions A, B, R_{pp}, R_p, and the angle P used to describe the size and location of the pallet pins with respect to the lever staff. R_p and P are related to the drawing dimensions A and B by

$$R_p = \sqrt{A^2 + B^2} \tag{3.4}$$

$$P = 2\tan^{-1}\left(\frac{A}{B}\right) \tag{3.5}$$

The separation between the lever staff and escape wheel staff, S, the separation between the lever staff and balance staff, D, and the radius of the impulse pin from the balance axis, R_I, are the only other dimensions pertinent to this analysis.

Note that the fillets and rounds which would be found on any actual escape wheel have been neglected. It is also assumed for the purposes of

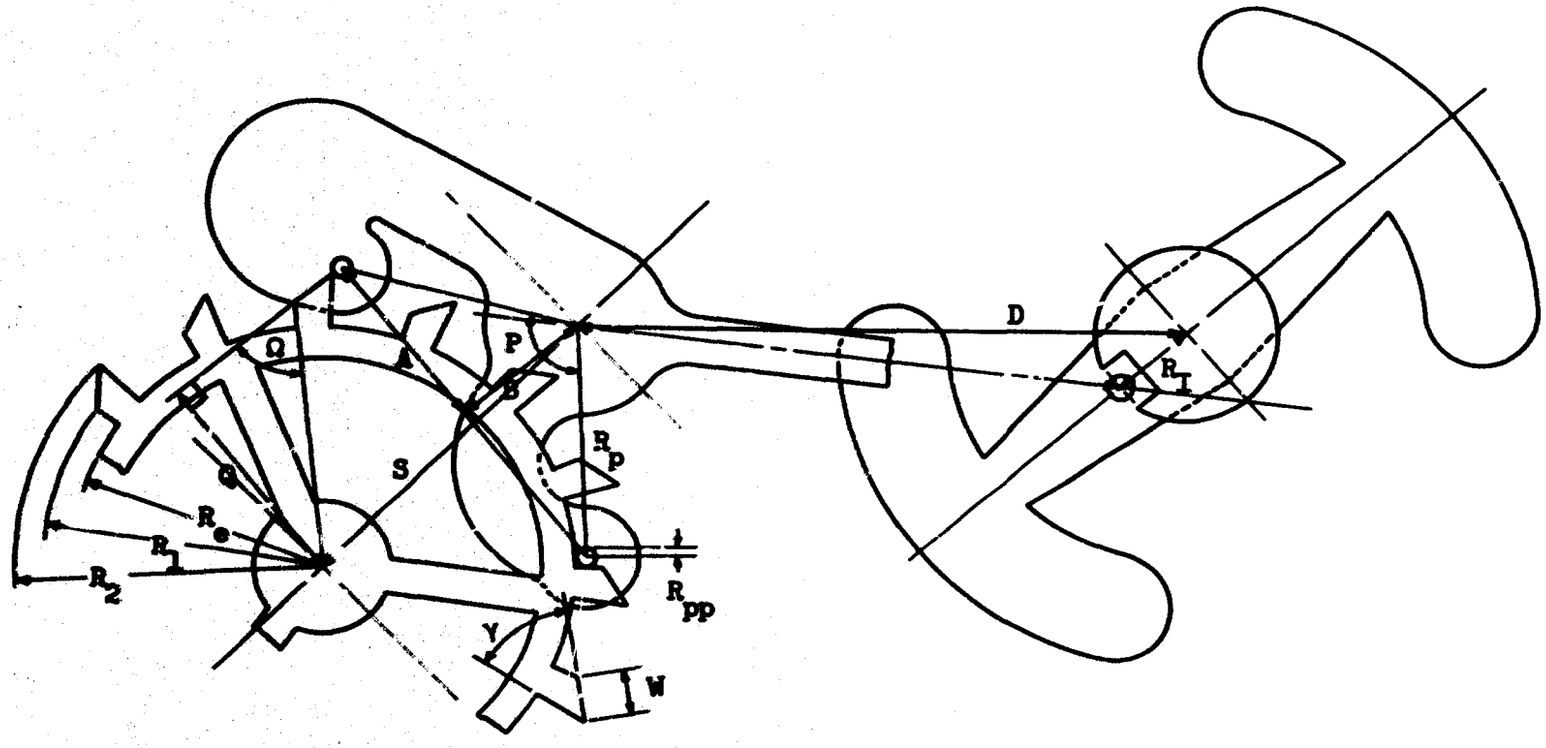

Figure 3. Basic dimensions defining the T5E1 escapement geometry.

this study that all of these dimensions are invariant for a given design. That is, there are no clearances in the pivots and the tolerance on every dimension is zero.

Escapement Effective Geometry

An "effective" geometry is defined using the following additional assumptions: (a) the pallet and impulse pins are treated as points; i.e., the pins are reduced to zero diameter; (b) there is no draw angle on the escape wheel tooth, that is, the unlocking face of the tooth lies on a radius; (c) the presence of a fork on the lever is neglected so that the impulse pin (point) may be considered as "striking" the lever when it reaches the centerline of the lever body; (d) the unlocking phase of the motion ends at $\beta = 0$; and (e) the angles δ and P and the dimensions S, D, and R_I are basic and will not be altered.

In order to reduce the pallet pin diameter to zero (i.e., $R_{ppe} = 0$)* and still have the motion of the escapement closely approximate that of the actual mechanism, it is necessary to slightly alter a number of the actual geometrical dimensions of the pallet and escape wheel. This new geometry is determined as follows.

The effective radius of the pallet pin (point) from the lever staff, R_{pe}, is determined from the requirement that ϵ change by $\frac{\pi}{N}$ radians in each half-cycle, where N is the number of teeth on the escape wheel.

Figures 4 and 5 schematically depict the geometrical situation between

---

*R_{ppe} denotes the "effective" value of R_{pp}; Q_e the "effective" value of Q, etc.

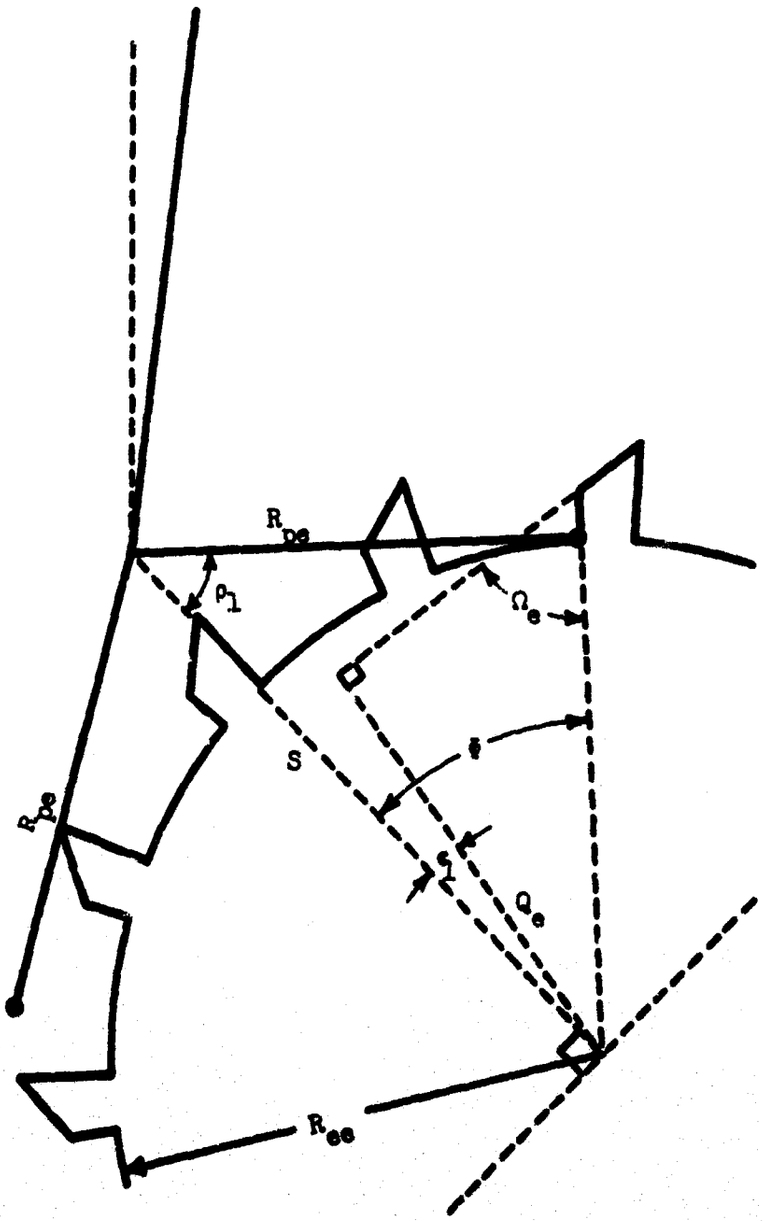

Figure 4. Geometrical situation at the beginning of the unlocking phase for the forward half-cycle.

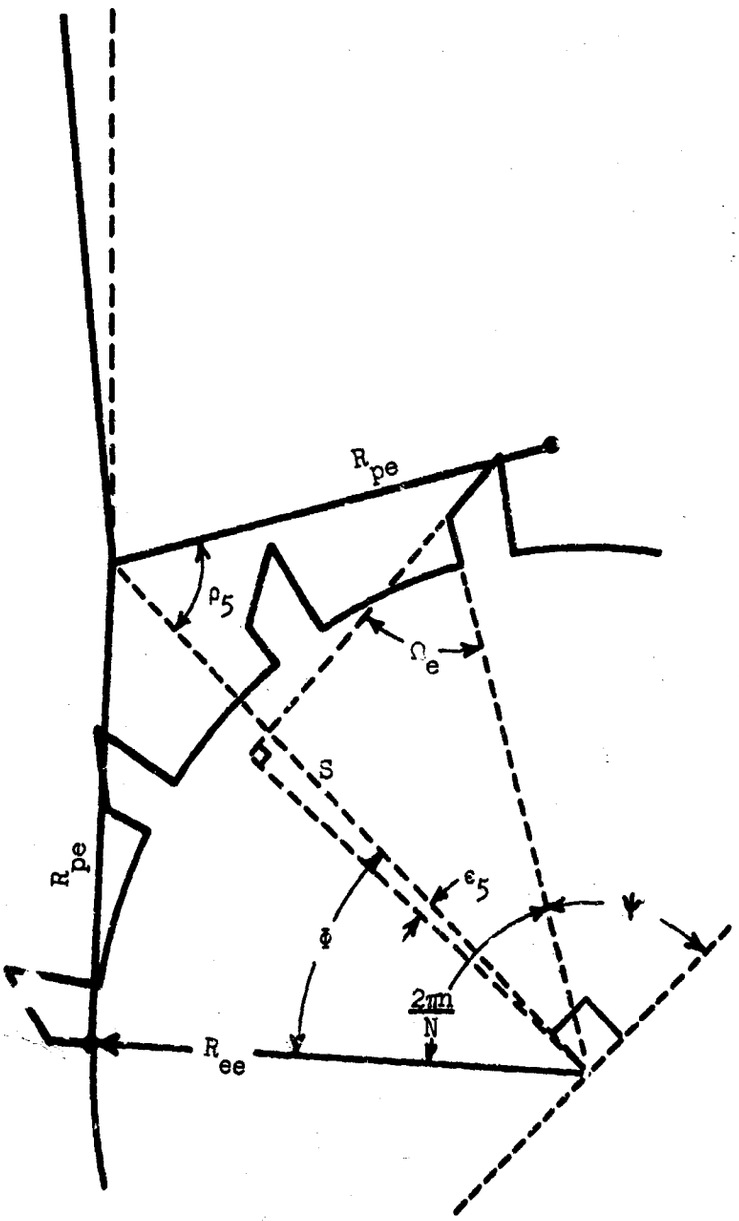

Figure 5. Geometrical situation at the end of relocking for the forward half-cycle. (Identical to situation at beginning of unlocking for the reverse half-cycle.)

the escape wheel and lever as it exists at the instant unlocking begins in the forward and reverse half-cycles, respectively. From these figures the following equations can be written.*

$$\Omega_e = \frac{\pi}{2} - \bar{\Phi} + \epsilon_1 \tag{3.6}$$

$$\Omega_e = \Psi + \epsilon_s \tag{3.7}$$

$$\Psi = \frac{\pi}{2} + \bar{\Phi} - n\left(\frac{2\pi}{N}\right) \tag{3.8}$$

Here n is the number of teeth spanned by the pallet pins. (For the T5E1 escapement used for this analysis, n is three as shown in Figure 3.) But a basic requirement when treating the pallet pins as points and assuming R_p equal for both pins is that

$$\epsilon_1 - \epsilon_s = \frac{\pi}{N} \tag{3.9}$$

Combining equations (3.6) through (3.9) to obtain $\bar{\Phi}$

$$\bar{\Phi} = \frac{\pi}{N}\left(n + \frac{1}{2}\right) \tag{3.10}$$

Then, from the law of cosines, the effective value of R_p is given by

$$R_{pe} = \sqrt{S^2 + R_{ee}^2 - 2SR_{ee}\cos\bar{\Phi}} \tag{3.11}$$

where R_{ee} is defined as

$$R_{ee} = R_e + R_{pp} \tag{3.12}$$

The effective value of R_1 is determined using the assumed condition

---

*Later in this report (see section 5), values of ϵ measured in the counter-clockwise sense from reference line S are regarded as negative angles. Equations (3.7) and (3.9) have been written in a manner consistent with this designation; i.e., $\epsilon_s < 0$.

that unlocking ends at $\beta_2 = 0$ for both the forward and reverse half-cycles. If $\beta_2 = 0$, then $\beta_2 = \frac{P}{2}$ and the line joining the escape wheel and lever staffs must bisect the lever angle P at the end of unlocking as shown in Figure 6. From the law of cosines, R_{1e} is then found to be

$$R_{1e} = \sqrt{R_{pe}^2 + S^2 - 2R_{pe}S\cos\left(\frac{P}{2}\right)} \tag{3.13}$$

The effective value of R_2 is determined from the assumption that as one pallet pin leaves the escape wheel tooth impulse face at the end of impulse, the other pin strikes the root of the escape wheel as shown in Figure 7. From Figure 7 and the law of cosines

$$R_{2e}^2 = R_{pe}^2 + S^2 - 2R_{pe}S\cos\beta_4 \tag{3.14}$$

but $$\cos\beta_4 = \cos(P-\xi) = \cos P\cos\xi + \sin P\sin\xi \tag{3.15}$$

By the law of sines

$$\sin\xi = \frac{R_{ee}\sin\bar{\Phi}}{R_{pe}} \tag{3.16}$$

and from the figure

$$\cos\xi = \frac{S - R_{ee}\cos\bar{\Phi}}{R_{pe}} \tag{3.17}$$

Substituting (3.16) and (3.17) in (3.15)

$$\cos\beta_4 = \frac{S\cos P}{R_{pe}} - \frac{R_{ee}}{R_{pe}}\left(\cos P\cos\bar{\Phi} - \sin P\sin\bar{\Phi}\right) \tag{3.18}$$

Then, using the identity for cos $(P+\bar{\Phi})$ and substituting in (3.14)

$$R_{2e} = \sqrt{R_{pe}^2 + S^2 - 2S\left[S\cos P - R_{ee}\cos(P+\bar{\Phi})\right]} \tag{3.19}$$

where $\bar{\Phi}$ is defined by equation (3.10).

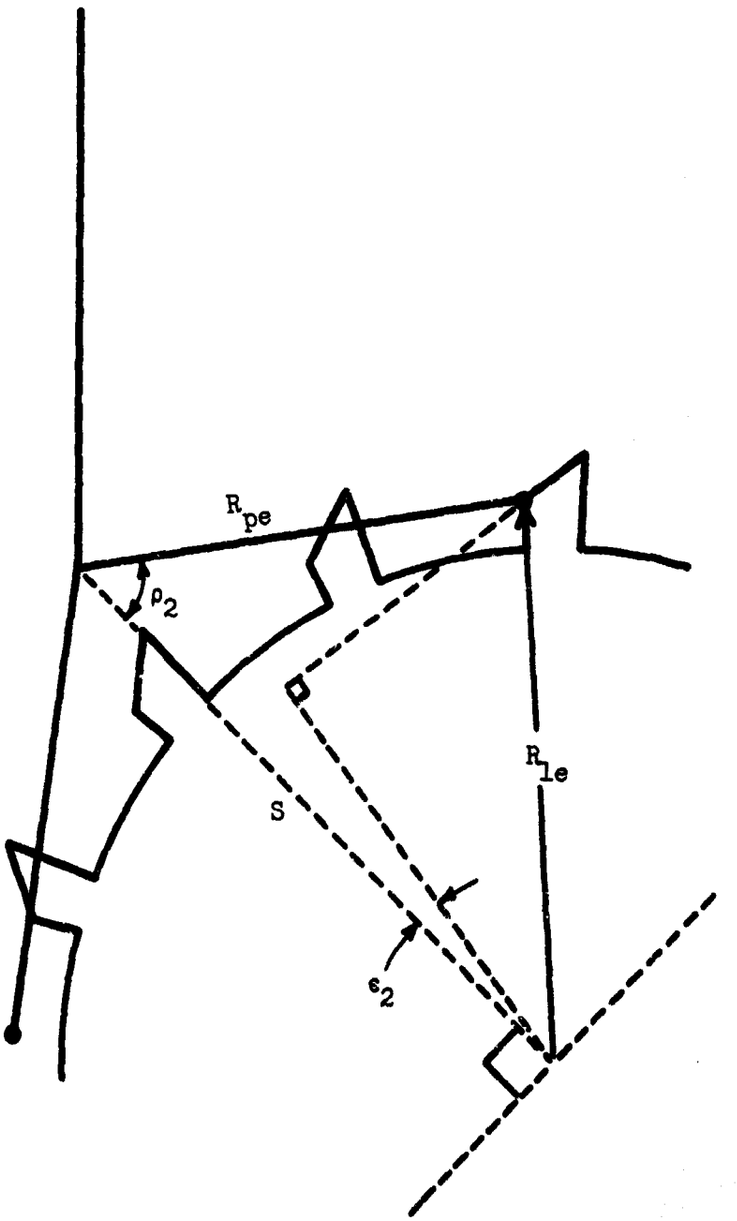

Figure 6. Geometrical situation at the end of unlocking.

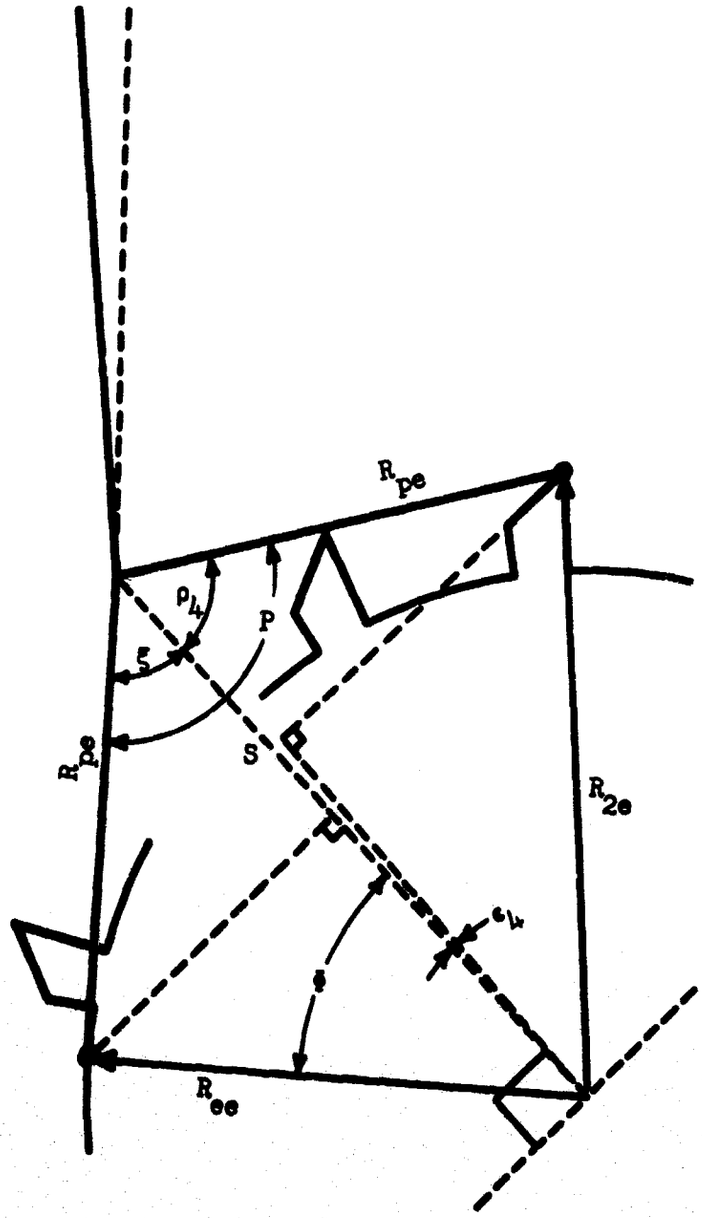

Figure 7. Geometrical situation at the end of impulse.

Using the above results in equations (3.1, (3.2), and (3.3)

$$W_e = R_{2e}\cos\gamma - \sqrt{R_{1e}^2 - R_{2e}^2\sin^2\gamma} \tag{3.20}$$

$$Q_e = R_{2e}\sin\gamma \tag{3.21}$$

$$\Omega_e = \sin^{-1}\left(\frac{R_{2e}}{R_{1e}}\sin\gamma\right) \tag{3.22}$$

A comparison of the effective geometry as determined by the procedure just outlined and the original geometry of a T5E1 escapement is presented in Table 2. Except for R_{pp}, the percentage change in the geometric parameters is small, the largest change being about a 9 percent reduction in length of the escape wheel tooth impulse face. Note also that $R_{pe} \neq R_p$. this is a result of assuming that the angle P and the center distance S are basic to the design.

TABLE 2

COMPARISON OF ORIGINAL AND EFFECTIVE GEOMETRY FOR T5E1 ESCAPEMENT

Quantity	Original	Effective	Change	% Change
N	15.0000	15.0000		
n	3.0000	3.0000		
R_I	0.0567	0.0567		
D	0.4005	0.4005		
S	0.2374	0.2374		
P	1.8621	1.8621		
Y	0.8727	0.8727		
R_{DP}	0.0061	0.0000	-0.0061	-100.00
R_D	0.1603	0.1589	-0.0014	- 0.90
R_e	0.1685	0.1746	0.0061	3.62
R_1	0.1840	0.1912	0.0072	3.93
R_2	0.2019	0.2077	0.0058	2.88
W	0.0301	0.0274	-0.0027	- 8.84
Q	0.1547	0.1591	0.0044	2.88
Ω	0.9983	0.9828	-0.0155	- 1.55

4. ESCAPEMENT KINEMATICS

Before proceeding to the equations of motion, the kinematic equations governing the interaction of the escapement components must be developed. The end points used to define the phases of motion of the escapement are given in Table 1. During the unlocking, "catch-up", and impulse phases, some or all of the basic components are interacting. Hence, for these phases, there are constraint relationships involving angular displacements which are determined by the geometry of the components.

Coupling Equations Between The Lever and Balance

From the beginning of unlocking until the end of impulse the balance and lever are interacting. The kinematic constraint equation governing this action is of the form $\beta = \beta(\rho)$. $\beta(\rho)$ is obtained from Figure 8 using the law of sines.

$$\beta = \sin^{-1}\left[\frac{\rho}{R_2}\sin\left(\frac{\rho}{2}-\rho\right)\right] - \left(\frac{\rho}{2}-\rho\right) \qquad (4.1)$$

Coupling Equations Between The Escape Wheel And Lever

Throughout the unlocking and impulse phases of the motion all three basic components of the escapement interact. The balance and hairspring assembly is coupled to the lever which is coupled to the escape wheel. Consequently, during these phases, the kinematic constraint equations are $\beta = \beta(\rho)$ and $\epsilon = \epsilon(\rho)$. $\beta(\rho)$ is given above. The $\epsilon = \epsilon(\rho)$ relationship must be examined in both the forward and reverse half-cycles because of the asymmetric nature of the escapement action.

As mentioned earlier in section 2 of the report, the escape wheel moves during the unlocking phases of the motion. Even though it is assumed that there is no draw angle on the teeth, this motion will still exist. Consequently, there exists a function $\epsilon_u = \epsilon_u(\rho)$ during unlocking. However,

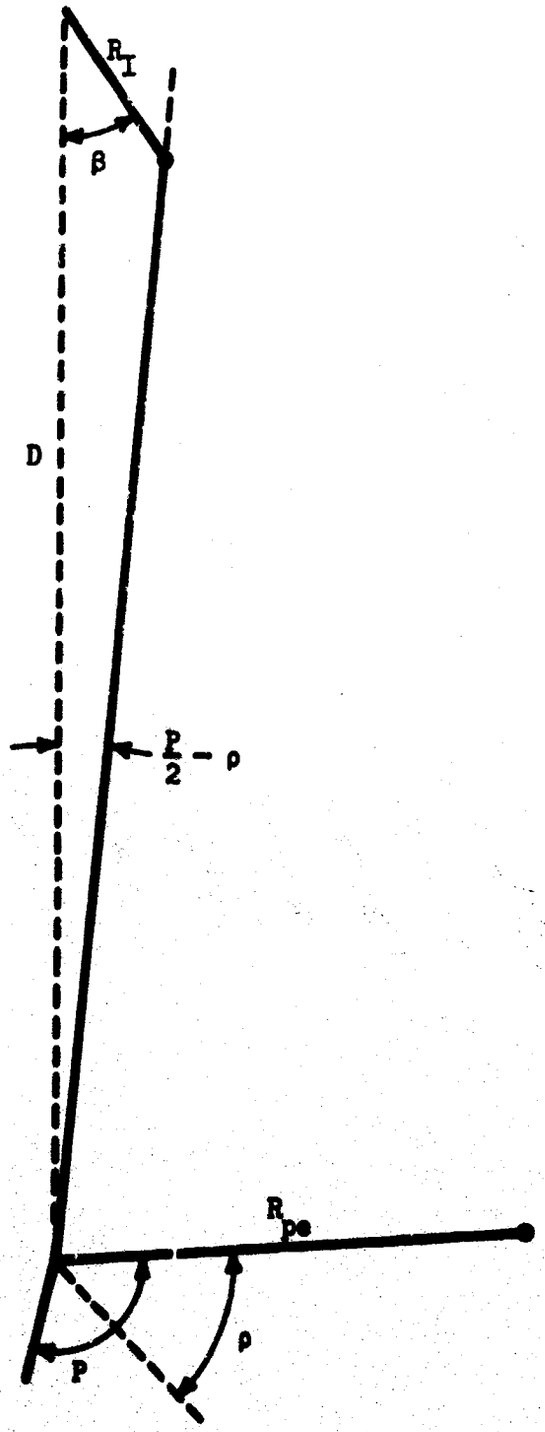

Figure 8. Geometrical interaction between the balance and lever.

as can be seen from Figures 4 and 5, with the assumption of no draw angle, the geometry is such that the driving torque exerted on the lever by the escape wheel is negligible during the unlocking phases. Therefore, for the purposes of this analysis, the assumption of no draw angle on the escape wheel teeth is taken to imply that there is no driving torque transmitted from the escape wheel to the lever (and balance) during the unlocking phase.*

The $\epsilon_i = \epsilon_i(\rho)$ relationships for the impulse phases of the motion are developed as follows. For the forward impulse phase the situation is as shown in Figure 9 and the following relationships are obtained.

$$\epsilon_f = \varphi - \alpha \tag{4.2}$$

$$\sin\varphi = \frac{Q_s}{R_f} \tag{4.3}$$

$$\sin\alpha = \frac{R_f^2 + S^2 - R_{ps}^2}{2SR_f} \tag{4.4}$$

Combining these expressions to obtain $\epsilon_f = \epsilon_f(\rho)$

$$\epsilon_f = \sin^{-1}\left(\frac{Q_s}{R_f}\right) - \sin^{-1}\left(\frac{R_f^2 + S^2 - R_{ps}^2}{2SR_f}\right) \tag{4.5}$$

where the dependence on ρ results from

$$R_f = \sqrt{R_{ps}^2 + S^2 - 2R_{ps}S\cos\rho} \tag{4.6}$$

---

*This implication is later modified for the purpose of including unlocking friction in the mathematical model (refer to section 4 and appendix C). In future work, it is planned to include the provision for a draw angle in the mathematical model so the function $\epsilon_u = \epsilon_u(\rho)$ for unlocking will be brought in at that time.

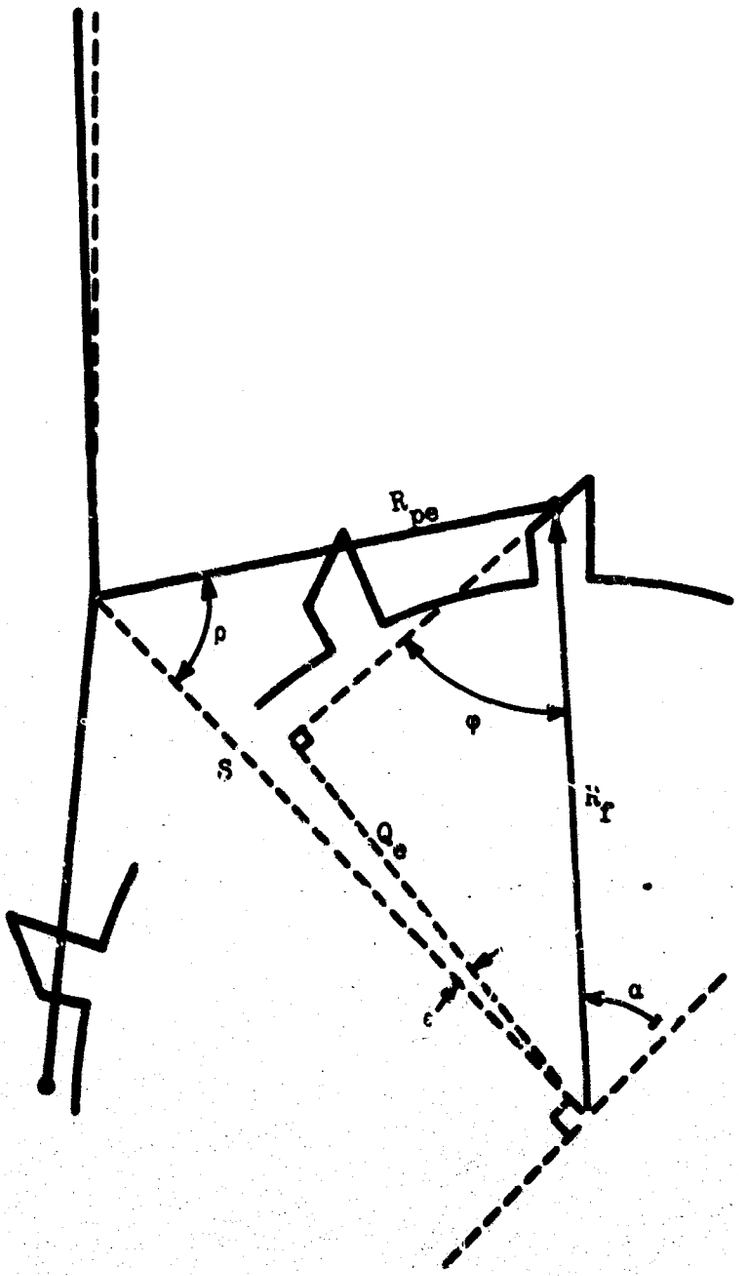

Figure 9. Geometrical interaction between the escape wheel and lever during forward impulse.

Appropriate geometry for the impulse portion of the reverse half-cycle is shown in Figure 10. It follows that

$$\epsilon_r = -\frac{\pi}{2} + \eta + \delta \qquad (\epsilon_r < 0) \tag{4.7}$$

$$\eta = n\left(\frac{2\pi}{N}\right) - \cos^{-1}\left(\frac{Q_s}{R_r}\right) \tag{4.8}$$

and

$$\sin\delta = \frac{R_r^2 + S^2 - R_{ps}^2}{2SR_r} \tag{4.9}$$

Combining (4.7), (4.8), and (4.9) to obtain $\epsilon_r = \epsilon_r(\rho)$

$$\epsilon_r = -\frac{\pi}{2} + \frac{2\pi n}{N} - \cos^{-1}\left(\frac{Q_s}{R_r}\right) + \sin^{-1}\left(\frac{R_r^2 + S^2 - R_{ps}^2}{2SR_r}\right) \tag{4.10}$$

where

$$R_r = \sqrt{R_{ps}^2 + S^2 - 2R_{ps}S\cos(P-\rho)} \tag{4.11}$$

Calculation of Interval Angles

The angular position of each component at each of the end points given in Table 1 is a function of the escapement geometry. These end point displacements are determined with the aid of the coupling equations (4.1), (4.5), and (4.10) as follows.

The initial position of the escape wheel is obtained by combining equations (3.6) and (3.10) and solving for ϵ_1.

$$\epsilon_0 = \epsilon_1 = \Omega_e - \frac{\pi}{2}\left(1 - \frac{2n+1}{N}\right) \tag{4.12}$$

From equation (4.5) with R_r set equal to R_{le} and noting that

$$\sin\Omega_e = \frac{Q_s}{R_{le}} \tag{4.13}$$

obtain

$$\epsilon_1 = \Omega_e - \sin^{-1}\left(\frac{R_{le}^2 + S^2 - R_{ps}^2}{2SR_{le}}\right) \tag{4.14}$$

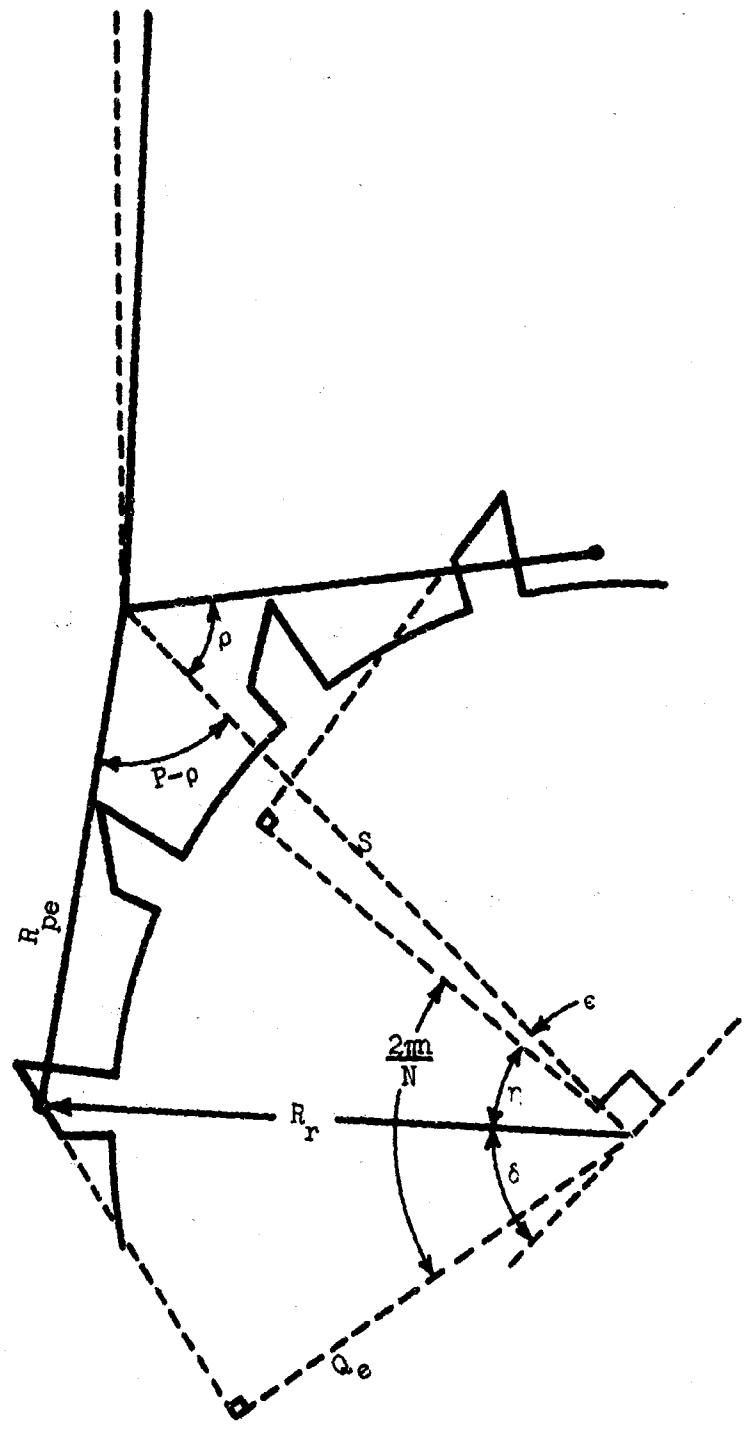

Figure 10. Geometrical interaction between the escape wheel and lever during reverse impulse.

ϵ_3 (and ϵ_9) and the corresponding value(s) of ρ, representing the position of the escape wheel and lever respectively at the "catch-up" displacement(s) β_3 (and β_9), depend on the input torque and β_m so they cannot be determined by purely geometrical considerations. The procedure that is used to determine these values is discussed later in section 6 of this report.

Again using equation (4.5) with R_f equal to R_{2e} and noting that

$$\sin\gamma = \frac{Q_s}{R_{2e}} \tag{4.15}$$

obtain $$\epsilon_4 = \gamma - \sin^{-1}\left(\frac{R_{2e}^2 + S^2 - R_{pe}^2}{2R_{2e}S}\right) \tag{4.16}$$

Using the fact that ϵ changes by $\frac{\pi}{N}$ radians per half-cycle

$$\epsilon_5 = \epsilon_6 = \epsilon_7 = \epsilon_4 - \frac{\pi}{N} \tag{4.17}$$

The values for ϵ_8 and ϵ_{10} are obtained by substituting R_{1e} and R_{2e} respectively into equation (4.10) and making use of (4.13) and (4.15).

$$\epsilon_8 = \Omega_e - \pi\left(1 - \frac{2n}{N}\right) + \sin^{-1}\left(\frac{R_{1e}^2 + S^2 - R_{pe}^2}{2R_{1e}S}\right) \tag{4.18}$$

$$\epsilon_{10} = \gamma - \pi\left(1 - \frac{2n}{N}\right) + \sin^{-1}\left(\frac{R_{2e}^2 + S^2 - R_{pe}^2}{2R_{2e}S}\right) \tag{4.19}$$

Since ϵ changes by $\frac{2\pi}{N}$ radians per cycle

$$\epsilon_{11} = \epsilon_{12} = \epsilon_4 - \frac{2\pi}{N} \tag{4.20}$$

Now consider the angular displacement of the lever during the "coupled" phases of the motion. Examination of Figure 9 shows that

$$\rho = \cos^{-1}\left(\frac{R_{pe}^2 + S^2 - R^2}{2R_{pe}S}\right) \tag{4.21}$$

Substituting the values R_{ee}, R_{1e}, and R_{2e} for R and noting the lever's symmetry of motion, the end point displacements of the lever are obtained.

$$\rho_0 = \rho_1 = \rho_{10} = \rho_{11} = \rho_{12} = \cos^{-1}\left(\frac{R_{pe}^2 + S^2 - R_{ee}^2}{2SR_{pe}}\right) \tag{4.22}$$

$$\rho_2 = \rho_3 = \cos^{-1}\left(\frac{R_{pe}^2 + S^2 - R_{1e}^2}{2SR_{pe}}\right) = \frac{\rho}{2} \tag{4.23}$$

and

$$\rho_4 = \rho_5 = \rho_6 = \rho_7 = \cos^{-1}\left(\frac{R_{pe}^2 + S^2 - R_{2e}^2}{2SR_{pe}}\right) \tag{4.24}$$

The end point displacements defining the "coupled" balance phases can now be determined by substituting the appropriate values of ρ into equation (4.1).

$$\beta_1 = \beta_{10} = \sin^{-1}\left[\frac{D}{R_2}\sin\left(\frac{\rho}{2} - \rho_1\right)\right] - \left(\frac{\rho}{2} - \rho_1\right) \tag{4.25}$$

$$\beta_2 = \beta_8 = 0 \tag{4.26}$$

and

$$\beta_4 = \beta_7 = \sin^{-1}\left[\frac{D}{R_2}\sin\left(\frac{\rho}{2} - \rho_4\right)\right] - \left(\frac{\rho}{2} - \rho_4\right) \tag{4.27}$$

β_0, β_3, β_5, β_6, β_9, β_{11} and β_{12} are geometrically indeterminant.

Table 3 gives the end point displacements (radians), calculated using the effective geometry given in Table 2, for each component of the T5E1 escapement. Note the movement of the escape wheel during the unlocking phases.

TABLE 3

ANGULAR POSITION (RADIANS) OF THE ESCAPEMENT COMPONENTS
AT THE END POINTS OF EACH PHASE OF THE MOTION

Position	β	ρ	ϵ
0	start	.82627	.14507
1	.72634	.82627	.14507
2	0	.93104	.14152
3	*	*	*
4	-.72634	1.03581	.02001
5	*	1.03581	-.06437
6	*	1.03581	-.06437
7	-.72634	1.03581	-.06437
8	0	.93104	-.06081
9	*	*	*
10	.72634	.82627	-.15963
11	*	.82627	-.27381
12	end	.82627	-.27381

*Indeterminate from geometrical considerations

5. EQUATIONS OF MOTION

Utilizing the effective geometry as defined in section 3 of this report, the equations of motion of the escapement components can be derived by applying the principles of Newtonian Mechanics.

The positive directions for the variables used in this analysis have been chosen such that β and ρ are positive when measured in the couter-clockwise sense whereas ϵ is positive when measured in the clockwise sense.

Phase Definitions

Within a cycle there are twelve phases, and the equations of motion will change from phase to phase. As related to the balance motion, these phase definitions for the forward half-cycle are:

1. Free swing of the balance from maximum amplitude β_m to β_1 where unlocking begins.
2. A collision, assumed instantaneous and inelastic, occurs at β_1 when the impulse pin on the balance strikes the lever. Unlocking of the escape wheel then proceeds from β_1 to β_2.
3. Balance and lever continue to rotate as the escape wheel accelerates to overtake them. The escape wheel "catches-up" to the lever and balance at β_3.
4. Another instantaneous, inelastic collision occurs when the live impulse face of the escape wheel tooth strikes the entrance pallet pin. A period of impulse then ensues from β_3 to β_4.
5. The freely rotating balance and escape wheel continue their motion until, at β_5, the exit pallet pin locks on the locking face of another escape wheel tooth.
6. The balance rotates freely to the top of its swing, β_6.

Although possessing different end-point designations, the phases of the reverse half-cycle are similarly defined.

Phase 1 Equations

During the free swing of the balance it is assumed that the only torques acting on the balance are: (a) the hairspring restoring torque, and (b) a frictional torque, T_s, at the balance pivot due to hairspring side thrust (see appendix A).

With the assumption that

$$T_s = L\beta \tag{5.1}$$

where L is a constant, the equation of motion is

$$I_B\ddot{\beta} = -K\beta + L\beta \tag{5.2}$$

I_B is the moment of inertia of the balance; K is the spring constant.

Phase 2 Equations

Unlocking of the escape wheel begins as the impulse pin strikes the lever at β_1 (see Figure 11). Let F_{BL} be the force the balance exerts on the lever, and F_{IB} the reaction force of the lever on the balance. Y_L' and Y_B are the respective lever arms of these forces about the lever and balance pivots.

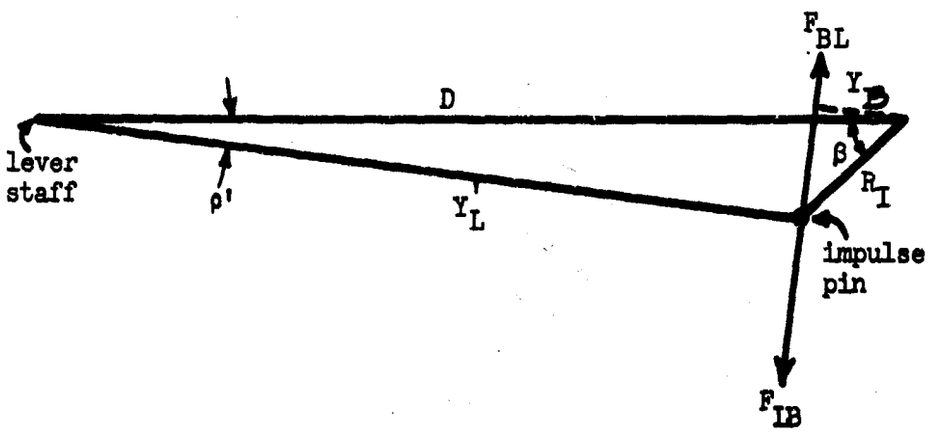

Figure 11. Interaction between the balance and lever during unlocking.

The impulse on the balance, ϑ_B, is

$$\vartheta_B = \int Y_B F_{LB}\,dt = I_B\dot{\beta}_{1a} - I_B\dot{\beta}_{1b} \qquad (5.3)$$

where $\dot{\beta}_{1a} < 0$; $\dot{\beta}_{1b} < 0$; $|\dot{\beta}_{1a}| < |\dot{\beta}_{1b}|$.

$\dot{\beta}_{1b}$ and $\dot{\beta}_{1a}$ represent the angular velocities of the balance before and after the collision, respectively.

The impulse on the lever, ϑ_L, is

$$\vartheta_L = \int Y_L' F_{BL}\,dt = I_L\dot{\rho}_{1a} - I_L\dot{\rho}_{1b} \qquad (5.4)$$

where $\dot{\rho}_{1a} > 0$; $\dot{\rho}_{1b} = 0$.

I_L is the moment of inertia of the lever.

The ratio of these impulses is

$$\frac{\vartheta_L}{\vartheta_B} = \frac{\int Y_L' F_{BL}\,dt}{\int Y_B F_{LB}\,dt} = \frac{Y_L' \int F_{BL}\,dt}{Y_B \int F_{LB}\,dt} \qquad (5.5)$$

Both of these impulses must be considered positive even though $F_{BL} = -F_{LB}$ because of the arbitrary choice of positive directions for ρ and β. Hence

$$\frac{\vartheta_L}{\vartheta_B} = \frac{Y_L'}{Y_B} = \frac{I_L\dot{\rho}_{1a}}{I_B(\dot{\beta}_{1a} - \dot{\beta}_{1b})} \qquad (5.6)$$

After the collision the lever and balance are coupled so that

$$Y_L'\dot{\rho}_{1a} = -Y_B\dot{\beta}_{1a} \qquad (5.7)$$

or

$$\frac{d\rho}{d\beta} = -\frac{Y_B}{Y_L'} \qquad (5.8)$$

Presence of the minus sign is dictated again because of the choice of positive directions for the variables. Eliminating $\dot{\beta}_{1a}$ between equations (5.6) and (5.7) gives

$$\dot{\beta}_{1a} = \frac{I_{12}}{I_{11}} \dot{\beta}_{1b} \tag{5.9}$$

where $$I_{11} = I_B + X_1^2 I_L \quad * \tag{5.10}$$

and $$X_1 = \frac{Y_B}{Y_L} \tag{5.11}$$

is the lever arm ratio between the balance and pallet lever evaluated at $\beta = \beta_1$.

The remainder of the phase 2 motion involves the rotation of the coupled balance and lever until unlocking of the escape wheel is achieved at $\beta_2 = 0$.

Consider first the motion of the pallet lever. It is assumed that the only torques acting on the lever during this portion of phase 2 are: (a) a torque in the positive sense due to the push of the impulse pin on the lever, and (b) a frictional torque (T_{Lf}) in the negative sense arising from the drag of the entrance pallet pin on the locking face of the escape wheel tooth (see appendix C). Consequently the equation of motion of the lever is

$$I_L \ddot{\rho} = T_{BL} - T_{Lf} \tag{5.12}$$

*The first subscript on I is used to denote the functional form whereas the second designates that value of β at which X (and later on Z) is to be evaluated.

or $$I_L \ddot{\beta} = Y_L' F_{BL} - T_{Lf} \tag{5.13}$$

where $Y_L' = Y_L'(\beta)$, $T_{Lf} = T_{Lf}(\beta)$.

In addition to the torques present during the free period of motion, the balance experiences the reaction torque of the lever due to their coupling. Its equation of motion is now

$$I_B \ddot{\beta} = -K\beta + L\beta + Y_B F_{LB} \tag{5.14}$$

with $Y_B = Y_B(\beta)$.

Using $F_{IB} = F_{BL}$ (since both result in positive torques on their respective components) and equations (5.8) and (5.13), the differential equation of motion can finally be written as

$$I_1 \ddot{\beta} + \tfrac{1}{2} \dot{I}_1 \dot{\beta} + (K-L)\beta = T_f \tag{5.15}$$

where $$I_1 = I_B + X^2 I_L \tag{5.16}$$

$$T_f = X T_{Lf} \tag{5.17}$$

and $$X = X(\beta) = \frac{Y_B}{Y_L'} \ . \tag{5.18}$$

The functional relationship for $X(\beta)$ is derived in appendix B.

Phase 3 Equations

At the instant of unlock the coupled balance and pallet lever have a finite velocity while the escape wheel is stationary. Hence the balance

and pallet lever will "run away" from the escape wheel and there will be a time lag before the beginning of impulse. During this time lag the escape wheel will be accelerated sufficiently by the torque, T_a, delivered through the gear train to catch up with the other components and provide the impulse.

The equation of motion for the escape wheel during this period is

$$I_E\ddot{\epsilon} = -T_a \tag{5.19}$$

A minus sign is required here since T_a is applied in such a direction as to decrease ϵ.

Except for the absence of the frictional torque, the equation of motion for the balance and pallet lever is similar to that which applied during unlocking. Thus

$$I_1\ddot{\beta} + \tfrac{1}{2}\dot{I}_1\dot{\beta} + (K+L)\beta = 0 \tag{5.20}$$

The sign on the $I\beta$ term is reversed because β has become negative while the sense of this torque has not changed.

Phase 4 Equations

An instantaneous, inelastic collision is assumed to occur when the escape wheel catches up to the lever and balance at β_3. Let F_{EL} represent the force exerted on the lever by the escape wheel at impact, F_{LE} the reaction force, and Y_L and Y_E the lever arms for these forces, respectively (see Figure 12). The equations of motion of the components can now be written as

$$I_E\ddot{\epsilon} = -T_a + Y_E F_{LE} \tag{5.21}$$

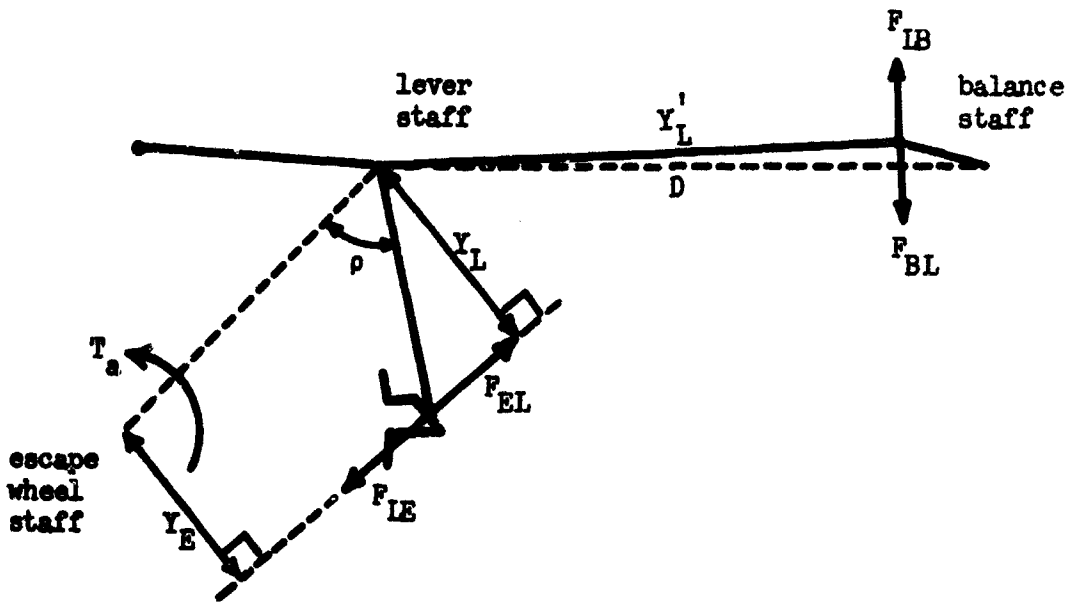

Figure 12. Interaction between the balance, lever, and escape wheel at forward "catch-up."

$$I_L\ddot{\rho} = Y_L F_{BL} - Y_L' F_{EL} \tag{5.22}$$

$$I_B\ddot{\beta} = -Y_B F_{LB} - K\beta - L\beta \tag{5.23}$$

These equations are coupled by the common forces and the constraint equations

$$Y_E\dot{\epsilon} = -Y_L\dot{\rho} \tag{5.24}$$

which is equivalent to

$$\frac{d\epsilon}{d\rho} = -\frac{Y_L}{Y_E} \quad * \tag{5.25}$$

and $$Y_L'\dot{\rho} = -Y_B\dot{\beta} \tag{5.26}$$

or $$\frac{d\rho}{d\beta} = -\frac{Y_B}{Y_L'} \tag{5.27}$$

*The minus sign is inserted because ρ increases in the forward half-cycle while ε decreases; all lever arms are treated as positive quantities. The analogue of equation (5.25) for the reverse half-cycle has a positive sign. See Table 3.

The first two constraint equations are valid only after the collision occurs and coupling has been achieved. Note that $\beta = \beta_3$ is a constant for this collision.

By eliminating the common forces and substituting for $\ddot{\gamma}$ in terms of $\ddot{\beta}$ one can derive the single equation

$$I_1\ddot{\beta} + (K+L)\beta + XZ_f T_a = -I_g X Z_f \ddot{\epsilon} \qquad (5.28)$$

where $Z_f = \frac{Y_L}{Y_E}$. (5.29)

It is found that this ratio is asymmetric in the two half-cycles; the subscript f refers to the forward half-cycle, r to the reverse half-cycle. The functional relationship for $Z(\beta)$ is derived in appendix B. This equation may now be integrated and the appropriate boundary conditions applied. Assuming that the collision is truly instantanteous, the integral of the terms on the left involving β and T_a may be neglected; it follows that

$$\dot{\beta}_{3a} = \frac{I_{23}\dot{\beta}_{3b} + X_3 Z_{f3} I_g \dot{\epsilon}_{3b}}{I_{23}} \qquad (5.30)$$

where $I_{23} = I_3 + X_3^2 I_L + X_3^2 Z_{f3}^2 I_g$ (5.31)

Subscripts b and a refer to angular speeds before and after the collision, respectively.

With the entrance pallet pin now in contact with the live face of the escape wheel tooth, an impulse is delivered by the escape wheel to the balance through the pallet lever and impulse pin until the end of the impulse face is reached. This impulse supplies energy to the balance to make up for losses and thereby maintain its motion at a given amplitude.

During the impulse period the equations of motion for the components together with the constraint equations are identical to those given above for the "catch-up" collision. Once again the common forces may be eliminated and the constraint equations used to substitute for $\ddot{\epsilon}$ and $\ddot{\rho}$. Each of the lever arms that enter these coupling equations are functions of β and will therefore vary during this period. As a result, when substitutions for $\ddot{\epsilon}$ and $\ddot{\rho}$ are made, each will involve a $\dot{\beta}$ term. The resulting equation of motion is

$$I_2\ddot{\beta} + \tfrac{1}{2}\dot{I}_2\dot{\beta} + (K+L)\beta = -XZ_f T_e \qquad (5.32)$$

with $$I_2 = I_B + X^2 I_L + X^2 Z_f^2 I_E \qquad (5.33)$$

Phase 5 Equations

As the entrance pallet pin leaves the impulse face of the escape wheel tooth and the impulse period ends, the exit pallet pin strikes the escape wheel root and the lever ceases to rotate. The escape wheel then rotates through a small additional displacement until the exit pallet pin locks on the locking face of another escape wheel tooth. Meanwhile, the balance, which has been rotating freely toward the top of its swing, has reached the position $\beta = \beta_5$. For this period the equations of motion of the components are, therefore,

$$I_E\ddot{\epsilon} = -T_e \qquad (5.34)$$

$$\ddot{\rho} = 0 \qquad (5.35)$$

$$I_B\ddot{\beta} = -K\beta - L\beta \qquad (5.36)$$

Phase 6 Equations

With the escape wheel now locked, the balance wheel continues to the top of its swing. Its equation of motion is

$$I_8\ddot{\beta} = -K\beta - L\beta \tag{5.37}$$

The first half-cycle of the motion is now completed.

Second Half-Cycle

The sequence of events during the second half-cycle is similar to that in the first and will not be treated in detail. In the interest of completeness, however, the equations of motion during the remaining six phases are given.

Phase 7

$$I_8\ddot{\beta} = -K\beta + L\beta \tag{5.38}$$

Phase 8

$$\dot{\beta}_{7a} = \frac{I_8}{I_{17}}\dot{\beta}_{7b} \quad ; \quad I_{17} = I_1(\beta_7) \tag{5.39}$$

$$I_1\ddot{\beta} + \tfrac{1}{2}\dot{I}_1\dot{\beta} + (K+L)\beta = T_f \tag{5.40}$$

Phase 9

$$I_8\ddot{\epsilon} = -T_a \tag{5.41}$$

$$I_1\ddot{\beta} + \tfrac{1}{2}\dot{I}_1\dot{\beta} + (K+L)\beta = 0 \tag{5.42}$$

Phase 10

$$\dot{\beta}_{9a} = \frac{I_{19}\dot{\beta}_{9b} - X_9 Z_{r9} I_8 \dot{\epsilon}_{9b}}{I_{29}} \quad ; \quad \dot{\epsilon}_{9b} < 0 \tag{5.43}$$

$$I_2\ddot{\beta} + \tfrac{1}{2}\dot{I}_2\dot{\beta} + (K+L)\beta = XZ_r T_a \tag{5.44}$$

Phase 11

$$I_e\ddot{\epsilon} = -T_a \tag{5.45}$$

$$\ddot{\rho} = 0 \tag{5.46}$$

$$I_b\ddot{\beta} = -K\beta - L\beta \tag{5.47}$$

Phase 12

$$I_b\ddot{\beta} = -K\beta - L\beta \tag{5.48}$$

This treatment has reduced the problem to solving a set of differential equations which describe the motion of an "equivalent" balance system. The effects of the lever and escape wheel are taken into account through the presence of their "reflected" moments of inertia in these equations.

A more elegant derivation of the preceding equations of motion is presented in appendix D.

6. METHOD OF SOLUTION

The heart of the problem of solving the equations of motion lies in handling the nonlinear, coupled differential equations which describe the unlocking, catch-up, and impulse phases. Indeed, these equations are even more formidable than they appear at first glance because T_f, X, and Z are complex functions of β. Also, only X is symmetric for forward and reverse motion (see appendix B). In addition, since there are two degrees of freedom during catch-up, the only way to obtain an accurate value of β_3 is through an iteration process.

Since attempts at an analytic solution of the exact equations have so far proven unsuccessful, a step-by-step method of approximate solution was chosen in which the motion of the balance was considered in small increments. Values of X, Z, and T_f were assumed constant for each increment. This assumption makes the $\dot{I}$ terms equal to zero and allows an analytic solution of the resulting differential equations.

A digital computer program was set up using the solution equations of motion. The final conditions of one step are used as the initial conditions of the next step, and new values of X, Z and T_f are computed for each step. Input to the program was the equilibrium values of maximum amplitude and applied torque, β_m and T_a; output was the oscillation period of the balance. An alternate approach to the solution of the nonlinear differential equations of motion is to program the computer to solve the exact equations using one of the numerical integration procedures available for this purpose.

A brief outline of the computation procedure used in the step-by-step solution method is as follows.

Phase 1: An analytic solution of the exact equation of motion can be obtained. Using the initial conditions $\beta = \beta_m$, and $\dot{\beta} = 0$, at $t = 0$, the solution is

$$\beta = \beta_m \cos \omega t \quad ; \quad \omega^2 = \frac{K-L}{I_s} \tag{6.1}$$

Inversion of this equation yields

$$t = \frac{1}{\omega} \cos^{-1}\left(\frac{\beta}{\beta_m}\right) \tag{6.2}$$

The duration of this phase, T, can now be calculated by substituting $\beta = \beta_1$ into this expression. Once T is determined $\dot{\beta}_{1b}$ can be found from the derivative of the $\beta(t)$ equation.

Phase 2: $\dot{\beta}_{1a}$ is determined by equation (5.9). Initial conditions for the first increment ($\Delta\beta$) are

$$\beta_0 = \beta_1 \; ; \; \dot{\beta}_0 = \dot{\beta}_{1a} \; ; \; t = 0.$$

The approximate equation of motion is

$$I_1 \ddot{\beta} + (K-L)\beta = T_f \tag{6.3}$$

and its solution can be written as

$$\beta = A \cos(\omega t - \varphi) + F \tag{6.4}$$

where

$$F = \frac{T_f}{K-L} \quad ; \quad \omega^2 = \frac{K-L}{I_1} \tag{6.5}$$

$$A = \sqrt{\frac{\dot{\beta}_0^2}{\omega_0^2} + (\beta_0 - F_0)^2} \tag{6.6}$$

$$\varphi = \tan^{-1} \frac{\dot{\beta}_0}{\omega_0(\beta_0 - F_0)} \tag{6.7}$$

and $\omega_o = \omega(\beta_o)$; i.e. $\omega_o^2 = \frac{K - L}{I_{10}}$ where $I_{10} = I_1(\beta_o)$ and $F_o = F(\beta_o)$.

Recall that T_f is assumed constant within the increment.

Solving for the time increment gives

$$t = \frac{1}{\omega}\left[\varphi + \cos^{-1}\left(\frac{\beta - F_o}{A}\right)\right] \qquad (6.8)$$

with $\beta = \beta_o + \Delta\beta$

and $\omega = \omega(\beta)$.

Note that the ω which enters the constants A and φ of the solution is evaluated at the beginning of the increment (β_o) whereas the ω in the inverted equation is evaluated at the end ($\beta_o + \Delta\beta$).

The angular speed at the end of the increment is determined from

$$\dot{\beta} = -A\omega \sin(\omega t - \varphi) \qquad (6.9)$$

again with $\omega = \omega(\beta)$. T is replaced by T + t, t is reset to zero, β_o and $\dot{\beta}_o$ are replaced by β and $\dot{\beta}$, new values for the lever arm ratio and unlocking friction torque are computed, and the whole process is repeated for each increment $\Delta\beta$ until phase 2 is completed.

Phase 3: Final conditions for phase 2 serve as initial conditions for phase 3. There are now two degrees of freedom in the system.

The approximate solution to the equation of motion of the balance is identical to the solution in phase 2 except the expression (K-L) is everywhere replaced by (K+L) and T_f is set equal to zero.

The analytical solution of the exact equation of motion of the escape wheel is

$$\epsilon = \epsilon_2 - \frac{T_e}{2I_e}t^2 \qquad (6.10)$$

where $\epsilon = \epsilon_a$ and $\dot{\epsilon} = 0$ at $t = 0$.

β_3 is now determined in the following manner. An incremental step in β is taken and the elapsed time calculated as explained before. This time is substituted into the ϵ (t) equation and the position of the escape wheel is determined. This value of ϵ is then substituted into the constraint equations ((4.1) and (4.5)) in order to calculate where the balance would be if the escape wheel had caught up to the other two components. If this value of β is greater (remember $\beta < 0$ here) than the value set by the incremental step, the escape wheel has had insufficient time to catch up so another incremental step is taken. By repeating this procedure, and using an iterative process to correct for overshoot, an accurate value of β_3 is obtained.

A simplified method of calculating β_3 was attempted by assuming that the coupled balance and lever have a constant angular speed during the catch-up period. The lever arm ratio XZ_f is approximated by a first order polynomial in β, i.e.

$$XZ_f = \frac{d\epsilon}{d\beta} \approx c_0 + c_1\beta \qquad (6.11)$$

These two assumptions together with the equation of motion of the escape wheel allow the derivation of an explicit expression for β_3. The results obtained using this method were somewhat inaccurate, however, because of the relatively large values of β_3 which occur in the operation of the T5E1 escapement. Although the difference in values of β_3 calculated by both methods seems relatively small ($\sim 2\%$), subsequent work on the energy analysis discussed in section 7 of this report showed that the steady-state conditions for the mechanism were very sensitive to the value of β_3. Thus, the more elaborate procedure for calculating β_3 was deemed necessary.

Phase 4: $\dot{\beta}_{3a}$ is determined by equation (5.30). Initial conditions are

$$\beta_o = \beta_3 \; ; \; \dot{\beta}_o = \dot{\beta}_{3a} \; ; \; t = 0.$$

The approximate equation of motion during this period is

$$I_2\ddot{\beta} + (K+L)\beta = -XZ_f T_a \tag{6.12}$$

and its solution is

$$\beta = A\cos(\omega t - \varphi) - G \tag{6.13}$$

where $$G = \frac{XZ_f T_a}{K+L} \; ; \quad \omega^2 = \frac{K+L}{I_2} \tag{6.14}$$

$$A = \sqrt{\frac{\dot{\beta}_o^2}{\omega_o^2} + (\beta_o + G_o)^2} \tag{6.15}$$

$$\varphi = \tan^{-1} \frac{\dot{\beta}_o}{\omega_o(\beta_o + G_o)} \tag{6.16}$$

and $G_o = G(\beta_o)$, $\omega_o = \omega(\beta_o)$ as before. X and Z_f are assumed constant within any one increment and are evaluated at β_o. The remainder of the procedure is analogous to that discussed for phase 2.

In a similar manner the step-by-step method is used to complete the remaining phases of the cycle.

One problem with this method of solution was the difficulty of guessing the correct value of the input torque, T_a, for a given equilibrium amplitude of oscillation since these two parameters are not unrelated. Attempts were made with an iterative approach to correct the initial guess after each cycle until convergence to the correct value occurred. Although the program should eventually converge to the correct value, the convergence rate was totally unsatisfactory and computer time was excessive. A solution of this problem is discussed in the following section of this report.

7. ENERGY ANALYSIS

In order to obtain an accurate value of equilibrium torque (to required accuracy of 10^{-3} dyne-cm) for a given amplitude, an energy analysis of the escapement was carried out and programmed on the computer. The output from this program (T_a versus β_m) is used in the differential equations of motion to obtain the period or beat rate of the system as described in section 6.

Before the actual analysis itself can be presented it is necessary to derive expressions for the angular speed at the end points of each phase of the motion. An expression for β_6, the angular displacement at the end of the first half-cycle, is also required. Each of the relationships presented is obtained by application of the law of conservation of energy.

Phase 1: Energy is dissipated in this phase by the side thrust effect; so

$$\frac{1}{2}K\beta_m^2 = \frac{1}{2}K\beta_1^2 + \frac{1}{2}I_8\dot{\beta}_{1b}^2 + \int_{\beta_m}^{\beta_1}(-L\beta)\,d\beta \qquad (7.1)$$

or

$$\dot{\beta}_{1b}^2 = \left(\frac{K-L}{I_8}\right)(\beta_m^2 - \beta_1^2) \qquad (7.2)$$

Phase 2: The collision at β_1 which initiates the unlocking phase is assumed to be instantaneous and inelastic. As a result

$$I_8\dot{\beta}_{1b} = I_{11}\dot{\beta}_{1a} \qquad (7.3)$$

where I_{11} represents I_1 evaluated at β_1. Consequently

$$\dot{\beta}_{1a} = \frac{I_8}{I_{11}}\sqrt{\left(\frac{K-L}{I_8}\right)(\beta_m^2 - \beta_1^2)} \qquad (7.4)$$

During the unlocking portion of this phase, energy is dissipated by both the side thrust effect and unlocking friction. Thus

$$\frac{1}{2}K\beta_1^2 + \frac{1}{2}I_{11}\dot{\beta}_{1a}^2 = \frac{1}{2}I_{12}\dot{\beta}_2^2 + \int_{\beta_1}^{0}(-L\beta)d\beta + \int_{\beta_1}^{0}(-T_f)d\beta \qquad (7.5)$$

where $$T_f = \mu T_a U(\beta) \qquad (7.6)$$

and μ is the coefficient of friction (see appendix C). Since the expression $\int U(\beta)d\beta$ is a function of the geometry only, it can be evaluated once and for all. Utilizing the Gauss guadrature method, the result for the T5E1 escapement is[5]

$$\int_0^{\beta_1} U(\beta)d\beta = 0.090945 = g \qquad (7.7)$$

Substitution of this value and simplification leads to the following equation

$$\dot{\beta}_2^2 = \frac{1}{I_{12}}\left[(K-L)\beta_1^2 + \frac{I_{11}}{I_{11}}(K-L)(\beta_m^2-\beta_1^2) - 2\mu g T_a\right] \qquad (7.8)$$

Phase 3: β_3 is determined by the iteration process discussed in section 6 of this report once the value of $\dot{\beta}_2$ is known. The angular speed of the balance at the end of the "catch-up" can then be determined from the relationship

$$\frac{1}{2}I_{12}\dot{\beta}_2^2 = \frac{1}{2}K\beta_3^2 + \frac{1}{2}I_{11}\dot{\beta}_{3b}^2 + \int_0^{\beta_3} L\beta d\beta \qquad (7.9)$$

where side thrust now represents the only dissipative effect. It therefore follows that

$$\dot{\beta}_{3b}^2 = \frac{I_{12}\dot{\beta}_2^2 - (K+L)\beta_3^2}{I_{11}} \qquad (7.10)$$

Phase 4: The "catch-up" collision is also assumed to be instantaneous and inelastic. As previously discussed in section 5 of this report, it is found that

$$\dot{\beta}_{3a} = \frac{I_{13}\dot{\beta}_{3b} + X_3 Z_{43} I_g \dot{\epsilon}_{3b}}{I_{23}} \tag{7.11}$$

where I_{23} represents I_2 evaluated at β_3. $\dot{\epsilon}_{3b}$ is calculated from the equation of motion of the escape wheel and the elasped time during "catch-up" as determined in the iteration process.

During the remainder of this phase energy is delivered to the balance system through impulse and lost through the side thrust effect; thus

$$\tfrac{1}{2}K\beta_3^2 + \tfrac{1}{2}I_{23}\dot{\beta}_{3a}^2 = \tfrac{1}{2}K\beta_4^2 + \tfrac{1}{2}I_{24}\dot{\beta}_4^2 + \int_{\beta_3}^{\beta_4} L\beta\, d\beta - \int_{\beta_3}^{\beta_4} XZ_4(-T_a)\, d\beta \tag{7.12}$$

The minus sign on T_a must be inserted because the torque is applied to the balance in the negative sense. Here the product XZ represents the lever arm ratio which reduces the torque T_a applied to the escape wheel as it is transmitted through the lever to the balance system. Note that the lower limit β_3, on the integrals, is not fixed; i.e., it is a function of β_m and T_a. Evaluation of the integral involving T_a in equation (7.12) is somewhat simplified by noting that equations (5.25) and (5.27) show that

$$XZ_4 = \frac{d\epsilon_4}{d\beta} \tag{7.13}$$

so that $$\int_{\beta_3}^{\beta_4} XZ_4(-T_a)\, d\beta = T_a \int_{\epsilon_4}^{\epsilon_3} d\epsilon = T_a(\epsilon_3 - \epsilon_4)$$

Using equations (4.1) and (4.5), ϵ_3 can be determined once β_3 is known.

With this result and the fact that $\beta_4 = -\beta_1$, equation (7.12) can be solved for $\dot{\beta}_4^2$; the result is

$$\dot{\beta}_4^2 = \frac{I_{23}\dot{\beta}_{2a}^2 - (K+L)(\beta_1^2 - \beta_3^2) + 2T_a(\epsilon_3 - \epsilon_4)}{I_{24}} \qquad (7.14)$$

Phases 5 and 6: As the escape wheel is relocked by the lever, the balance swings towards its maximum position dissipating energy through the side thrust effect. It follows that

$$\tfrac{1}{2}K\beta_4^2 + \tfrac{1}{2}I_3\dot{\beta}_4^2 = \tfrac{1}{2}K\beta_6^2 + \int_{\beta_4}^{\beta_6} L\beta\,d\beta \qquad (7.15)$$

or
$$\beta_6^2 = \beta_1^2 + \frac{I_3\dot{\beta}_4^2}{K+L} \qquad (7.16)$$

The first half-cycle is now complete.

In a similar manner, the following expressions can be derived for the second half-cycle:

Phase 7:

$$\tfrac{1}{2}K\beta_6^2 = \tfrac{1}{2}K\beta_7^2 + \tfrac{1}{2}I_3\dot{\beta}_{7b}^2 + \int_{\beta_6}^{\beta_7} (-L\beta)\,d\beta \qquad (7.17)$$

But
$$\beta_7 = -\beta_1$$

so
$$\dot{\beta}_{7b}^2 = \left(\frac{K-L}{I_3}\right)(\beta_6^2 - \beta_1^2) \qquad (7.18)$$

or
$$\dot{\beta}_{7b}^2 = \left(\frac{K-L}{K+L}\right)\dot{\beta}_4^2 \qquad (7.19)$$

Phase 8:

$$\dot{\beta}_{7a} = \frac{I_3}{I_{17}}\dot{\beta}_{7b} \qquad (7.20)$$

or, since $I_{17} = I_{11}$,

$$\dot{\beta}_{7a} = \frac{I_8}{I_{11}} \sqrt{\frac{K-L}{I_8}} \sqrt{\beta_6^2 - \beta_1^2} \tag{7.21}$$

Now $$\tfrac{1}{2}K\beta_7^2 + \tfrac{1}{2}I_{17}\dot{\beta}_{7a}^2 = \tfrac{1}{2}I_{18}\dot{\beta}_8^2 + \int_{\beta_7}^{0}(-L\beta)\,d\beta + \tag{7.22}$$

But $I_{18} = I_{12}$; $$+ \int_{\beta_7}^{0}(-T_f)\,d\beta$$

thus $$\tfrac{1}{2}K\beta_1^2 + \tfrac{1}{2}I_{11}\dot{\beta}_{7a}^2 = \tfrac{1}{2}I_{12}\dot{\beta}_8^2 + \tfrac{1}{2}L\beta_1^2 + \int_0^{\beta_1} T_f\,d\beta \tag{7.23}$$

or $$\dot{\beta}_8^2 = \frac{1}{I_{12}}\left[\frac{I_8}{I_{11}}(K-L)(\beta_6^2 - \beta_1^2) + (K-L)\beta_1^2 - 2\mu g T_a\right] \tag{7.24}$$

Phase 9:

$$\tfrac{1}{2}I_{18}\dot{\beta}_8^2 = \tfrac{1}{2}K\beta_9^2 + \tfrac{1}{2}I_{19}\dot{\beta}_{9b}^2 + \int_0^{\beta_9} L\beta\,d\beta \tag{7.25}$$

$$\dot{\beta}_{9b}^2 = \frac{I_{12}\dot{\beta}_8^2 - (K+L)\beta_9^2}{I_{19}} \tag{7.26}$$

Phase 10:

$$\dot{\beta}_{9a} = \frac{I_{19}\dot{\beta}_{9b} - X_9 Z_{r9} I_E \dot{\epsilon}_{9b}}{I_{29}} \tag{7.27}$$

The minus sign is required because $\dot{\epsilon}_{9b} < 0$.

$$\tfrac{1}{2}K\beta_9^2 + \tfrac{1}{2}I_{29}\dot{\beta}_{9a}^2 = \tfrac{1}{2}K\beta_{10}^2 + \tfrac{1}{2}I_{210}\dot{\beta}_{10}^2 + \int_{\beta_9}^{\beta_{10}} L\beta\,d\beta + \int_{\beta_9}^{\beta_{10}} X Z_r T_a\,d\beta \tag{7.28}$$

But $$\int_{\beta_9}^{\beta_{10}} XZ_r T_a \, d\beta = -T_a \int_{\epsilon_9}^{\epsilon_{10}} \frac{d\epsilon}{d\beta} d\beta = T_a(\epsilon_9 - \epsilon_{10}) \qquad (7.29)$$

Since $$\beta_{10} = \beta_1$$

it follows that

$$K\beta_9^2 + I_{29}\dot{\beta}_{9a}^2 = K\beta_1^2 + I_{210}\dot{\beta}_{10}^2 + L(\beta_1^2 - \beta_9^2) - 2T_a(\epsilon_9 - \epsilon_{10}) \qquad (7.30)$$

or $$\dot{\beta}_{10}^2 = \frac{I_{29}\dot{\beta}_{9a}^2 - (K+L)(\beta_1^2 - \beta_9^2) + 2T_a(\epsilon_9 - \epsilon_{10})}{I_{210}} \qquad (7.31)$$

Note that $I_{210} \neq I_{24}$ because $Z_{r10} \neq Z_{f4}$.

Phases 11 and 12: For steady-state motion

$$\tfrac{1}{2}K\beta_{10}^2 + \tfrac{1}{2}I_8\dot{\beta}_{10}^2 = \tfrac{1}{2}K\beta_m^2 + \int_{\beta_{10}}^{\beta_m} L\beta \, d\beta \qquad (7.32)$$

or $$\dot{\beta}_{10}^2 = \left(\frac{K+L}{I_8}\right)(\beta_m^2 - \beta_1^2) \qquad (7.33)$$

This completes the second half-cycle.

Equivalent Balance System Energy Balance

As shown in section 5 of this report, the equations of motion of the main components may be combined with the constraint equations to derive equations which describe an "equivalent" escapement system. This "equivalent" system possesses a displacement-dependent moment of inertia which arises due to the presence of the "reflected" moments of inertia of the lever and escape wheel. An energy analysis of the equivalent escapement system is presented below; steady-state conditions are assumed throughout.

The energy balance conditions for the equivalent escapement may be depicted schematically as shown in Figure 13.

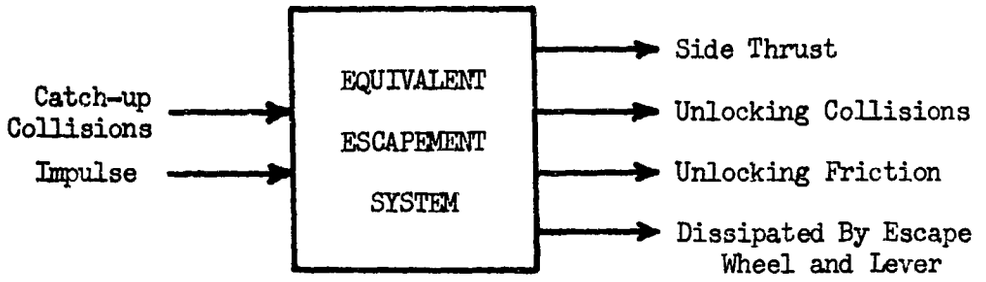

Figure 13. Schematic diagram of equivalent escapement energy balance.

Loss mechanisms which have been considered are: (a) side thrust losses, (b) unlocking collisions, (c) unlocking friction, and (d) dissipation by the escape wheel and lever upon unlocking. Of these, only a and c are identical in both half-cycles since, in general, $-\beta_6 \neq \beta_m$, and $-\beta_3 \neq \beta_9$, etc. As a result, the angular speed of the balance system just prior to the unlocking collision and at the end of the impulse phase in the reverse half-cycle differs from the speeds at the corresponding points in the forward half-cycle. Losses through mechanisms b and d are therefore different in each half-cycle.

With the assumption that the radial side thrust is directly proportional to balance displacement, the energy loss due to this effect per cycle is

$$L_{ST} = 2\left[\int_0^{\beta_m} L\beta d\beta + \int_0^{\beta_c} L\beta d\beta\right] \qquad (7.34)$$

or $$L_{ST} = L(\beta_m^2 + \beta_6^2) \tag{7.35}$$

Since the unlocking collisions are assumed to be inelastic and instantaneous, the loss through this mechanism can be calculated from the difference in kinetic energies before and after the collisions. Thus

$$L_{UC} = \tfrac{1}{2} I_B(\dot{\beta}_{1b}^2 + \dot{\beta}_{7b}^2) - \tfrac{1}{2} I_{11}(\dot{\beta}_{1a}^2 + \dot{\beta}_{7a}^2) \tag{7.36}$$

Upon substitution of equations (7.2), (7.4), (7.18), and (7.21) this equation may be written as

$$L_{UC} = \tfrac{1}{2}(K-L)\left(1 - \frac{I_B}{I_{11}}\right)(\beta_m^2 + \beta_6^2 - 2\beta_1^2) \tag{7.37}$$

During the unlocking of the escape wheel energy is dissipated by friction. This loss per cycle is given by

$$L_{UF} = 2\int_0^{\beta_1} T_f \, d\beta \tag{7.38}$$

or $$L_{UF} = 2\mu T_a \int_0^{\beta_1} U(\beta)\, d\beta \tag{7.39}$$

where $T_f = \mu T_a U(\beta)$ (see appendix C). Substitution for the integral from equation (7.7) yields the result

$$L_{UF} = 2\mu g T_a \tag{7.40}$$

Both the lever and escape wheel have a finite velocity at the end of the impulse phase of the motion. Whatever energy they possess at the instant they are uncoupled from the balance is dissipated as the escaped

wheel relocks. The loss of energy can be expressed as

$$L_{SL} = \tfrac{1}{2} I_{24} \dot{\beta}_4^2 - \tfrac{1}{2} I_8 \dot{\beta}_4^2 + \tfrac{1}{2} I_{210} \dot{\beta}_{10}^2 - \tfrac{1}{2} I_8 \dot{\beta}_{10}^2 \qquad (7.41)$$

Substitution of equations (7.14) and (7.33) into this expression gives

$$L_{SL} = \left(\frac{K+L}{2}\right)\left[\left(\frac{I_{24}}{I_8} - 1\right)\left(\beta_6^2 - \beta_1^2\right) + \left(\frac{I_{210}}{I_8} - 1\right)\left(\beta_m^2 - \beta_1^2\right)\right] \qquad (7.42)$$

The total losses for the entire cycle are, obviously, the sum of the individual losses; i.e.

$$L_T = L_{ST} + L_{UC} + L_{UF} + L_{SL} \qquad (7.43)$$

After substitution for each of those losses, it can be shown that

$$L_T = \frac{\beta_m^2}{2}\left[K\left(\frac{I_{210}}{I_8} - \frac{I_8}{I_{11}}\right) + L\left(\frac{I_{210}}{I_8} + \frac{I_8}{I_{11}}\right)\right] +$$

$$+ \beta_1^2\left[K\left(\frac{I_8}{I_{11}} - \frac{I_{24}+I_{210}}{2I_8}\right) - L\left(\frac{I_8}{I_{11}} + \frac{I_{24}+I_{210}}{2I_8}\right) + 2L\right] \qquad (7.44)$$

$$+ \frac{\beta_6^2}{2}\left[K\left(\frac{I_{24}}{I_8} - \frac{I_8}{I_{11}}\right) + L\left(\frac{I_{24}}{I_8} + \frac{I_8}{I_{11}}\right)\right] + 2\mu g T_a$$

Each of the quantities on the right hand side of this expression is a constant, independent of amplitude, except for β_6, T_a, and, of course, β_m.

Energy is supplied to this equivalent system by: (a) catch-up collisions, and (b) impulse. Although there must be a net loss of energy in the entire system as a result of the catch-up collisions, the effect of the collisions on the equivalent escapement is to add energy.

The energy supplied to the equivalent escapement as a result of the catch-up collisions at β_3 and β_9 is

$$G_{cc} = \tfrac{1}{2} I_{23} \dot{\beta}_{3a}^2 - \tfrac{1}{2} I_{13} \dot{\beta}_{3b}^2 + \tfrac{1}{2} I_{29} \dot{\beta}_{9a}^2 - \tfrac{1}{2} I_{19} \dot{\beta}_{9b}^2 \qquad (7.45)$$

Substitution of equation (5.30) for $\dot{\beta}_{3a}$ and equation (5.43) for $\dot{\beta}_{9a}$ yields

$$G_{cc} = \frac{1}{2 I_{23}} \left[I_{13} \dot{\beta}_{3b} + X_3 Z_{f3} I_E \dot{\epsilon}_{3b} \right]^2 - \tfrac{1}{2} I_{13} \dot{\beta}_{3b}^2 + \qquad (7.46)$$

$$+ \frac{1}{2 I_{29}} \left[I_{19} \dot{\beta}_{9b} - X_9 Z_{f9} I_E \dot{\epsilon}_{9b} \right]^2 - \tfrac{1}{2} I_{19} \dot{\beta}_{9b}^2$$

With the exception of I_E, each of the terms in equation (7.46) depends, in some manner, upon either the applied torque T_a, or the magnitudes of the catch-up angles, or both. This becomes evident when equations (7.8), (7.10), (7.24), and (7.26) are used to substitute for $\dot{\beta}_{3b}$ and $\dot{\beta}_{9b}$. $\dot{\epsilon}_{3b}$ and $\dot{\epsilon}_{9b}$ may be determined either from the equation of motion of the escape wheel (equations (5.34) and (5.45) or by equating the kinetic energy of the escape wheel just prior to the catch-up collisions to the work done by the applied torque; i.e.

$$\tfrac{1}{2} I_E \dot{\epsilon}_{3b}^2 = T_a (\epsilon_2 - \epsilon_3) \quad ; \quad \epsilon_2 > \epsilon_3 \qquad (7.47)$$

and

$$\tfrac{1}{2} I_E \dot{\epsilon}_{9b}^2 = T_a (\epsilon_8 - \epsilon_9) \quad ; \quad \epsilon_8 > \epsilon_9 \qquad (7.48)$$

An alternative expression for G_{cc} may be derived in the following way. Consider the catch-up collision in the forward half-cycle. Equations (7.10) and (7.11) may be solved for the kinetic energy of the equivalent balance system immediately before and after the catch-up collision, respectively. After subtraction of these two expressions and the substitution of equations (7.8) for $\dot{\beta}_2^2$ and (7.14) for $\dot{\beta}_4^2$, the energy gain can be written as

$$
\begin{aligned}
{}_fG_{cc} = &-\frac{(K-L)I_B}{2I_{11}}\beta_m^2 + \frac{(K+L)I_{24}}{2I_B}\beta_6^2 + T_a[\epsilon_4-\epsilon_3+2\mu g] + \\
&+\beta_1^2\left[L + \frac{K}{2}\left(\frac{I_B}{I_{11}} - \frac{I_{24}}{I_B}\right) + \frac{L}{2}\left(\frac{I_B}{I_{11}} - \frac{I_{24}}{I_B}\right)\right]
\end{aligned}
\tag{7.49}
$$

In a similar manner, an expression can be obtained for the reverse half-cycle collision. The total gain can therefore be written as

$$
\begin{aligned}
G_{cc} = &\frac{\beta_m^2}{2}\left[K\left(\frac{I_{210}}{I_B} - \frac{I_B}{I_{11}}\right) + L\left(\frac{I_{210}}{I_B} + \frac{I_B}{I_{11}}\right)\right] + \\
&+\frac{\beta_6^2}{2}\left[K\left(\frac{I_{24}}{I_B} - \frac{I_B}{I_{11}}\right) + L\left(\frac{I_{24}}{I_B} + \frac{I_B}{I_{11}}\right)\right] + \\
&+\beta_1^2\left[K\left(\frac{I_B}{I_{11}} - \frac{I_{24}+I_{210}}{2I_B}\right) - L\left(\frac{I_B}{I_{11}} + \frac{I_{24}+I_{210}}{2I_B} - 2\right)\right] \\
&+T_a(\epsilon_4-\epsilon_3+\epsilon_{10}-\epsilon_9+2\mu g)
\end{aligned}
\tag{7.50}
$$

Note that ϵ_3 and ϵ_9 are the values of ϵ at which the catch-up collisions occur.

The energy supplied to the equivalent balance system during the impulse portions of the motion is

$$G_I = \int_{\beta_3}^{\beta_4} \dot{X} Z_f (-T_a)\, d\beta + \int_{\beta_9}^{\beta_{10}} \dot{X} Z_r T_a\, d\beta \qquad (7.51)$$

But $$XZ_f = \frac{d\epsilon}{d\beta}$$

and $$XZ_r = -\frac{d\epsilon}{d\beta}$$

in the first and second half-cycles, respectively. Therefore

$$G_I = T_a(\epsilon_3 - \epsilon_4 + \epsilon_9 - \epsilon_{10}) \qquad (7.52)$$

The total energy gain for the entire cycle is

$$G_T = G_{cc} + G_I \qquad (7.53)$$

or

$$G_T = \tfrac{1}{2} I_{23} \dot{\beta}_{3a}^2 - \tfrac{1}{2} I_{13} \dot{\beta}_{3b}^2 + \tfrac{1}{2} I_{29} \dot{\beta}_{9a}^2 - \tfrac{1}{2} I_{19} \dot{\beta}_{9b}^2 + T_a(\epsilon_3 - \epsilon_4 + \epsilon_9 - \epsilon_{10}) \qquad (7.54)$$

By equating the total losses per cycle to the total gains per cycle a relationship between β_m and T_a for steady-state motion of the escapement can be obtained. However, this relationship is transcendental because the expression for G_{cc} contains terms which are dependent upon β_m and T_a. At first sight, it appears that the substitution of equation (7.50) for G_{cc} into the energy balance equation would lead to a useful relationship between β_m and T_a. Unfortunately, this approach leads only to the identity

$l = 1$. In retrospect, this result is not surprising because only one requirement, namely the conservation of energy, has been applied to derive all of these relationships. Consequently, a simple, explicit expression for T_a in terms of β_m cannot be found.

A self-consistent, iterative method of solving the energy balance equation has proven effective. Define B in such a way that equation (7.44) can be written as

$$L_T = B + 2\mu g T_a \tag{7.55}$$

The energy balance equation then becomes

$$B + 2\mu g T_a = G_{cc} + T_a(\epsilon_3 - \epsilon_4 + \epsilon_9 - \epsilon_{10}) \tag{7.56}$$

This equation can be rewritten as

$$T_a = \frac{G_{cc} - B}{C} \tag{7.57}$$

where $$C = 2\mu g - \epsilon_3 + \epsilon_4 - \epsilon_9 + \epsilon_{10} \, . \tag{7.58}$$

But evaluation of B requires a knowledge of β_6, C the values of the catch-up angles, and G_{cc} the speeds before and after each of the catch-up collisions. An initial guess is now made for T_a at a given amplitude β_m. This estimate is used in equation (7.1) through (7.33) to calculate the quantities needed and they are fed into equation (7.57) to calculate a "new" T_a. This procedure continues until convergence to the correct value occurs. After the first few passes the corrections to T_a, i.e., the difference between each of the "old" and "new" values, are used in a linear interpolation scheme to considerably enhance the convergence rate.

Total System Energy Balance

An energy analysis similar to that already presented may be carried out for the entire escapement mechanism. The various energy exchange mechanisms of the total system may be pictured schematically as shown in Figure 14.

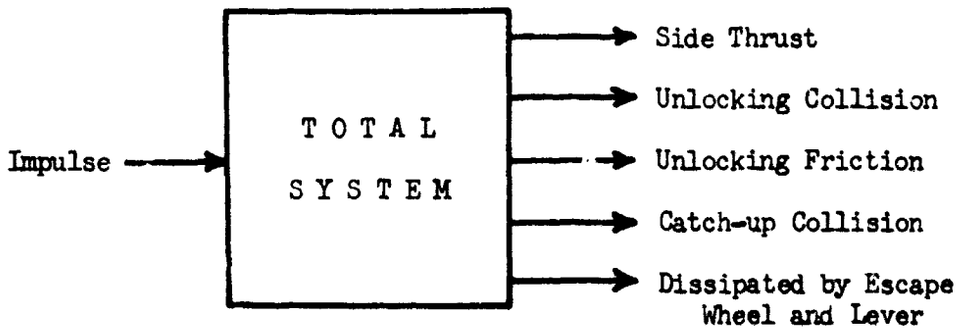

Figure 14. Schematic diagram of total system energy balance.

Loss mechanisms which have been considered for the total system are: (a) side thrust losses, (b) unlocking collisions, (c) unlocking friction, (d) catch-up collisions, and (e) dissipation by the escape wheel and lever upon relocking. The derivation of expressions for losses a, b, and c proceeds in the same manner as presented for the equivalent balance system with identical results (see equations (7.35), (7.37), and (7.40)).

Although the catch-up collisions were responsible for an addition of energy to the equivalent escapement system, these collisions must result in a net loss of energy when the total system is considered. This loss

can be written simply as the difference in kinetic energies of the total system immediately before and after the collisions occur; i. e.

$$L'_{cc} = \tfrac{1}{2} I_{13} \dot{\beta}^2_{3b} + \tfrac{1}{2} I_g \dot{\epsilon}^2_{3b} - \tfrac{1}{2} I_{23} \dot{\beta}^2_{3a} + \\ + \tfrac{1}{2} I_{19} \dot{\beta}^2_{9b} + \tfrac{1}{2} I_g \dot{\epsilon}^2_{9b} - \tfrac{1}{2} I_{29} \dot{\beta}^2_{9a} \tag{7.59}$$

Upon substitution of equations (7.47) and (7.48), this equation becomes

$$L'_{cc} = T_a(\epsilon_2 - \epsilon_3 + \epsilon_8 - \epsilon_9) - G_{cc} \tag{7.60}$$

where G_{cc} is given by equation (7.45).

Uncoupling of the escape wheel and lever from the balance occurs at the completion of the impulse phase in each half-cycle. Whatever energy the former two possess at this instant is dissipated upon relocking of the escape wheel. Also, additional energy is supplied to the escape wheel by T_a during the period between uncoupling and relocking. (Recall that the model escapement is defined in such a way that the motion of the lever ceases at the end of impulse. See Figure 2e.) Therefore, the total energy dissipated by the escape wheel and lever is

$$L'_{EL} = L_{EL} + \int_{\epsilon_4}^{\epsilon_5} (-T_a)\, d\epsilon + \int_{\epsilon_{10}}^{\epsilon_{11}} (-T_a)\, d\epsilon \tag{7.61}$$

or

$$L'_{EL} = L_{EL} + T_a(\epsilon_4 - \epsilon_5 + \epsilon_{10} - \epsilon_{11}) \tag{7.62}$$

where L_{EL} is given by equation (7.42).

The sum of the losses per cycle for the total system is

$$L'_T = L_{ST} + L_{UC} + L_{UF} + T_a(\epsilon_2 - \epsilon_3 + \epsilon_8 - \epsilon_9) - \\ - G_{cc} + L_{EL} + T_a(\epsilon_4 - \epsilon_5 + \epsilon_{10} - \epsilon_{11}) \tag{7.63}$$

$$L'_T = L_T - G_{cc} + T_a(\epsilon_2 - \epsilon_3 + \epsilon_4 - \epsilon_5 + \epsilon_8 - \epsilon_9 + \epsilon_{10} - \epsilon_{11}) \quad (7.64)$$

Or, using equation (7.55),

$$L'_T = T_a(\epsilon_2 - \epsilon_3 + \epsilon_4 - \epsilon_5 + \epsilon_8 - \epsilon_9 + \epsilon_{10} - \epsilon_{11} + 2\mu g) + B - G_{cc} \quad (7.65)$$

Energy is added to the total system through the impulse supplied by the torque applied to the escape wheel, T_a. In each cycle, the escape wheel rotates through an angle of $\frac{2\pi}{N}$ radians, where N is the number of teeth on the escape wheel. Consequently, the energy added to the total system per cycle is

$$G'_T = \int_{\epsilon_0}^{\epsilon_{12}} (-T_a)\, d\epsilon = T_a\left(\frac{2\pi}{N}\right) \quad (7.66)$$

Once again, the basic energy balance relationship for steady-state motion is obtained by equating losses to gains; thus

$$T_a\left(\frac{2\pi}{N}\right) = T_a(\epsilon_2 - \epsilon_3 + \epsilon_4 - \epsilon_5 + \epsilon_8 - \epsilon_9 + \epsilon_{10} - \epsilon_{11} + 2\mu g) + B - G_{cc} \quad (7.67)$$

The solution for T_a is

$$T_a = \frac{B - G_{cc}}{C'} \quad (7.68)$$

where $$C' = \frac{2\pi}{N} - \epsilon_2 + \epsilon_5 - \epsilon_8 + \epsilon_{11} - C \quad (7.69)$$

and C is given by equation (7.58). Equation (7.69) can be solved in the same, self-consistent manner discussed in the equivalent escapement energy analysis.

Both energy analyses presented in this section are, of course, equivalent as becomes evident upon comparison of equations (7.57) and (7.68). Equating both of these expressions leads to the identity

$$\epsilon_2 - \epsilon_5 + \epsilon_8 - \epsilon_{11} = \frac{2\pi}{N}$$

whose validity for the T5E1 can be verified by substitution of the appropriate values of ε from Table 3 in section 4.

8. RESULTS OF THE ANALYSIS

Both the differential equations of motion and the energy equations, outlined in sections 5 and 7 respectively of this report, make up the mathematical model of the detached lever escapement (hereafter referred to as the "model" escapement). To check the validity of the model, an analysis was made using the T5E1 escapement geometry.

As explained in section 6 of this report, the differential equations of motion were treated using a step-by-step method of solution. The accuracy of this method was checked in three different ways as follows.

1. Changing the size of the increment or step provides one test of accuracy. Table 4 shows the period of the escapement as calculated by the step-by-step method for $\beta_m = \pi$, $\mu = 0.3$, and L equal to 0.0 and 13.83. Note that a smaller increment or step is required for comparable accuracy when side thrust effects are included in the model. As a result of this comparison 40 steps per phase were used in obtaining all of the analytical results presented in this section.

TABLE 4

VARIATION OF THE PERIOD WITH THE NUMBER OF STEPS PER PHASE OF THE MOTION

Number of steps per phase of the motion	Period in Seconds	
	L = 0.0	L = 13.83
5	0.0401050	0.0401467
10	0.0401049	0.0401458
20	0.0401048	0.0401453
40	0.0401048	0.0401450
100	0.0401048	0.0401450

2. Comparing the angular velocity at various points in the cycle as predicted by both the energy solution and the step-by-step solution provides another test of accuracy. Such a comparison is shown in Table 5 for the case $\beta_m = \pi$, $\mu = 0.3$, and $L = 13.83$.

TABLE 5

COMPARISON OF ANGULAR VELOCITIES PREDICTED BY ENERGY ANALYSIS AND STEP-BY-STEP SOLUTION

Angular Velocity	Method of Computation		Percent Difference
	Step-by-step	Energy analysis	
$\dot{\beta}_2$	-477.858	-477.837	.0044
$\dot{\beta}_{3b}$	-475.555	-475.534	.0044
$\dot{\beta}_{3a}$	-481.860	-481.839	.0044
$\dot{\beta}_4$	-485.080	-484.955	.0258
$\dot{\beta}_8$	479.406	479.265	.0294
$\dot{\beta}_{9b}$	477.677	477.537	.0293
$\dot{\beta}_{9a}$	482.406	482.265	.0292
$\dot{\beta}_{10}$	483.708	483.460	.0513

The very nature of the step-by-step method should cause a build up of error in the solution; that is, once an error has crept into the solution in a single increment, it will be involved in setting the initial conditions for the next increment, etc. This condition is verified by the results presented in Table 5 which show a general increase in the

magnitude of the differences as the escapement proceeds through the cycle. Examination of the table also shows that the major discrepancy between these two methods arises during the impulse portions of the cycle. Indeed, the errors introduced during forward and reverse impulse (0.0214% and 0.0221% respectively) account for 85% of the total error shown (0.0513%).

3. A comparison of the balance amplitude at the end of the first cycle with the amplitude at the start of the cycle provides the final accuracy test of the step-by-step method. Under equilibrium conditions these two values should be equal. Any difference represents an error introduced by the step-by-step method of solution since the input torque as calculated by the energy analysis is accurate enough to give amplitude agreement to within 10^{-8} radians. Table 6 shows a comparison of these values for various initial amplitudes and the energy loss parameters of $\mu = 0.3$ and $L = 13.83$. Note that the difference is relatively small, the maximum amounting to only 0.14 degrees of arc.

TABLE 6

AMPLITUDE DIFFERENCES INTRODUCED BY THE STEP-BY-STEP METHOD OF SOLUTION

Nominal Amplitude	Amplitude in Radians		Difference Radians	Percent Difference
	Initial	Final		
45°	0.78540	0.78572	.00032	.041
90°	1.57080	1.57169	.00089	.057
135°	2.35619	2.35761	.00142	.060
180°	3.14159	3.14312	.00153	.049
225°	3.92699	3.92940	.00241	.061

The close correlation between values shown by these tests justify confidence in the validity of the step-by-step method of solution.

The results of the energy analysis concerning the equilibrium amplitude-input torque variation under several energy loss conditions are shown in Table 7. These data are plotted in Figure 15. An experimental curve is also shown in this figure for purposes of comparsion.

TABLE 7

EQUILIBRIUM TORQUES FOR VARIOUS AMPLITUDES AND LOSS CONDITIONS

β_m	Equilibrium Torque in dyne-cm					
	$\mu = 0.0$ $L = 0.0$	$\mu = 0.2$ $L = 0.0$	$\mu = 0.3$ $L = 0.0$	$\mu = 0.0$ $L = 13.83$	$\mu = 0.2$ $L = 13.83$	$\mu = 0.3$ $L = 13.83$
45°		51.4	60.6	124.9	149.2	165.2
90°	307.3	376.8	417.7	622.7	743.6	823.6
135°	752.2	910.6	1008.6	1452.5	1734.5	1921.3
180°	1374.5	1657.8	1835.5	2614.0	3121.8	3458.2
225°	2174.4	2618.2	2898.6	4107.5	4905.5	5734.3

When comparing the experimental results it is necessary to account for the fact that the experimental model is a complete timer which includes a gear train, whereas the mathematical model includes only the three escapement components. In obtaining experimental data, torque is supplied by means of dead weights driving a ball bearing mounted pulley which is flexibly coupled to the low speed shaft in the gear train. There is no means of accurately measuring the much smaller torque actually delivered to the fast moving escape wheel. (In fact, this torque is not instan-

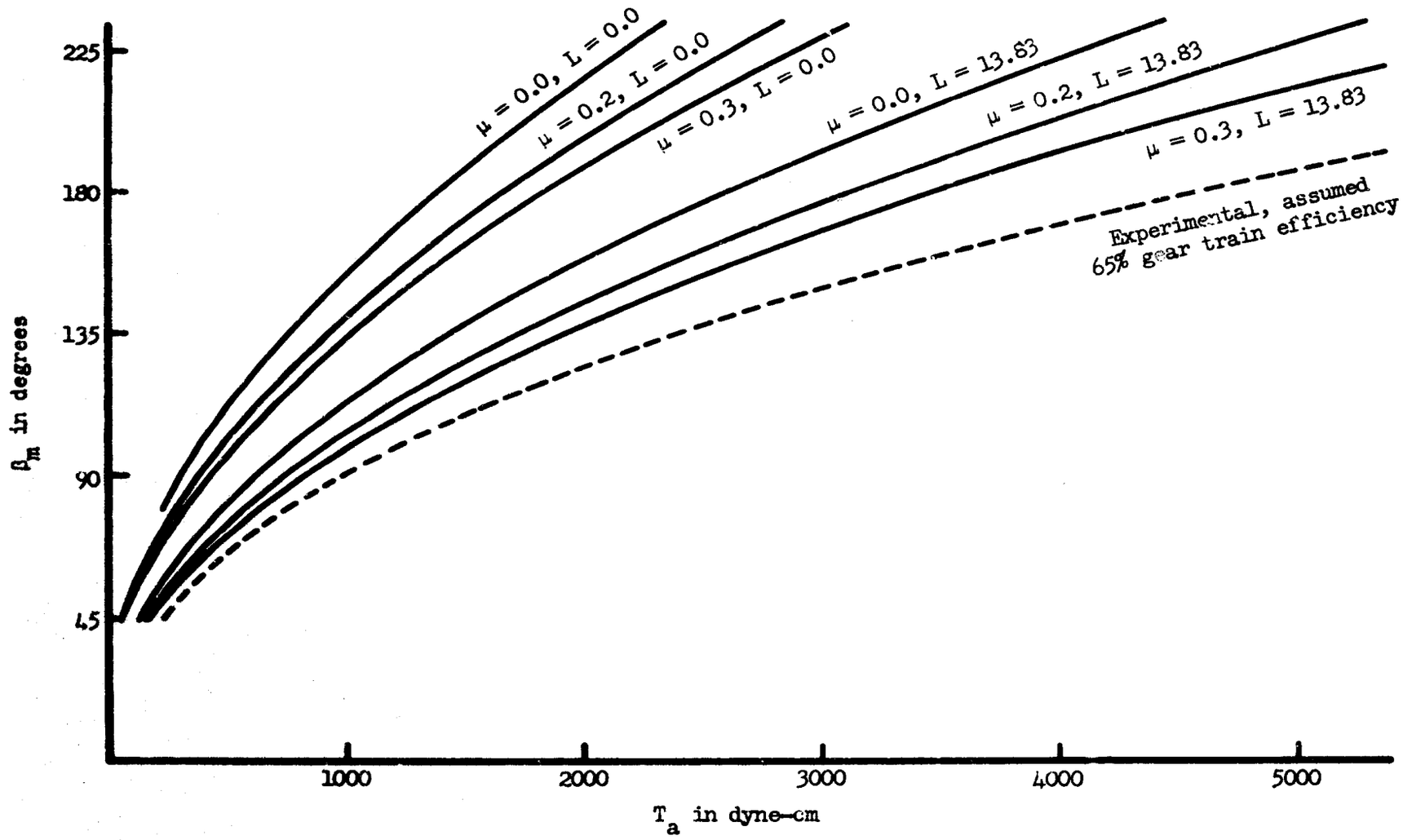

Figure 15. Equilibrium amplitude as a function of input torque for several loss conditions.

taneously constant due to the nonlinear transmission properties of gear teeth.)

In converting the experimental torques to compare with analytical values applied at the escape wheel, a gear train efficiency of 65% was assumed in order to account for losses due to friction. This is a reasonable figure for a nonprecision, 3 stage step-up gear train of 159.7 to 1 ratio. It was also assumed that this efficiency is essentially constant (independent of transmitted torque) over the range of input torque considered.

Since the experimental curve in Figure 15 could have been relocated by the assumption of a different value for the efficiency or by assuming a constant error in the measurement of the experimental input torque, no conclusions can be drawn based on the closeness of the fit. It is felt, however, that the close correlation between the shape of the experimental curve and the $\mu = 0.3$, $L = 13.83$ curve shows that the model is essentially valid in respect to its amplitude versus torque behavior.

The data from Table 7 are displayed in another way in Figure 16 where the input torque for steady-state conditions is plotted against the square of the balance amplitude. Apparently, from this figure, there exists a linear relationship between T_a and β_m^2 of the form

$$T_a = a\beta_m^2 + b \qquad (8.1)$$

However, an attempt to fit the data to such a curve shows the relationship to be near-linear but not exact.

A word of caution should be interjected here concerning the reliability of the data for the loss conditions of $\mu = 0$, and $L = 0$. Under

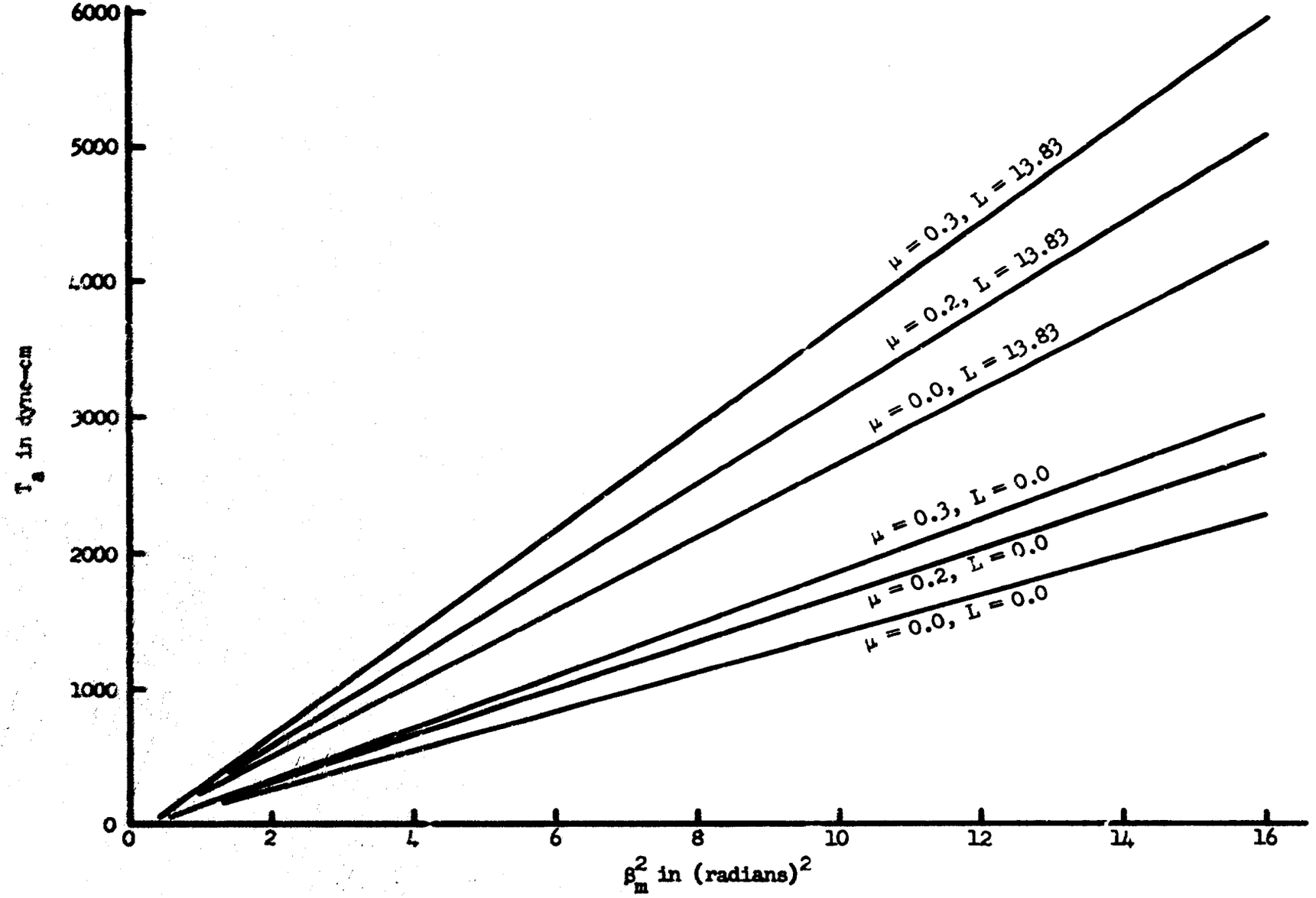

Figure 16. Equilibrium torque as a function of the square of the amplitude for several loss conditions.

these conditions catch-up occurs very near the end of the live impulse face of the escape wheel - so near, in fact, that the slight discrepancies in the two methods of solution resulted in the occurrence of a catch-up collision in the energy analysis but not in the step-by-step solution for the forward half-cycle. For this reason, eventhough catch-up always occurred in both solutions for the reverse half-cycle, the data for these loss conditions should be viewed with some suspicion, at best.

Values of the applied torque from Table 7 were used in the step-by-step solution of the equations of motion to determine the period of oscillation. A typical computer output is shown in appendix E for the conditions $\beta_m = \pi$, $\mu = 0.3$, $L = 13.83$. Data from this output are plotted in Figure 17 to show the angular position of the balance as a function of time. The most striking feature of this $\beta(t)$ curve is that it is apparently a true cosine curve. Indeed, no apparent deviation from a true cosine curve can be seen even when the scales are expanded by a factor of 10. Thus, in this respect, the model shows that departures in the motion of the balance from that of an idealized, undamped harmonic oscillator upon coupling the balance to the other basic components of the escapement is slight.

Another means of illustrating this fact is provided by Figure 18. Here the data from appendix E have been plotted in a phase-plane diagram; i.e., β has been plotted as a function of $\dot{\beta}/\omega_B$ where $\omega_B = \sqrt{\frac{K}{I_B}}$. An ideal, undamped harmonic oscillator is characterized by a circular plot in such a phase-plane diagram. Although the departure from ideal behavior shown by the circle is now evident, it is again seen to be slight. Maximum deviation occurs just prior to the forward catch-up collision and amounts to about 4.3%.

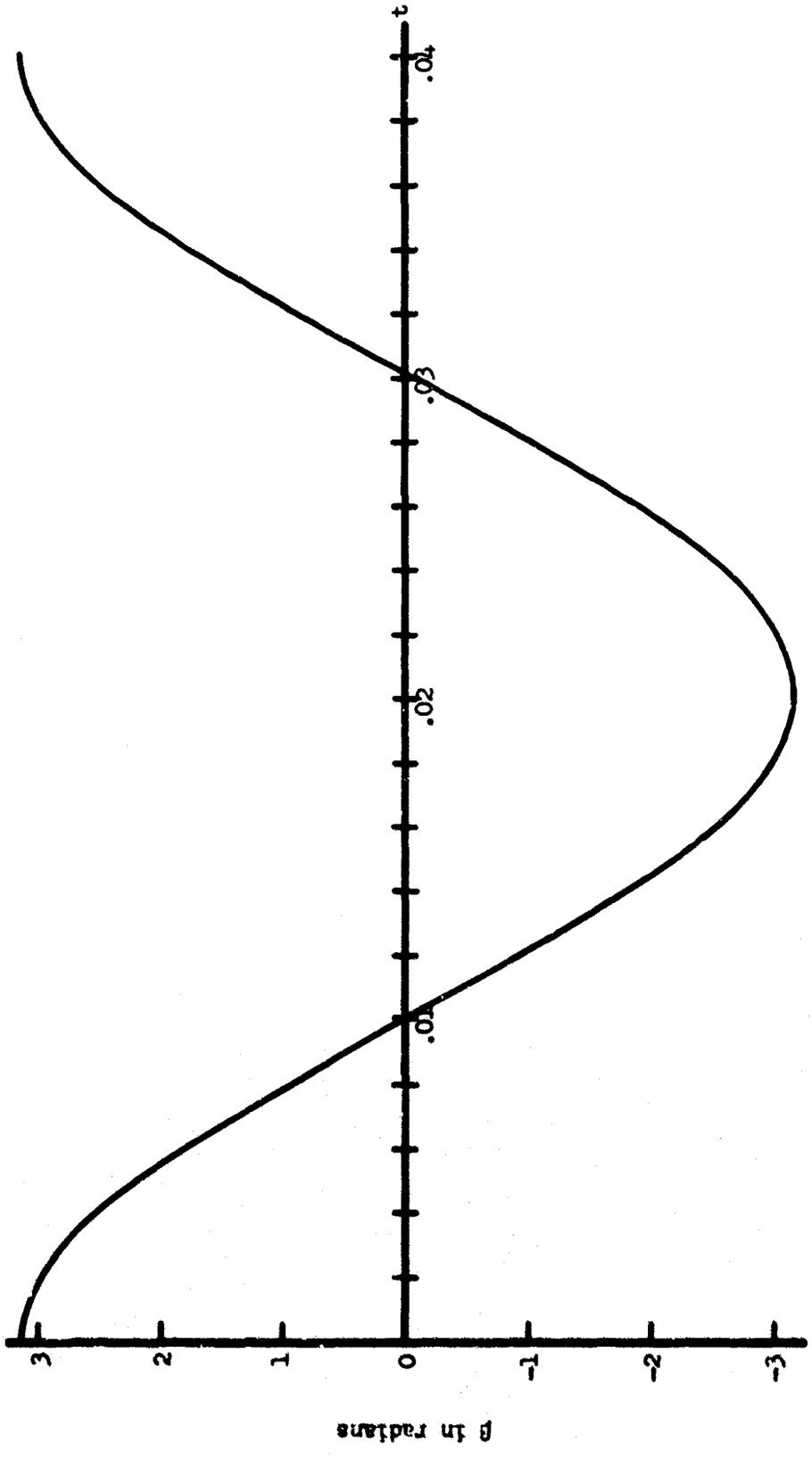

Figure 17. Angular position of the balance as a function of time.

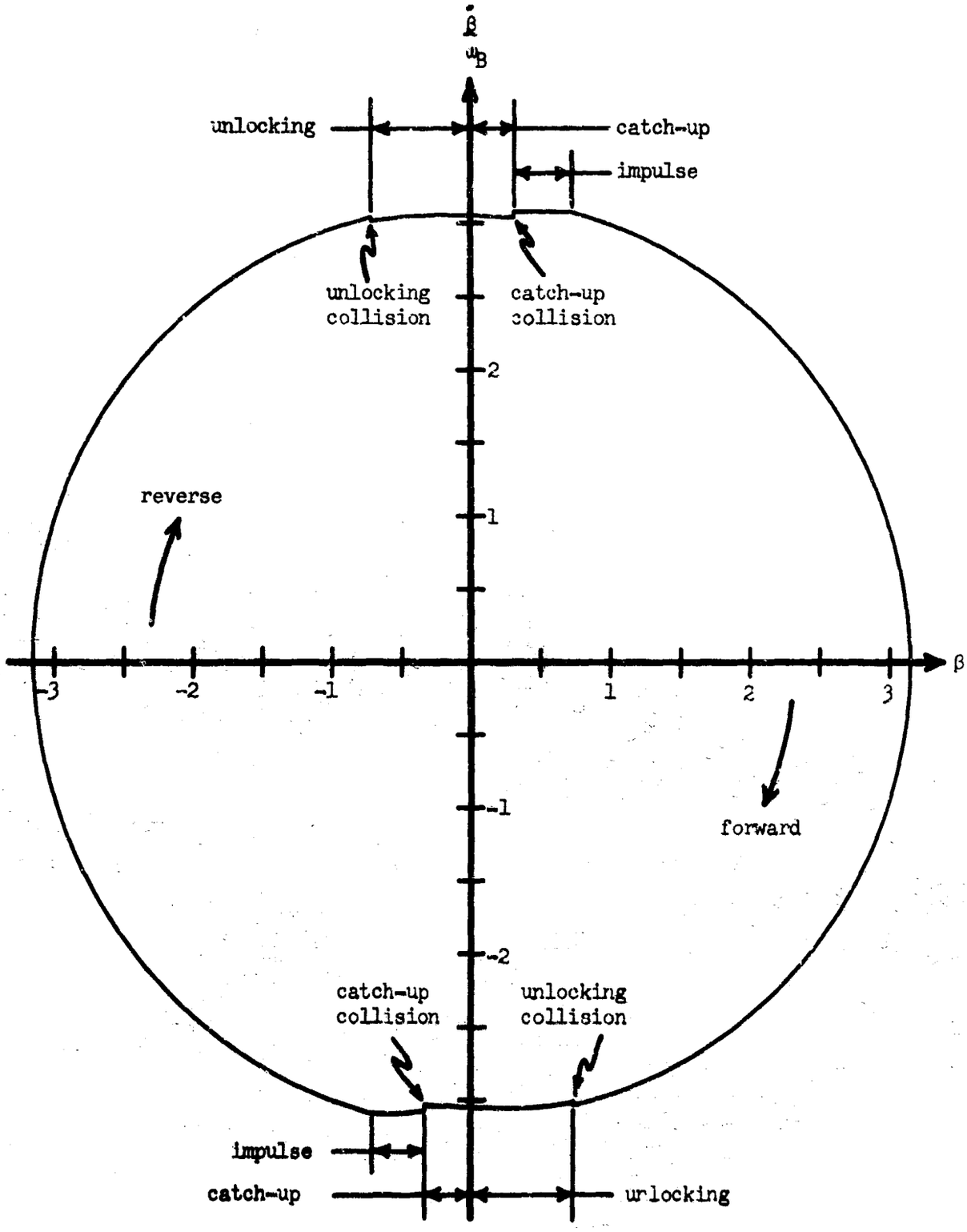

Figure 18. Phase-plane diagram of the equivalent escapement. ($\beta_m = \pi$, $\mu = 0.3$, $L = 13.83$)

The primary use for the outputs from step-by-step solutions such as appendix E was to study the torque sensitivity of the model T5E1 escapement. Results of this study are summarized in Table 8. Values of μ and L used, for each amplitude studied, were 0.3 and 13.83, respectively. The calculated beat rate is compared with the beat rate for a freely oscillating balance system having $I_B = 0.0374$ gm-cm^2 and K = 921.9 dyne-cm. These values were obtained by measuring T5E1 components and they produce a beat rate of 49.9754 bps. The beat rate fracti: (BRF) is plotted as a function of the square of the amplitude in Figure 19 where

$$BRF = 1 - \frac{\pi(\text{actual beat rate})}{\omega_B} \qquad (8.2)$$

and $\omega_B^2 = \frac{K}{I_B}$.

TABLE 8

BEAT RATE FRACTION USING ENERGY LOSS
PARAMETERS $\mu = 0.3$ and L = 13.83

Amplitude	Applied Torque dyne-cm	Beat Rate beats/sec	B R F in %
45°	165.2	49.204	1.543
90°	823.6	49.664	.623
135°	1921.3	49.766	.419
180°	3458.2	49.817	.317
225°	5734.3	49.848	.255

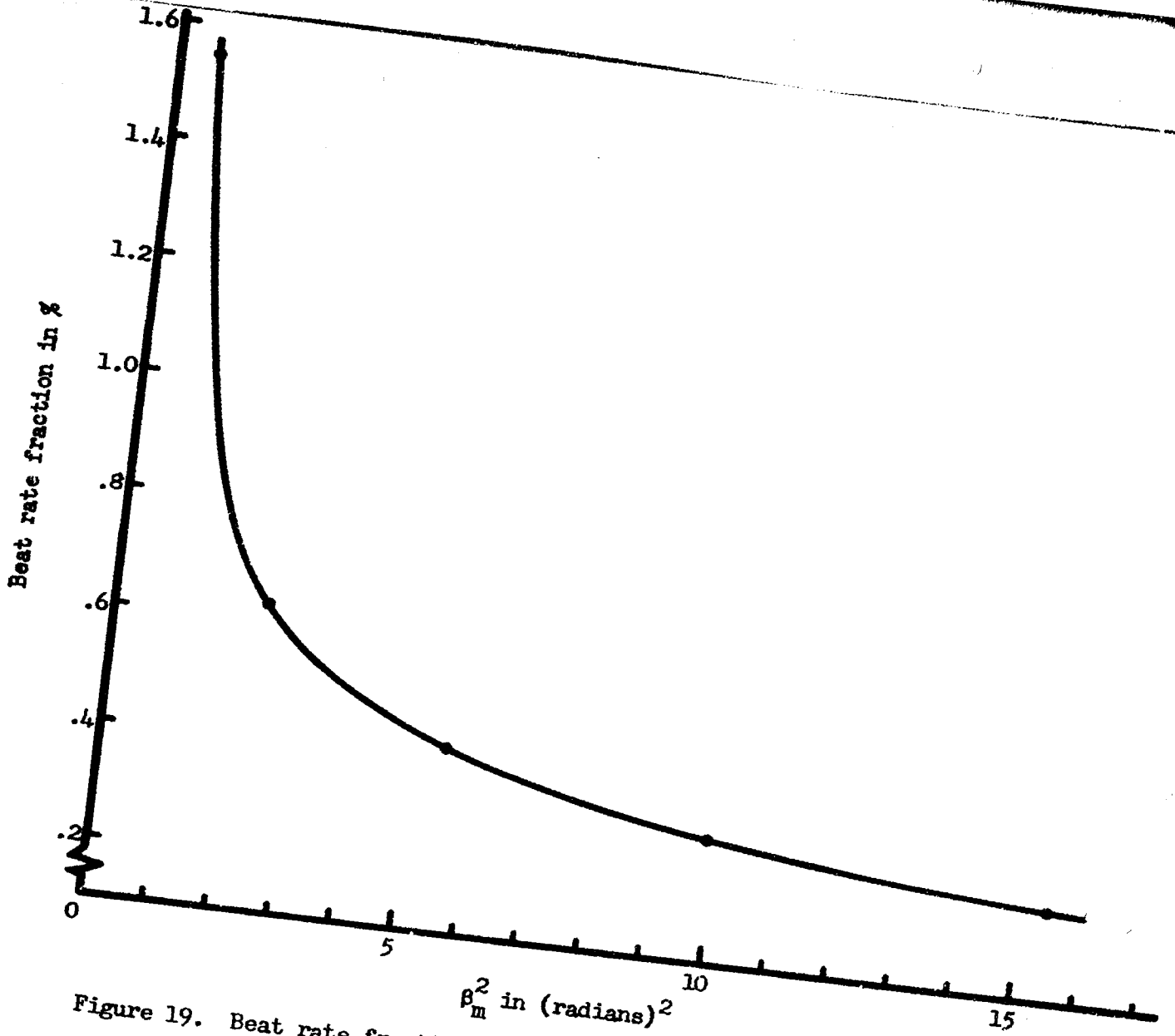

Figure 19. Beat rate fraction as a function of the square of the amplitude. ($\beta_m = \pi$, $\mu = 0.3$, $L = 13.83$)

It is evident from the curve that the model obeys the generally accepted maxim that large balance amplitude promotes good timekeeping.

In Figure 20, beat rate errors predicted by the model are compared with experimental torque sensitivity data taken on three different escapements at HDL. The points on the analytical curve were obtained by using the beat rate for 135° amplitude in the third column of Table 8 as a reference value and comparing the beat rate at the other amplitudes to this reference value. The beat rate error for 45° of amplitude falls off scale and is not shown in the figure. The analytical values of torque in dyne-centimeters at the escape wheel were converted to estimated torques in inch-ounces at the timer main shaft by applying the 159.7 to 1 gear train ratio and assumed 65% gear train efficiency. A comparison of the analytical T5E1 curve with the experimental curves of the higher beat rate timers shows general agreement in shape, but the model will have to be improved in order to obtain better agreement with the 50 bps T5E1 experimental results. Eventually, with improvements in the mathematical model and armed with the results of design parameter investigations, it is expected that an explanation can be found for the increase in rate of the 50 bps experimental curve as the torque decreased from 12 to 5 inch-ounces.

The action of the escapement during the catch-up and impulse phases of the motion is illustrated by Figure 21. Values of the balance displacement during forward impulse were determined from the computer outputs of the step-by-step solutions for various energy loss conditions and amplitudes. These values are shown plotted as a function of the

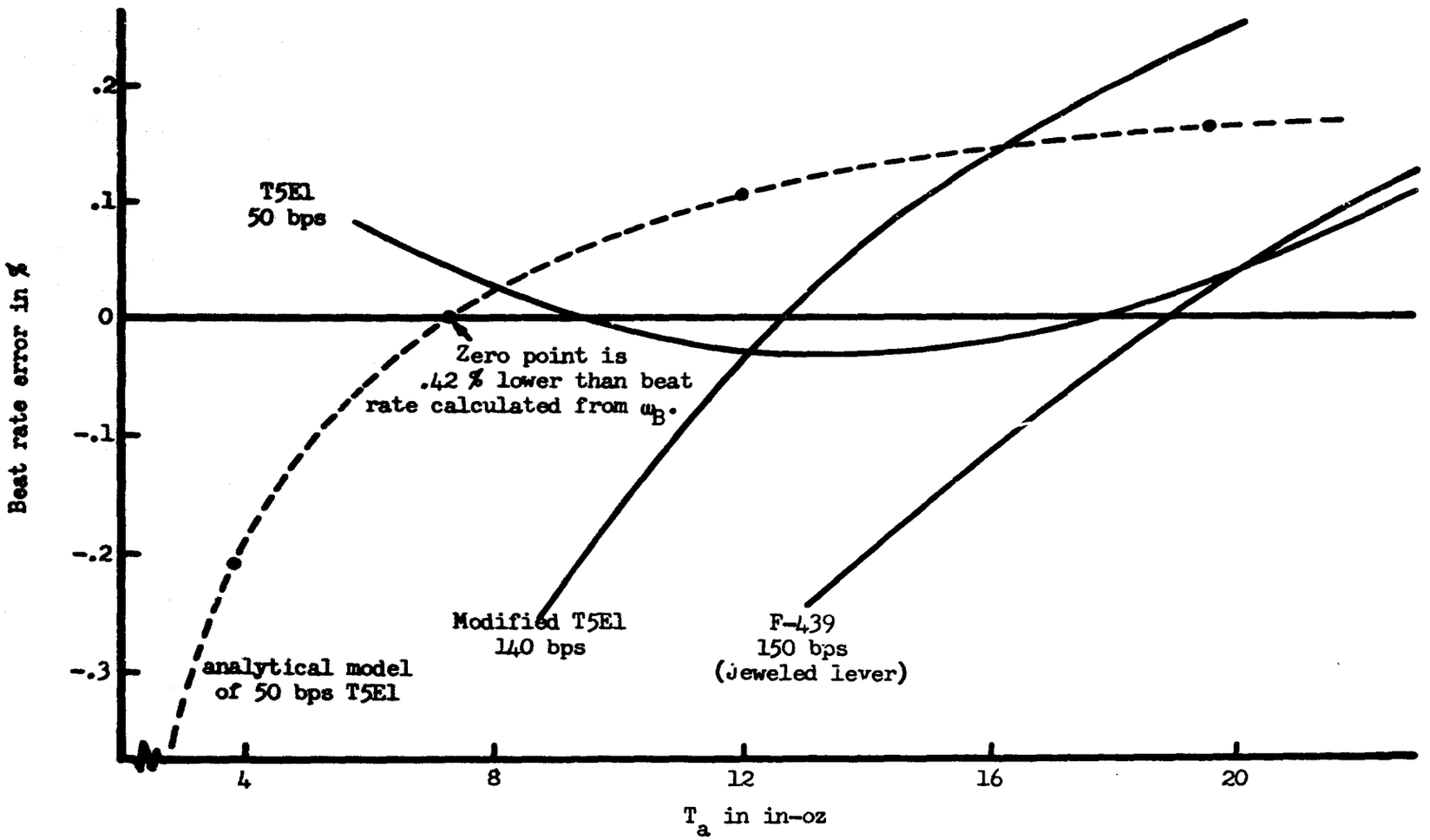

Figure 20. Comparison of analytical and experimental torque sensitivity of the escapement.

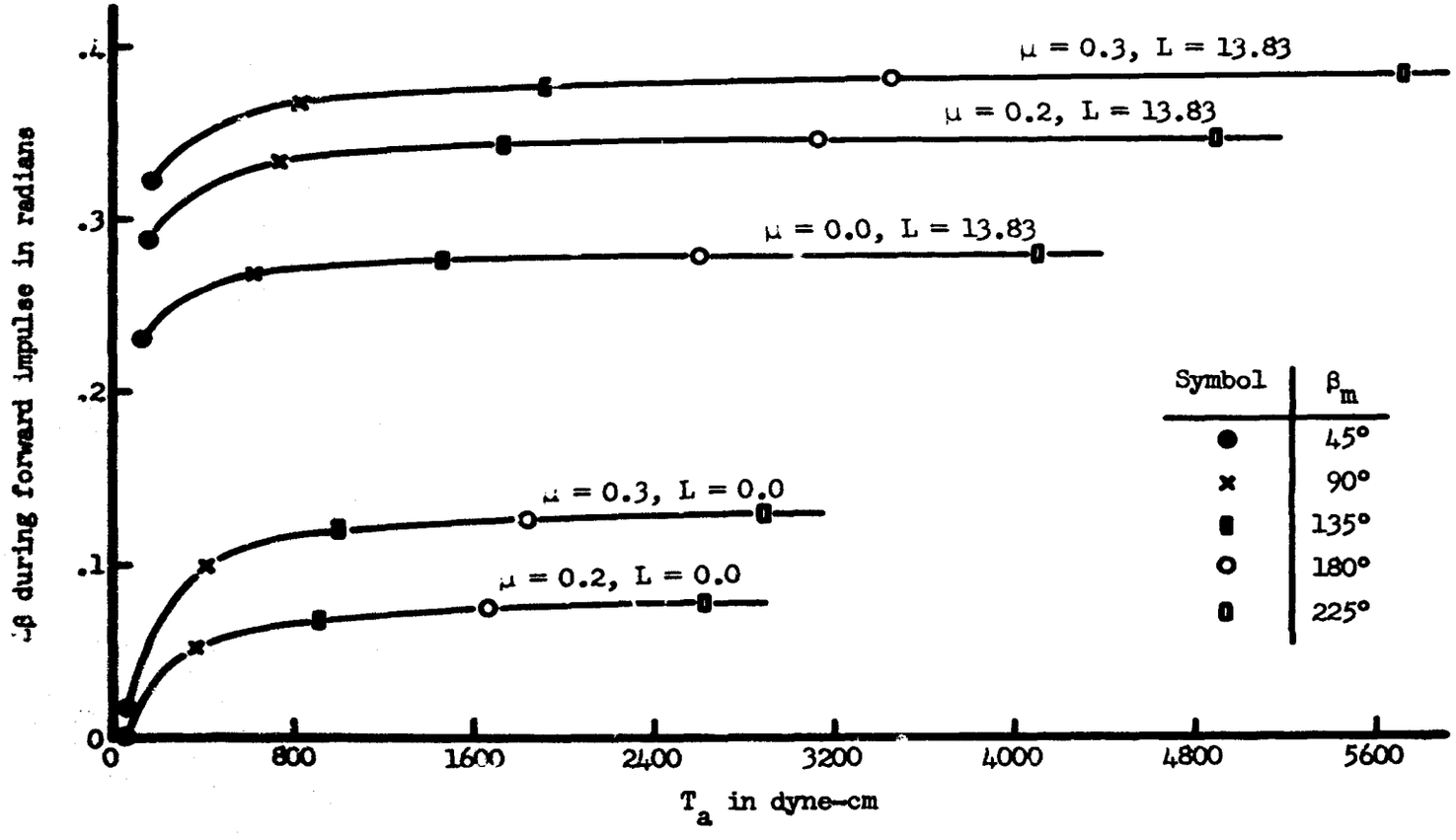

Figure 21. Balance displacement during the forward impulse phase of the motion. (The maximum possible value of $\Delta\beta$ is β_4 which is .726 radians.)

applied torque. The curves show that the impulse is delivered over very small balance displacements except when the energy losses are increased by the side thrust of the balance spring. Note especially that the losses due to side thrust are so large that the input torque required for a given equilibrium amplitude is nearly doubled when side thrust is considered. A curve for the conditions of $\mu = 0$ and $L = 0$ is not shown in this figure because, as mentioned previously, catch-up did not occur in the forward half-cycle in both the energy solution and step-by-step solution.

It is apparent from Figure 21 that the balance displacement during forward impulse ($\Delta\beta$) increases with the applied torque. Or, in other words, the higher the torque, the sooner catch-up occurs. With the inclusion of the hairspring side thrust, impulse is delivered to the balance over only 44 to 53% of the possible interval. This corresponds to using only 39 to 48% of the live impulse face of the escape wheel to deliver the forward impulse. Similar results were obtained during the reverse half-cycle with the exception that catch-up occurred sooner in every case. Consequently, the balance displacement during reverse impulse is larger (by about 6%) than during forward impulse.

Available high speed movies of a detached pin-lever escapement were studied in an effort to verify the behavior during the catch-up and impulse phases as predicted by the model. Some of these films, taken at about 7000 frames per second, were made of a 200 bps escapement whose equilibrium amplitude was about 90°. Observations made as a result of the study of eight films were:

1. The catch-up angle varied with the applied torque. As the

applied torque decreased, the balance displacement during impulse decreased (catch-up angle increased).

2. The entrance pallet pin was struck by the escape wheel 35-65% up the live impulse face of the escape wheel tooth; in most cases this was closer to 50-60%. Therefore, forward impulse was delivered to the balance over 40-50% of the live impulse face for most cases.
3. The exit pallet pin always caught up sooner than the entrance pallet pin, usually 15-40% up the live impulse face.

Each of the observations made is qualitatively consistent with the predictions of the model escapement. Of course, the stiffer hairspring required for a 200 bps escapement should cause larger side thrust effects. However, no observations were made which were in disagreement with the behavior predicted by the model.

Three films of the 50 bps T5E1 timing movement, taken at 4000 frames per second, were also studied. In these films, the catch-up phase was not discernible. It appeared as if the escape wheel tooth and pallet pin remained in contact at all times or, at best, catch-up occurred within the first few percent of the length of the live impulse face. Thus, these movies of the 50 bps movement indicate that additional energy loss mechanisms will have to be included in the mathematical model in order to obtain closer agreement between theory and experiment.

These high speed films were also studied to determine whether significant bouncing occurs during the impacts between the basic components of the escapement. Observations of the impacts of the pallet pins

showed either no noticeable bouncing or, in the case of the 200 bps movement, the possibility that all the energy was delivered to the balance upon impact with one big bounce occuring so as to exclude any further impulse. The nature of the films made it impossible to exclude this possibility. There was some evidence of slight bouncing during the impact of the impulse pin upon the lever fork. This possibility is disregarded here since the present model assumes inelastic collisions and does not contain the geometric details of the lever fork. Shinkle, in a similar study of the cylinder escapement[2], has found the time-keeping and amplitude properties of this escapement to be insensitive to bouncing. In the absence of firmer evidence to the contrary, this viewpoint has been adopted in the present work.

Data obtained from the computer output of the step-by-step solution can be used to calculate the magnitudes of the various energy losses and gains to determine their relative importance in the operation of the model escapement. A typical "energy balance" is shown in Table 9 for both the equivalent escapement and total system. Quantities listed in this table were calculated by substituting values of catch-up angles, angular speeds, etc., from appendix E into the relationships derived for the various energy loss and gain mechanisms in section 7 of this report. Thus Table 9 displays the energy balance for the conditions $\beta_m = \pi$, and $\mu = 0.3$, $L = 13.83$. All energies are in ergs.

TABLE 9

ENERGY BALANCE FOR THE CONDITIONS $\beta_m = \pi$, $\mu = 0.3$, and $L = 13.83$

EQUIV. ESCAPEMENT ENERGY BALANCE		TOTAL SYSTEM ENERGY BALANCE	
TOTAL ENERGY	4549.4	TOTAL ENERGY	4549.4
ENERGY GAINS		ENERGY GAINS	
Forward Catch-up Collision	160.6	Forward Input	723.3
Forward Impulse	187.6	Reverse Input	723.3
Reverse Catch-up Collision	119.4		
Reverse Impulse	166.5		
TOTAL GAINS	634.1	TOTAL GAINS	1446.6
ENERGY LOSSES		ENERGY LOSSES	
Forward Side Thrust	136.9	Forward Side Thrust	136.9
Forward Unlock Collision	34.0	Forward Unlock Collision	34.0
Forward Unlock Friction	94.2	Forward Unlock Friction	94.2
Forward Lever & Escape Wheel Dissipation	54.6	Forward Catch-up Collision	73.3
		Forward Lever & Escape Wheel Dissipation	345.9
Reverse Side Thrust	136.9	Reverse Side Thrust	136.9
Reverse Unlock Collision	34.2	Reverse Unlock Collision	34.2
Reverse Unlock Friction	94.2	Reverse Unlock Friction	94.2
Reverse Lever & Escape Wheel Dissipation	45.4	Reverse Catch-up Collision	57.3
		Reverse Lever & Escape Wheel Dissipation	439.7
TOTAL LOSSES	630.4	TOTAL LOSSES	1446.6

The small imbalance between total losses and gains occure because of the slight discrepancies between the energy analysis, by which the equilibrium torque is obtained, and the step-by-step method in which this value or torque is subsequently used. The small magnitude of the imbalance provides further proof of the validity of the step-by-step method of solution of the differential equations of motion.

Similar energy balance data were obtained for each of the other amplitudes studied using the same energy loss parameters; i.e., $\mu = 0.3$, and $L = 13.83$. These results are presented for the equivalent escapement in Figure 22. Numbers across the top of the figure represent the stored energy in the hairspring at the beginning of each cycle while those numbers along the top of the bars represent the total energy exchange per cycle. Note that the relative energy exchange per cycle increases from almost 10% to 14% as the amplitude increases. It is evident from the figure that side thrust losses are of significant magnitude; in fact, side thrust represents the dominant loss mechanism for the equivalent escapement. As discussed earlier in section 7, catch-up collisions result in a gain in energy by the equivalent escapement. Note the importance of these collisions as an energy gain mechanism by comparing with energy gains through impulse.

Figure 23 similarly displays the energy balance for the total system. Note that catch-up collisions are a loss mechanism for the total system. Dissipation by the escape wheel and lever upon relocking now accounts for over half the total losses. Side thrust losses are still dominant over the other loss mechanisms, however, usually accounting for about 20% of the total losses. The relative energy exchange per cycle gradually increases from about 24% to 32% as the amplitude increases.

Magnitudes of the energy losses through the various mechanisms considered are plotted for the total system in Figure 24 as a function of the total energy. Each of these losses and, as a result, their sum, apparently increase linearly with the total energy or, equivalently, with the square of the balance amplitude. Once again, however, it was

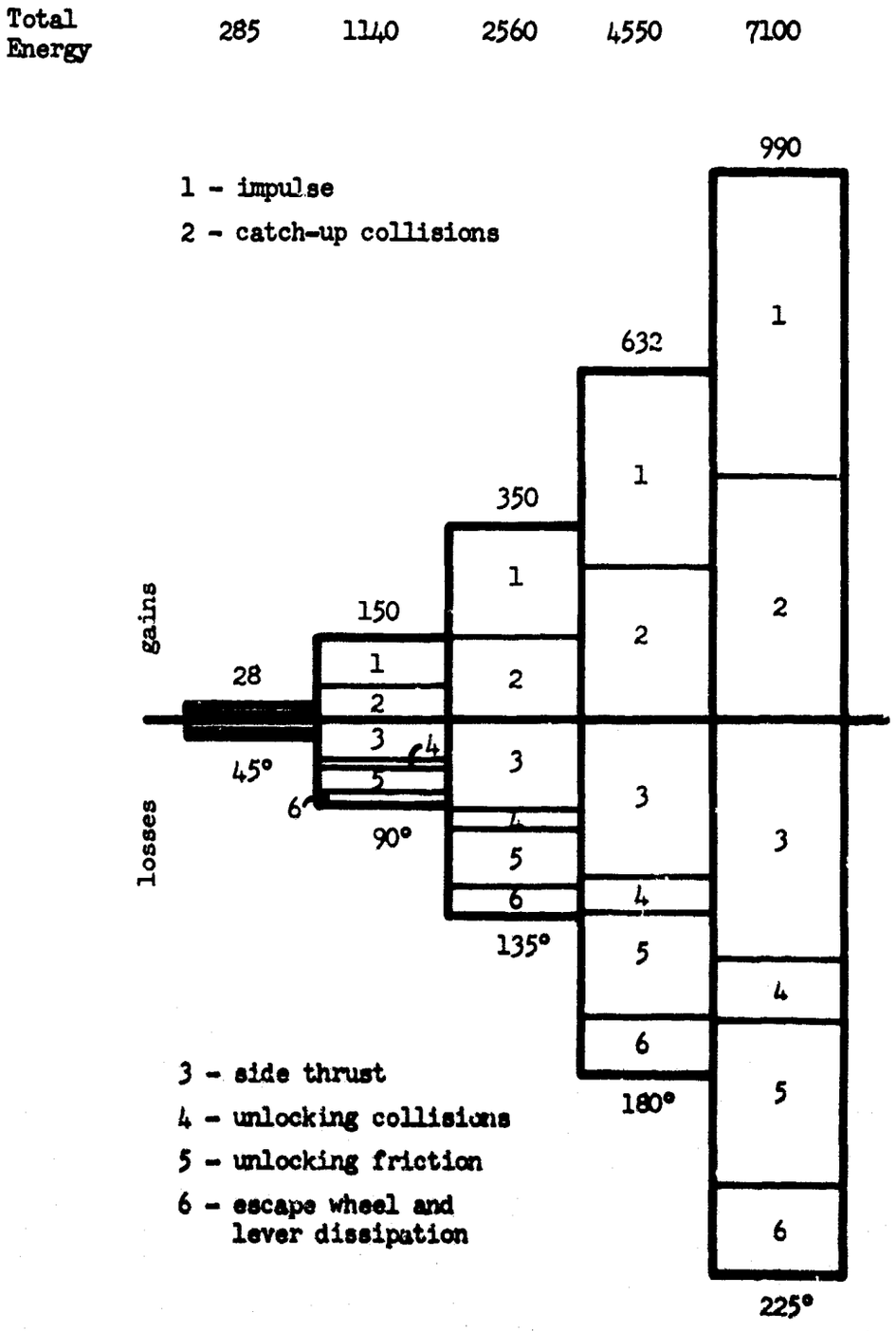

Figure 22. Energy balance for the equivalent escapement using energy loss parameters of $\mu = 0.3$ and $L = 13.83$.

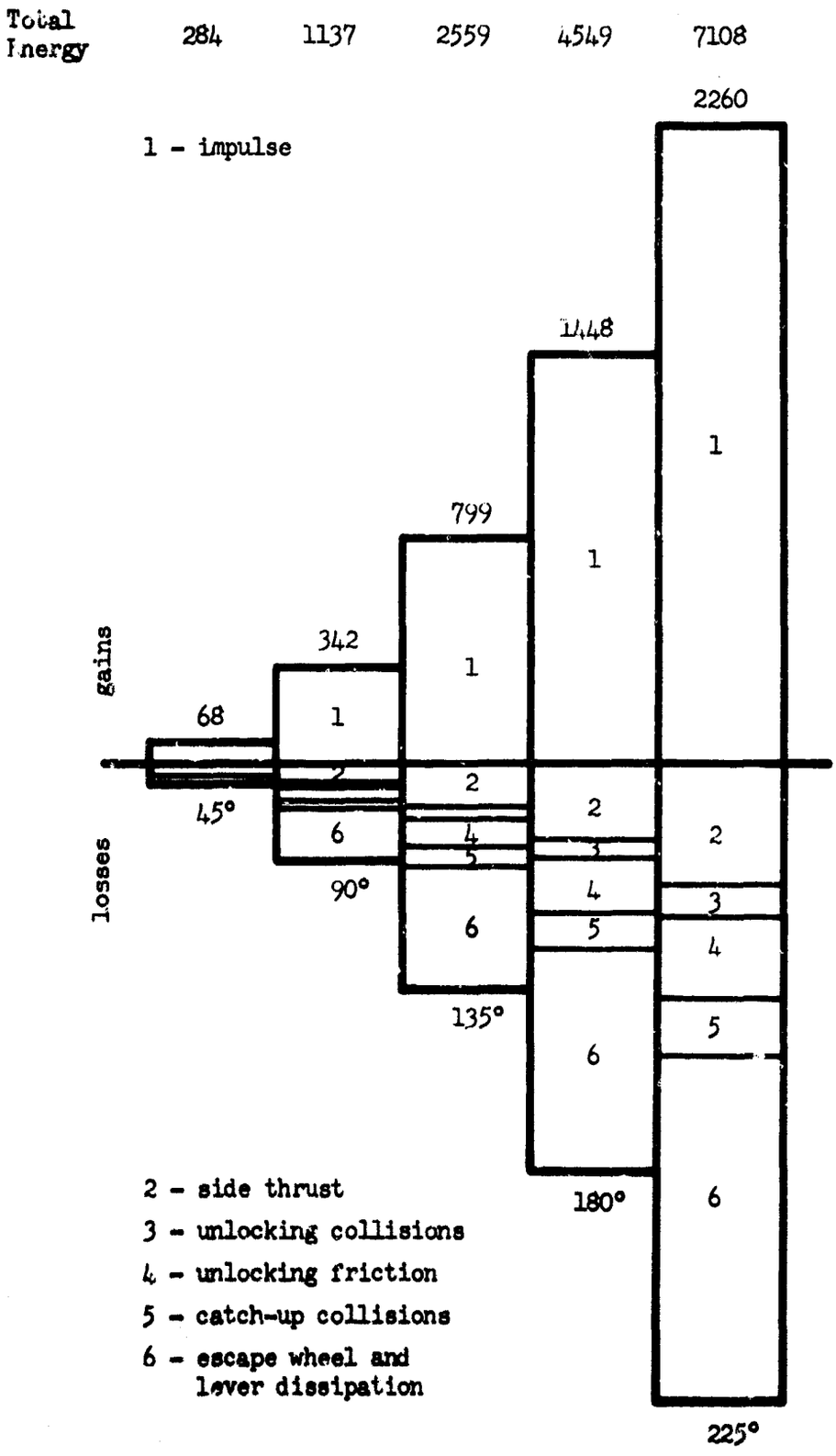

Figure 23. Energy balance for the total system using energy loss parameters of $\mu = 0.3$ and $L = 13.83$.

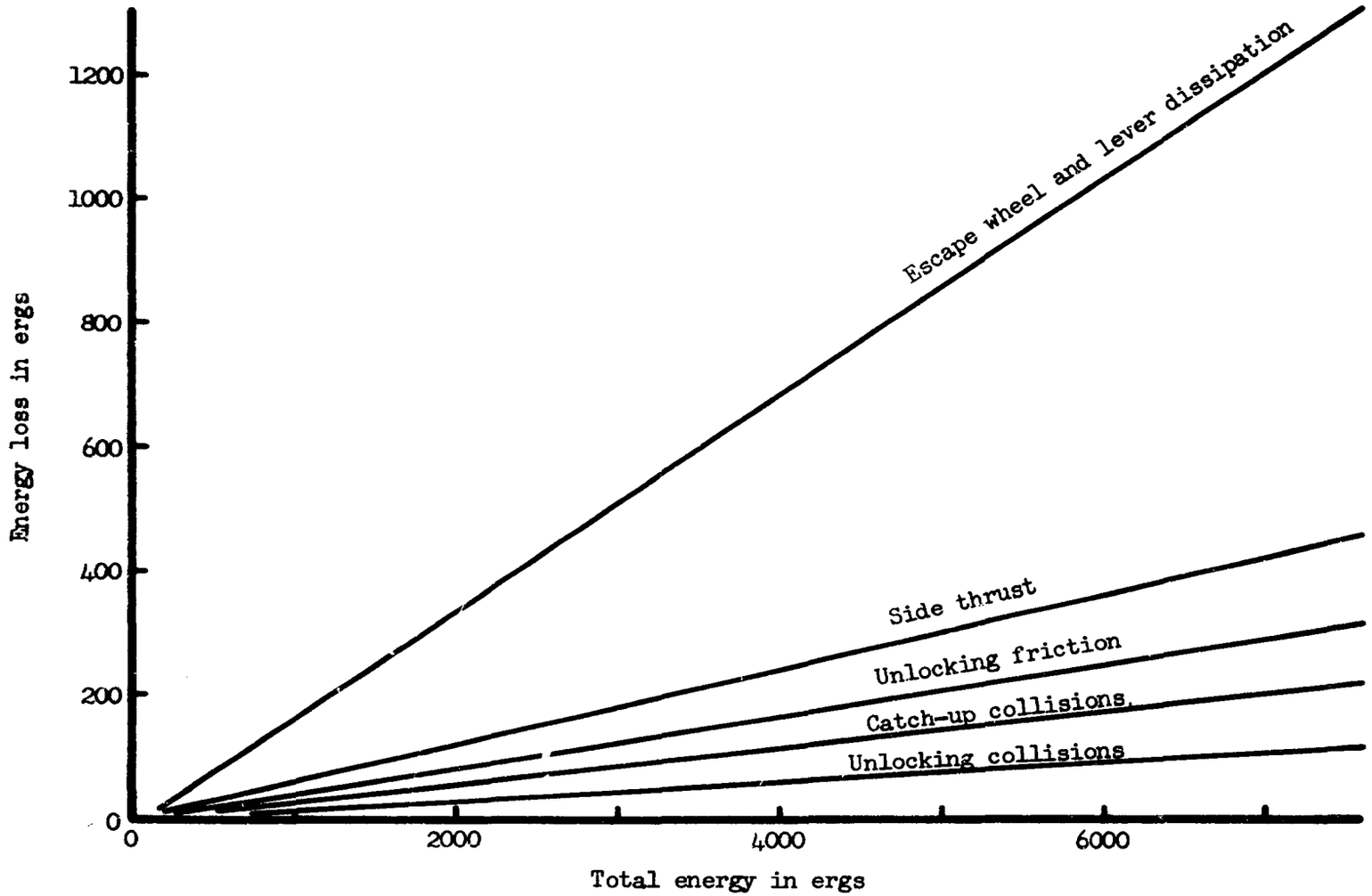

Figure 24. Total system energy losses as a function of the total energy. ($\mu = 0.3$, $L = 13.83$)

found through attempts at a numerical fit of the data that the relationship is not exactly linear. The apparent linearity is easily explained by reference to equations (7.35), (7.37), (7.40), (7.60), and (7.62) which are the relationships used to calculate each of the losses. These relationships include numerous constants and either β_m or β_6 or T_a or combinations thereof. But it has already been demonstrated that T_a is nearly linearly related to β_m^2. With the added fact that β_6 is usually just a few tenths of a percent greater than $-\beta_m$, it follows directly from these equations that each of the losses are almost linear functions of the total energy or β_m^2.

The total energy of the escapement will vary as the escapement proceeds through a cycle because of the various energy losses. Data taken from appendix E have been used to compute the total energy of the equivalent escapement at various points throughout the cycle for $\beta_m = \pi$, $\mu = 0.3$, and $L = 13.83$. These computations show that the maximum variation of the total energy from the initial value, E_o, is only about 4.3% of E_o and occurs just prior to the forward catch-up collision. Hence, in order to vividly illustrate this variation of the total energy, the quantity $\frac{E}{E_o} - 0.95$ has been plotted as a function of β in Figure 25 where E represents the total energy when the balance displacement is β. Instantaneous energy changes (radial lines) occur in this figure for each of the collisions because of the assumption of instantaneous collisions and because of energy dissipations by the escape wheel and lever upon relocking. Other than these instantaneous changes, the most rapid variation of the total energy occurs during the impulse phase of the motion as expected.

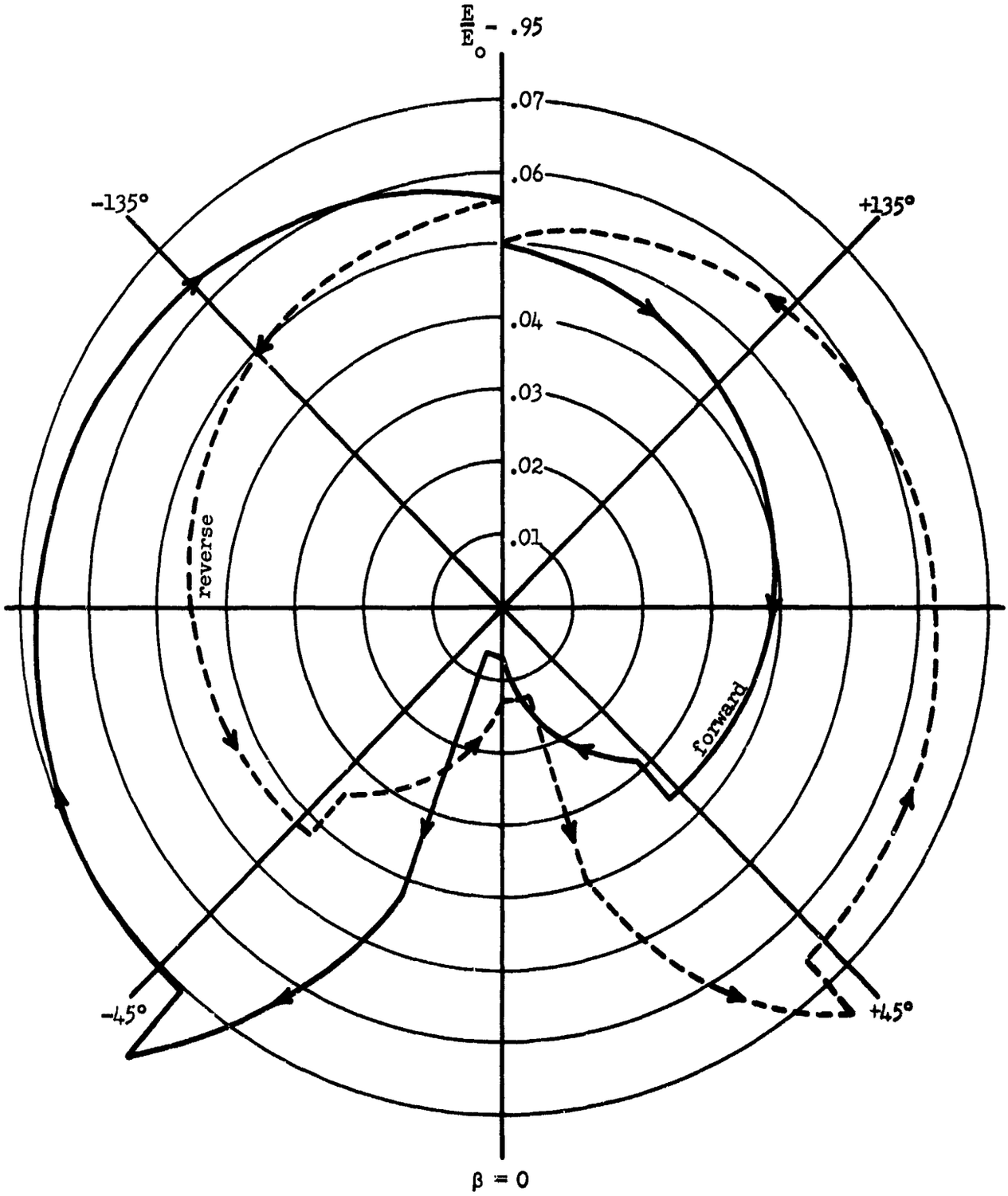

Figure 25. Energy variation of the equivalent escapement as a function of balance displacement. ($\beta_m = \pi$, $\mu = 0.3$, $L = 13.83$)

9. CONCLUSIONS AND RECOMMENDATIONS

The following conclusions can be drawn as a result of the analysis conducted to date.

1. A mathematical model of the detached lever escapement has been devised. The model has been analyzed both energetically and by approximate solution of the equations of motion. Excellent agreement between these two methods of approach justify confidence in the validity of the techniques employed.
2. Predictions made using the model have been compared with experimental data from an actual mechanism. The correlation between the analytical and experimental results of the equilibrium amplitude as a function of applied torque shows the model to be essentially valid in this respect. At least qualitative agreement has been found between the behavior of the model during catch-up and impulse and observations of high speed films of an actual escapement. Initial prediction of the torque sensitivity characteristic did not show close agreement with its experimental results so further modification of the model is indicated. However, no basic difficulties are envisioned because qualitative agreement was obtained when the model was compared to higher beat rate detached lever escapements.
3. The relative importance of the energy gain and loss mechanisms considered has been established. Although energy dissipation by the escape wheel and lever is predominant, hairspring radial side thrust effects have been shown to play a major role.

4. The catch-up portion of the cycle which occurs between unlocking and the beginning of impulse plays a decisive role in the properties of the mechanism. The requirement of a finite time to achieve coupling of the escape wheel to the lever and balance reduces the length of the live face of the escape wheel over which impulse is delivered to the balance. This reduction is very sensitive to the number and type of loss mechanisms considered.
5. The basic properties of the model are, at least to first order, amplitude dependent. Indeed, the input torque and each of the loss mechanisms have been shown to be <u>almost</u> linear functions of the square of the amplitude.

As a result of the analysis covered by this report, the following recommendations are presented:

1. Further modification of the basic model should be undertaken. Some features of the escapement which are not included in the present model but which are felt to be important are:
   a. The provision for unlocking to end before zero balance displacement.
   b. The addition of a draw angle on the escape wheel teeth.
   c. The addition of a variable geometry on the lever fork.
   d. The provision for frictional losses during impulse.
   e. The provision for elastic collisions during unlocking and impulse.

   By incorporating some or all of the features into the model, it should be possible to determine which produce significant changes in the properties of the escapement.

2. Computer studies of the present model as a function of the various parameters of the mechanism should be carried out. Analysis has shown the present model to be reasonable and it is felt that such studies could be profitably undertaken now. As stated in the introduction, it is suspected that an escapement's geometry, that is, the sizes, shapes, and inertias of its parts, govern the shape of its torque sensitivity curve. Shinkle has, in fact, shown[6] that the cylinder escapement can be altered to display any degree of torque sensitivity by changing the pallet geometry. Computer studies of the present model should show if an alteration of geometry would lead to a similar result for the detached lever escapement.
3. Further effort should be expended toward obtaining an analytical solution of the equations of motion. Although the approximate solutions that have been obtained have yielded considerable insight, they are no substitute for the analytical solutions. The phase-plane diagram showed small departures of the escapement from the behavior of an idealized, undamped harmonic oscillator. This fact indicates that the use of perturbation techniques of analysis might be a promising approach and worthy of investigation.

Eventhough the mathematical model established by the analysis was based on the T5E1 pin lever escapement design, the result is applicable to detached lever escapements in general. Any particular design can be

analyzed by using known values of the physical parameters and slightly revising some of the geometric equations describing the linkage ratios between the components.

For example, the Army's new XM577 mechanical time fuze uses a high beat rate detached pin lever escapement to gain increased accuracy over the older cylinder-type escapement designs. Because this fuse is used with spinning (up to 30,000 RPM) artillery projectiles, the friction torques seen by the timing movement will vary widely as the spin speed decays and as the fuze is used with different weapons having different spin rates. Other force perturbances result from yawing of the projectile in flight, changes in the coefficient of friction, and variations in tolerances of the mainspring, gears, plates, and other piece parts. These variations in escapement driving force must span a wide range, especially when thousands of fuzes are considered.

By clever design (and often at extra cost) many of the disturbing influences can be either reduced to negligible levels or compensated out. For instance, spin sensitive driving elements can be used to increase the torque at higher spins where the reaction friction torque is the greatest. Better lubricants can reduce friction and closer tolerances will result in more uniformity from unit to unit. However, variations in escapement driving force can never be completely eliminated. Therefore, it is highly desirable to make the escapement rate as insensitive to driving force variations (reduce its torque sensitivity) as possible so the highest accuracy can be achieved at the least cost in expensive design refinements.

The XM577 Escapement mainly differs from the T5E1 design in that 1) it employs a torsion-wire hairspring in place of the spiral type hairspring and, 2) it uses the "folded-lever" principle to achieve a "two-center" (escape wheel and balance on the same axis) configuration. Use of the torsion wire hairspring would make the balance side thrust forces negligible and this can be handled simply by setting the value of L equal to zero in the mathematical model. The folded lever can be included through minor changes in the geometric equations defining the linkage ratios X and Z. Thus the mathematical model developed under this contract should prove to be a valuable design aid for the Army's newest time fuzes.

APPENDIX A. HAIR SPRING SIDE THRUST

A freely oscillating spring-mass system subjected to a constant Coulomb friction drag has an amplitude that decays linearly with the number of oscillations. But experimental decay curves deviate from linearity. This deviation has, in the past, been ascribed to various effects, e.g., windage. Shinkle[7], however, has suggested that the source of the nonlinearity is the reaction at the balance pivots due to the side thrust of the hairspring.

Whenever the balance is displaced from its equilibrium position, the spiral-wound hairspring is distorted in such a way that, in addition to the restoring couple, a radial thrusting of the balance staff against the pivots occurs. Although the manner in which the side thrust depends upon amplitude is not presently known, it seems reasonable to assume that its magnitude is directly proportional to balance displacement. With this assumption the equation of motion of the freely swinging balance wheel becomes

$$I_b\ddot{\beta} = -K\beta \pm L\beta \qquad (A.1)$$

where the positive sign on the last term applies in the first and third quarter-cycles and the minus sign in the second and fourth. This difference in signs comes about because the side thrust torque always acts to oppose the motion of the balance. For this reason the side thrust torque maintains the same sense of direction as the balance passes through the equilibrium position while the sense of the hairspring restoring torque is reversed since it is always directed toward the equilibrium position.

Using the final conditions in the first quarter-cycle as the initial conditions in the second, etc., the motion of the damped balance is described by the following set of equations.

1st quarter-cycle

$$\beta = \beta_m \cos \omega t \quad ; \quad \omega^2 = \frac{K-L}{I_\theta} \tag{A.2}$$

$$\dot{\beta} = -\omega \beta_m \sin \omega t \tag{A.3}$$

2nd quarter-cycle

$$\beta = -\beta_m \sqrt{\frac{K-L}{K+L}} \sin \omega t \quad ; \quad \omega^2 = \frac{K+L}{I_\theta} \tag{A.4}$$

$$\dot{\beta} = -\beta_m \sqrt{\frac{K-L}{I_\theta}} \cos \omega t \tag{A.5}$$

3rd quarter-cycle

$$\beta = -\beta_m \sqrt{\frac{K-L}{K+L}} \cos \omega t \quad ; \quad \omega^2 = \frac{K-L}{I_\theta} \tag{A.6}$$

$$\dot{\beta} = \frac{\beta_m (K-L)}{\sqrt{I_\theta (K+L)}} \sin \omega t \tag{A.7}$$

4th quarter-cycle

$$\beta = \beta_m \left(\frac{K-L}{K+L}\right) \sin \omega t \quad ; \quad \omega^2 = \frac{K+L}{I_\theta} \tag{A.8}$$

$$\dot{\beta} = \frac{\beta_m (K-L)}{\sqrt{I_\theta (K+L)}} \cos \omega t \tag{A.9}$$

Time, t, has been reset to zero at the beginning of each quarter-cycle to simplify the application of initial conditions.

It follows from the last set of solutions that the amplitude of the nth damped oscillation, β_n, would be

$$\beta_n = \left(\frac{K-L}{K+L}\right)^n \beta_m \tag{A.10}$$

This expression was fitted to experimental data taken on a sample T5E1 escapement and a value of 13.83 dyne-centimeters per radian was obtained for L (K = 921.9 dyne-centimeters per radian). Values of β_n calculated with this L are shown as circles in Figure 26. Their close correlation with the experimental curve is evidence that side thrust effects play a major role in damping of the balance. Even closer correlation should be obtained by including a constant value of coulomb damping in addition to that induced by the side thrust. Constant damping is not included in this study because the damping force is independent of amplitude (or applied torque) and therefore should not influence the escapement's torque sensitivity to any significant degree.

Since the amplitude of oscillation decreases by the factor (K-L)/(K+L) in each cycle, the fractional change of energy per cycle for the freely oscillating balance assembly is

$$\frac{\Delta E}{E} = -\frac{4KL}{(K+L)^2} \qquad (A.11)$$

This equation predicts a 5.8% loss of energy per cycle for the T5E1 escapement model. Based on this result it can be concluded that side thrust effects represent one of the major loss mechanisms for this escapement. For escapements employing a torsion wire in place of the spiral type hairspring, the energy lost through balance pivot friction is expected to be a much smaller fraction of the total energy.

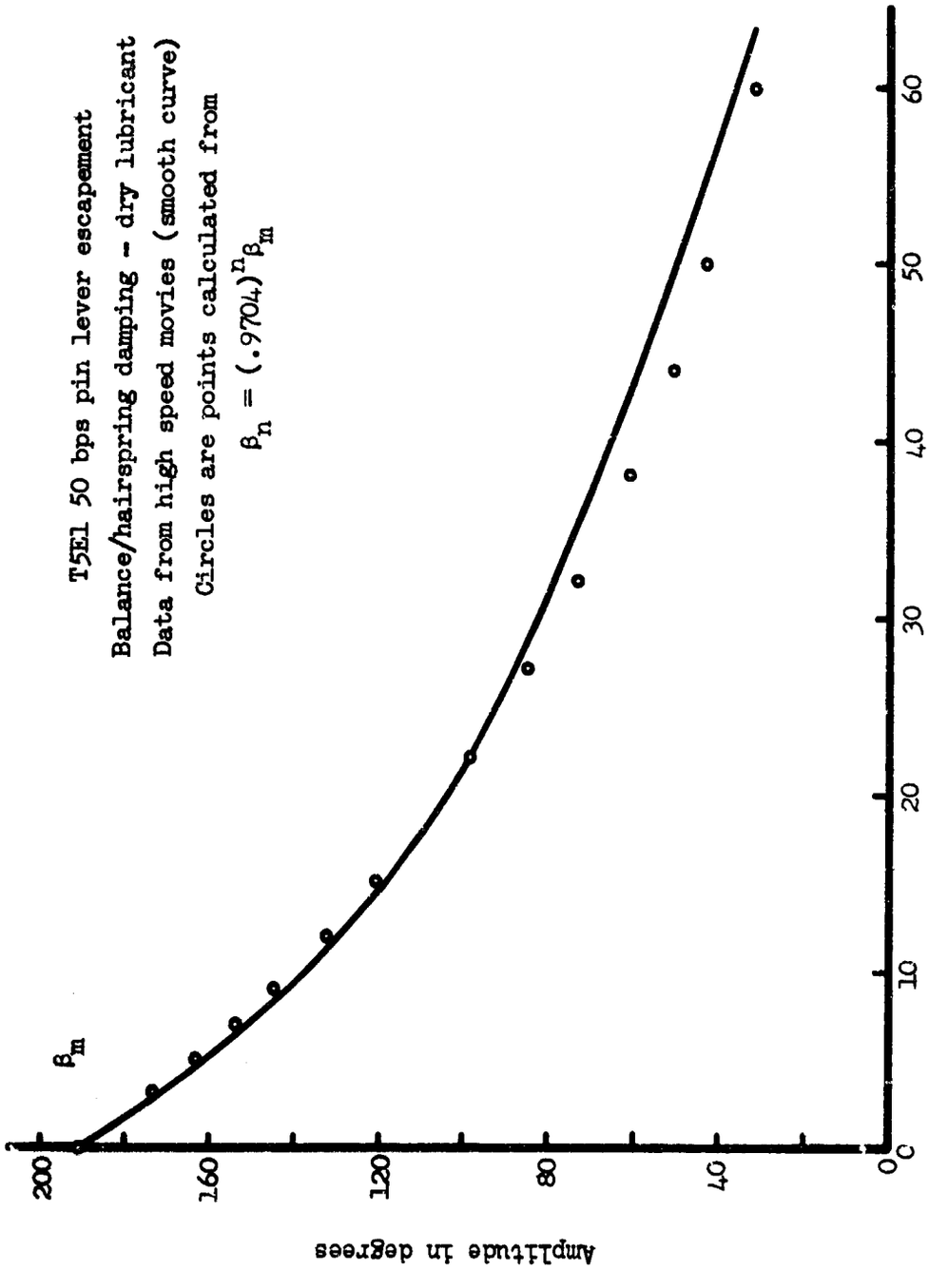

Figure 26. Amplitude decay for the T5E1 balance/hairspring system.

APPENDIX B: LEVER ARM GEOMETRY

Lever arms and their ratios appear in the equations of motion and the energy analysis for each of the coupled phases of the motion. This appendix is devoted to the derivation of analytic expressions for each of these quantities.

An intermediate position of the three coupled components during the forward impulse period is shown in Figure 27.

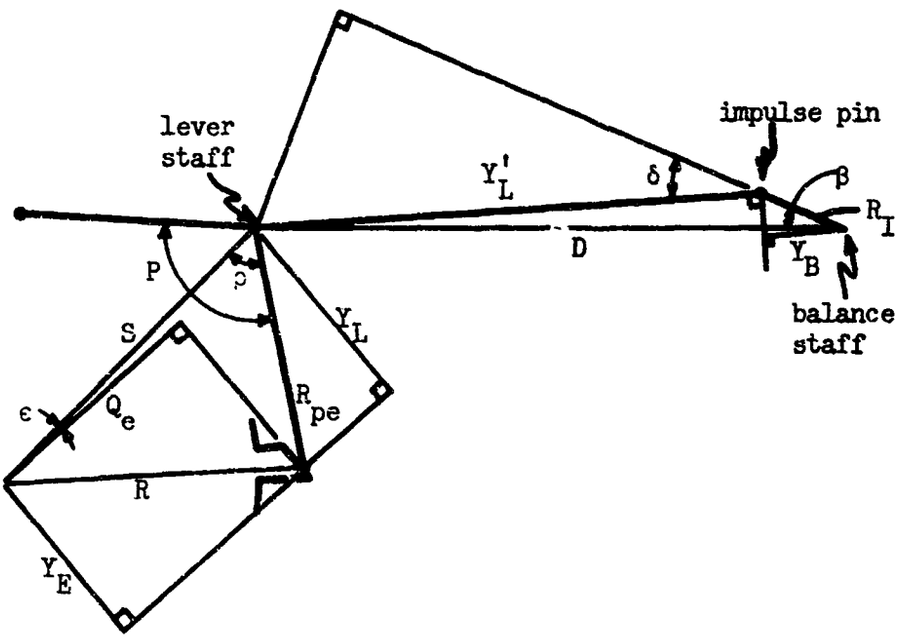

Figure 27. Interaction between the balance, lever, and escape wheel during the forward impulse phase of the motion.

It follows from this figure that

$$Y_B = R_I \cos\delta \qquad (B.1)$$

But $$\cos\delta = \frac{D\cos\beta - R_I}{Y_L'} \tag{B.2}$$

So $$Y_B = \frac{R_I}{Y_L'}(D\cos\beta - R_I) \tag{B.3}$$

By the law of cosines

$$Y_L' = \sqrt{D^2 + R_I^2 - 2DR_I\cos\beta} \tag{B.4}$$

Thus $$X = \frac{Y_B}{Y_L'} = \frac{R_I(D\cos\beta - R_I)}{D^2 + R_I^2 - 2DR_I\cos\beta} \tag{B.5}$$

or $$X = X(\beta) = \frac{\cos\beta - \frac{D}{R_I}}{\frac{D}{R_I} + \frac{R_I}{D} - 2\cos\beta} = -\frac{d\rho}{d\beta} \tag{B.6}$$

Because of the symmetric nature of the coupling between the balance and lever, this expression for $X(\beta)$ will apply during all of the coupled stages in both halves of the cycle. $X(\beta)$ for the T5E1 escapement is plotted in Figure 29.

The lever arms for the escape wheel-lever coupling are

$$Y_E = \sqrt{R^2 - Q_E^2} \tag{B.7}$$

where $$R^2 = R_{pe}^2 + S^2 - 2R_{pe}S\cos\rho \tag{B.8}$$

and $$Y_L = \sqrt{R_{pe}^2 - (S\cos\epsilon - Q_E)^2} \tag{B.9}$$

Also $$Y_L = Y_E + S\sin\epsilon \tag{B.10}$$

Therefore $$Z_f = \frac{Y_L}{Y_E} = 1 + \frac{S}{Y_E}\sin\epsilon = -\frac{d\epsilon}{d\rho} \qquad \text{(B.11)}$$

This equation together with the constraint equations, $\beta(\rho)$ and $\epsilon(\rho)$ (equations (4.1) and (4.5)), define $Z_f(\beta)$ during the forward impulse period.

The requirement that the escape wheel rotate in the same sense in each half-cycle imposes a restriction on the escape wheel tooth design - it must be asymmetric. This fact results in a different functional form for Y_L in each half-cycle which, in turn, causes the escapement to run asymmetrically. Typical geometry for the escape wheel and lever during reverse impulse is shown in Figure 28.

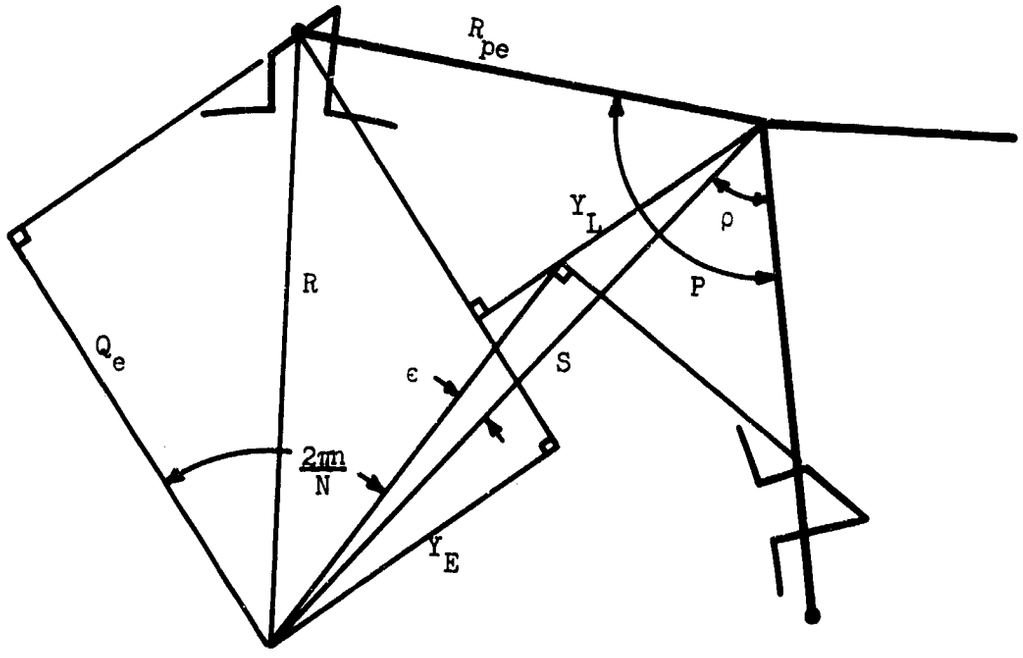

Figure 28. Interaction between the escape wheel and lever during the reverse impulse phase of the motion.

Again $$Y_E = \sqrt{R^2 - Q_E^2}$$

where $$R^2 = R_{pE}^2 + S^2 - 2R_{pE}S\cos(P-\rho) \qquad \text{(B.12)}$$

So Y_E has the same form during both halves of the cycle because $P-\rho$ varies during the reverse half-cycle in the same manner as ρ does in the forward half-cycle.

It also follows from the figure that

$$Y_E + Y_L = S\sin\left(\frac{2\pi n}{N} - \epsilon\right) \qquad \text{(B.13)}$$

Then $$Z_r = \frac{Y_L}{Y_E} = \frac{S}{Y_E}\sin\left(\frac{2\pi n}{N} - \epsilon\right) - 1 = \frac{d\epsilon}{d\rho} \qquad \text{(B.14)}$$

Using $\beta(\rho)$ and $\epsilon(\rho)$ for the reverse motion (equations (4.1) and (4.10)), $Z_r(\beta)$ for the reverse half-cycle may be determined.

$Z(\beta)$ and the product $XZ(\beta)$ for the T5E1 escapement are plotted in Figures 29 and 30. Note the significant difference in the forward and reverse values of Z (and consequently XZ) which is responsible for the assymetric ($\beta_m \neq -\beta_6$) motion of the escapement.

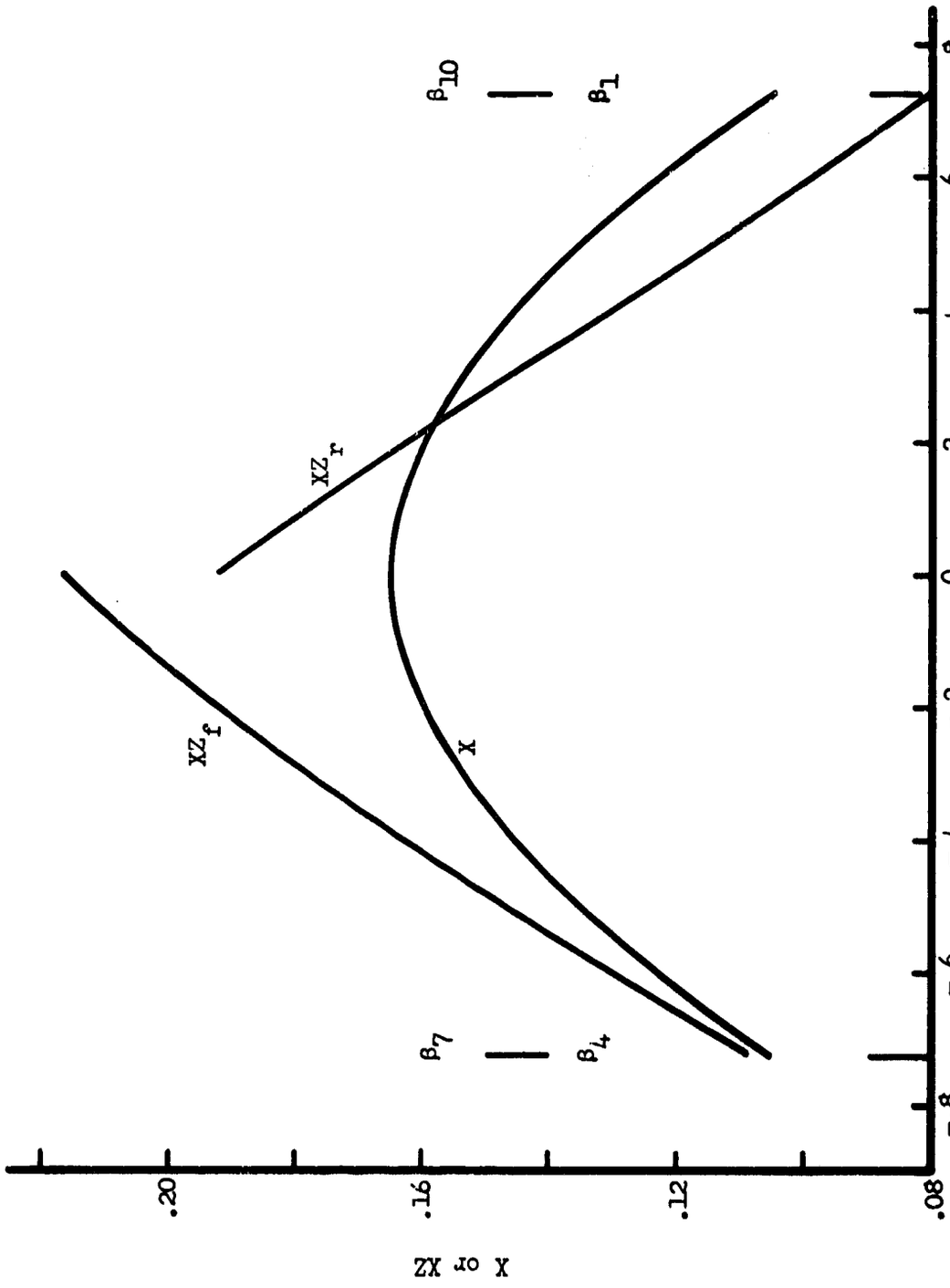

Figure 29. Lever arm ratios for the T5E1, forward and reverse half-cycles.

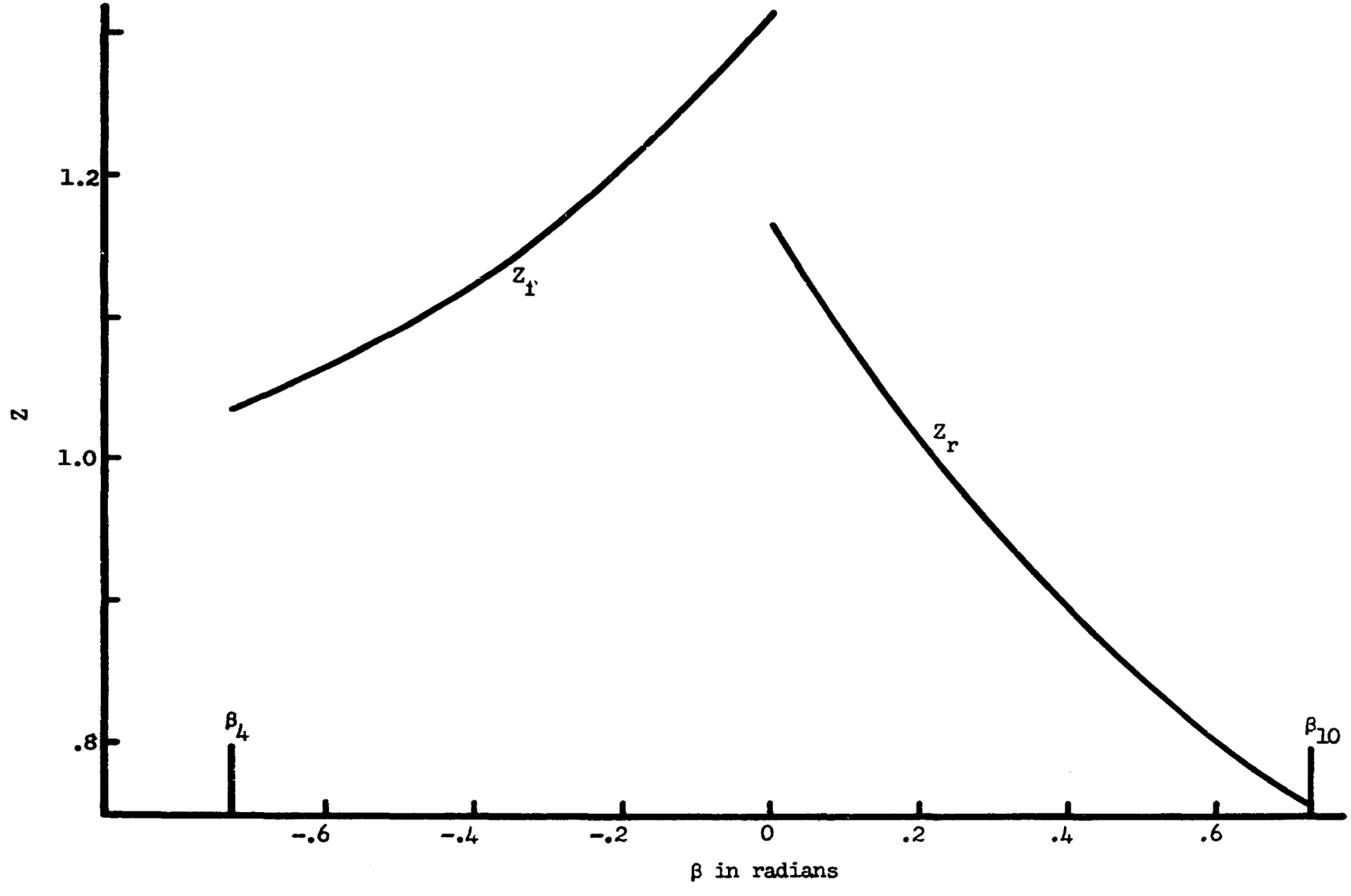

Figure 30. Lever arm ratio for the T5E1, forward and reverse half-cycles.

APPENDIX C: FRICTIONAL EFFECTS DURING UNLOCKING

During the unlocking portion of the phase 2 motion, the entrance pallet pin slides across the locking face of an escape wheel tooth. Because of the applied torque, there is a rather large normal reaction between the pin and the locking face. This leads to an appreciable frictional drag which is transmitted through the lever to the balance hairspring system.

As shown in Figure 31, the torque on the pallet lever due to the frictional drag is

$$T_{Lf} = Y_f f \tag{C.1}$$

From the figure

$$Y_f = S \sin\alpha = \frac{S R_{pe} \sin\rho}{R} \tag{C.2}$$

$$R^2 = R_{pe}^2 + S^2 - 2 R_{pe} S \cos\rho \tag{C.3}$$

Now $$T_e = R F_n \tag{C.4}$$

so that $$f = \mu F_n = \frac{\mu T_e}{R} . \tag{C.5}$$

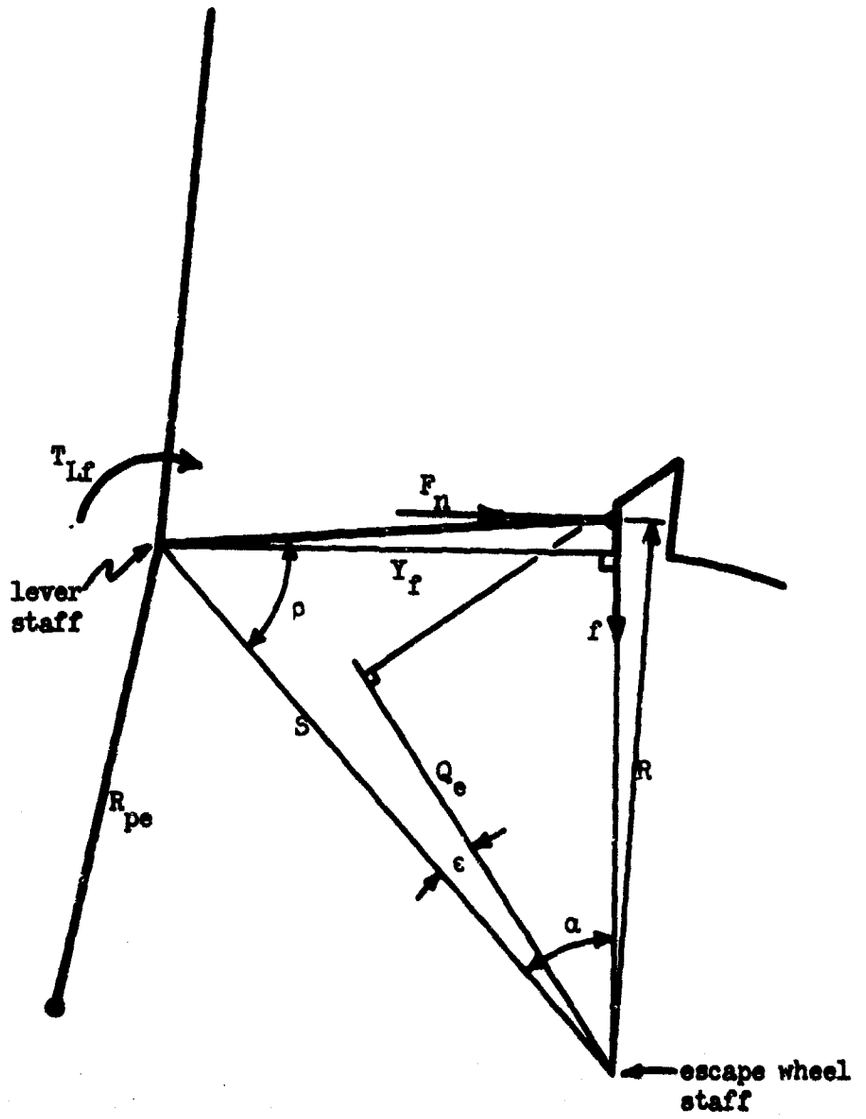

Figure 31. Interaction between the escape wheel and lever during the unlocking phase of the motion.

This torque is transmitted through the lever to the balance as the ratio of their lever arms, X. Thus

$$T_f = X T_{Lf} = \frac{X \mu T_a R_{pe} S \sin\rho}{R_{pe}^2 + S^2 - 2 R_{pe} S \cos\rho} \qquad (C.6)$$

This result together with the coupling equation (4.1) allows T_f to be written as

$$T_f = \mu T_a U(\beta) \qquad (C.7)$$

A similar treatment of unlocking friction for the reverse half-cycle gives an equation for T_f identical to that above except ρ is everywhere replaced by $(P-\rho)$. But $P-\rho$ in the second half-cycle varies in the same manner as ρ in the first half-cycle; T_f is therefore symmetric in the two half-cycles. The function $U(\beta)$ versus (β) for the T5E1 escapement is shown in Figure 32.

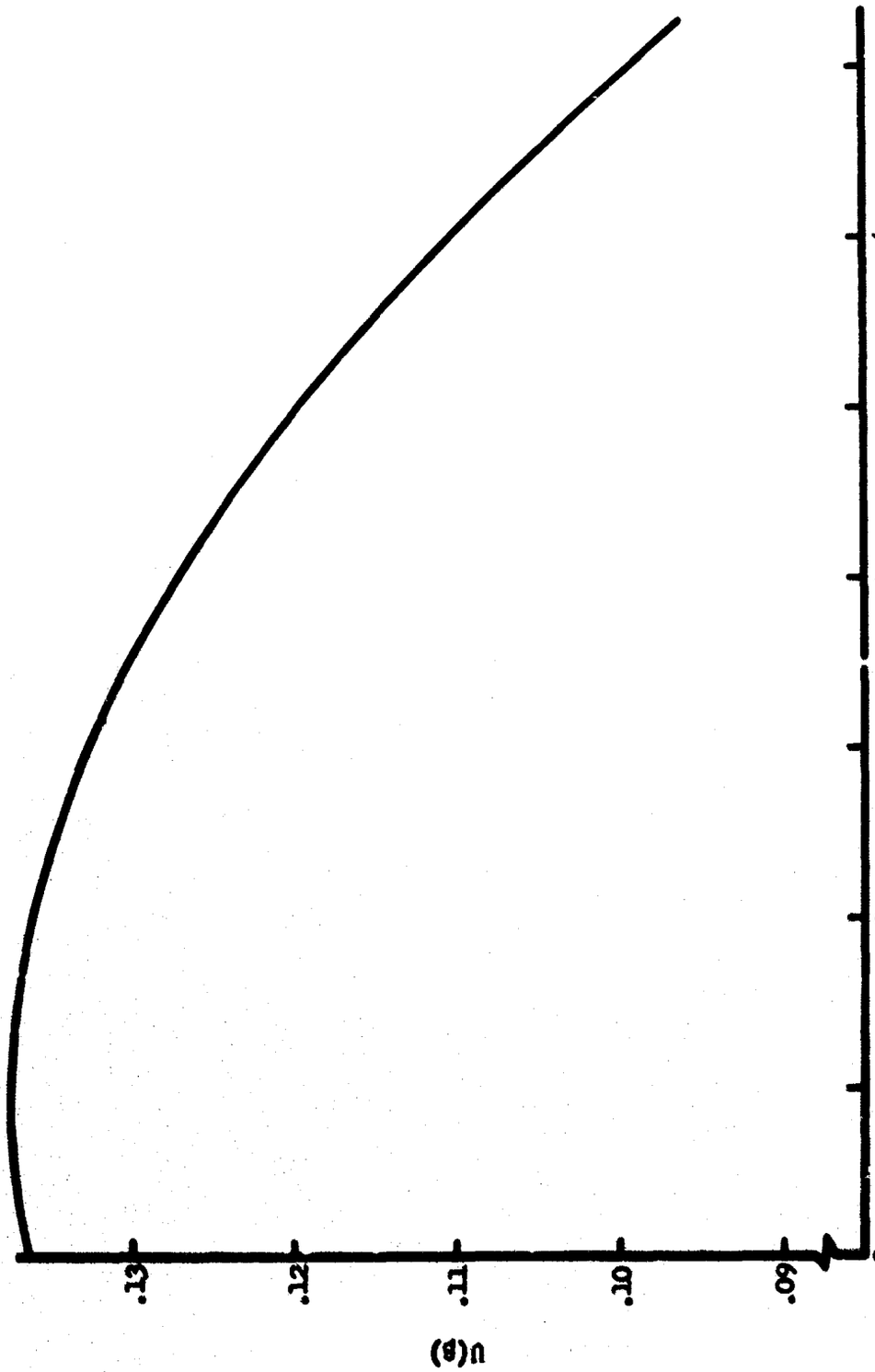

Figure 32. U(β) vs |β| for the TSEL.

APPENDIX D: ALTERNATIVE DERIVATION OF EQUATIONS OF MOTION

The equations of motion for the detached lever escapement may be derived using Lagrange's method.[8] This is a method for setting up equations of motion directly in terms of any convenient set of generalized coordinates.

Lagrange's equations are

$$\frac{d}{dt}\left(\frac{\partial \mathcal{L}}{\partial \dot{q}_i}\right) - \frac{\partial \mathcal{L}}{\partial q_i} = Q_i \qquad \text{(D.1)}$$

where $\mathcal{L} = T - V$

T = kinetic energy of system

V = potential energy of system

q_i = generalized coordinate

Q_i = generalized forces not derivable from a potential function; e.g., friction forces or time variant forcing functions.

Since Lagrange's equations are equivalent to Newton's equations of motion, they do not represent a new physical theory, but merely another way of expressing the same laws of motion.

The balance displacement β will be used as the generalized coordinate describing the motion of the system. Define λ as

$$\lambda = -\frac{\beta\dot{\beta}}{|\beta\dot{\beta}|} \qquad \text{(D.2)}$$

Thus λ is the sign of the term $-\beta\dot{\beta}$ according to the following table.

Quarter of motion	$\beta/\lvert\beta\rvert$	$\dot{\beta}/\lvert\dot{\beta}\rvert$	$-\beta\dot{\beta}/\lvert\beta\dot{\beta}\rvert$
1	+	-	+
2	-	-	-
3	-	+	+
4	+	+	-

λ is defined in this manner so that, in the equations of motion, the generalized damping force ($Q_\beta = \lambda L \beta$) due to hairspring side thrust always acts to decrease the angular velocity of the balance.

The derivations proceed as follows:

1. For the free motion of the balance:

$$T = \tfrac{1}{2} I_s \dot{\beta}^2$$

$$V = \tfrac{1}{2} K \beta^2$$

$$Q_s = \lambda L \beta$$

$$\mathcal{L} = \tfrac{1}{2}(I_s \dot{\beta}^2 - K\beta^2)$$

$$\frac{\partial \mathcal{L}}{\partial \beta} = I_s \dot{\beta} \quad ; \quad \frac{d}{dt}\left(\frac{\partial \mathcal{L}}{\partial \dot{\beta}}\right) = I_s \ddot{\beta}$$

$$\frac{\partial \mathcal{L}}{\partial \beta} = -K\beta$$

Therefore

$$I_s \ddot{\beta} + K\beta = \lambda L \beta$$

or $$I_s\ddot{\beta} + (K-\lambda L)\beta = 0 \qquad (D.3)$$

2. For the unlocking phase:

$$T = \tfrac{1}{2} I_s \dot{\beta}^2 + \tfrac{1}{2} X^2 I_L \dot{\beta}^2$$

where use has been made of the fact that inertias are reflected as the square of the lever arm ratio.

$$V = \tfrac{1}{2} K\beta^2$$

$$Q_s = \lambda L\beta + T_f$$

$$\mathcal{L} = \tfrac{1}{2}\left[(I_s + X^2 I_L)\dot{\beta}^2 - K\beta^2\right]$$

$$\frac{\partial \mathcal{L}}{\partial \dot{\beta}} = (I_s + X^2 I_L)\dot{\beta}$$

$$\frac{d}{dt}\left(\frac{\partial \mathcal{L}}{\partial \dot{\beta}}\right) = (I_s + X^2 I_L)\ddot{\beta} + 2X\dot{X} I_L \dot{\beta} \quad ; \quad X = X(\beta)$$

$$\frac{\partial \mathcal{L}}{\partial \beta} = \tfrac{1}{2} I_L \dot{\beta}^2 \left(\frac{\partial X^2}{\partial \beta}\right) - K\beta$$

$$\frac{\partial X^2}{\partial \beta} = \frac{\partial X^2}{\partial t} \Big/ \frac{\partial \beta}{\partial t} = \frac{2X\dot{X}}{\dot{\beta}}$$

So $$\frac{\partial \mathcal{L}}{\partial \beta} = X\dot{X} I_L \dot{\beta} - K\beta$$

Thus $$(I_s + X^2 I_L)\ddot{\beta} + 2X\dot{X} I_L \dot{\beta} - X\dot{X} I_L \dot{\beta} + K\beta = \lambda L\beta + T_f$$

or $$I_1\ddot{\beta} + \tfrac{1}{2}\dot{I}_1\dot{\beta} + (K-\lambda L)\beta = T_f \qquad (D.4)$$

where $$I_1 = I_B + X^2 I_L$$

3. For the catch-up phase:

One equation is the same as for the unlocking phase except that $T_f = 0$.

$$I_1\ddot{\beta} + \tfrac{1}{2}\dot{I}_1\dot{\beta} + (K-\lambda L)\beta = 0$$

Also note that λ has changed sign.

The second equation, describing the motion of the escape wheel, is simply

$$I_E\ddot{\epsilon} = -T_a \qquad (D.5)$$

4. For the impulse phase:

$$T = \tfrac{1}{2}I_B\dot{\beta}^2 + \tfrac{1}{2}X^2 I_L\dot{\beta}^2 + \tfrac{1}{2}(XZ)^2 I_E\dot{\beta}^2$$

$$V = \tfrac{1}{2}K\beta^2$$

$$Q_\beta = \lambda L\beta - XZT_a$$

$$\mathcal{L} = \tfrac{1}{2}\left[(I_B + X^2 I_L + X^2Z^2 I_E)\dot{\beta}^2 - K\beta^2\right]$$

$$\frac{\partial \mathcal{L}}{\partial \beta} = (I_B + X^2 I_L + X^2Z^2 I_E)\dot{\beta}$$

$$\frac{d}{dt}\left(\frac{\partial \mathcal{L}}{\partial \beta}\right) = (I_B + X^2 I_L + X^2Z^2 I_E)\ddot{\beta} + 2X\dot{X} I_L\dot{\beta} + 2XZ(\dot{X}Z + X\dot{Z})I_E\dot{\beta}$$

where $Z = Z(\beta)$.

$$\frac{\partial \mathcal{L}}{\partial \beta} = \left[X\dot{X}I_L + XZ(X\dot{Z}+\dot{X}Z)I_E\right]\dot{\beta} - K\beta$$

These expressions, when substituted into Lagrange's equation, give

$$I_2\ddot{\beta} + \tfrac{1}{2}\dot{I}_2\dot{\beta} + (K-\lambda L)\beta = -XZT_a \qquad \text{(D.6)}$$

with $I_2 = I_B + X^2 I_L + X^2Z^2 I_E$.

The function Z is not identical for both half-cycles (see Appendix B).

This Lagrangian method of derivation is a more elegant and less cumbersome approach to the equations of motion. It is not obvious, however, how the presence of the pallet lever and escape wheel are taken into account until the Newtonian approach is used. It then follows rather directly that their moments of inertia enter as the square of their lever arm ratios. In addition to this insight, Newtonian mechanics also provides a description of the various collisions.

APPENDIX E: A COMPUTER OUTPUT OF THE STEP-BY-STEP SOLUTION

Values of the equilibrium torque as determined from the energy analysis are used in the step-by-step solution of the equations of motion to calculate the period of the escapement. Certain dimensions and angles derived from the effective geometry are also input along with appropriate energy loss parameters. A list of typical input data is shown below.

ANGLE=	180.0000000000	BETAM=	3.1415926535
D =	.4005015106	P =	1.5620763648
RT =	.0567000000	RPE =	.1588641877
S =	.2374031381	OMEGA=	.9828312937
OE =	.1591115680	K =	921.9000000000
IB =	.0374000000	IP =	.0258000000
IE =	.0134000000	N =	40.0000000000
BETA1=	.7263352035	DD =	.0000000010
EPS2 =	.1415163064	EPS8 =	-.0608093111
TEETH=	15.0000000000	SPAN =	3.0000000000
TAU =	3458.2151000000	MU =	.3000000000
L =	13.8300000000		

IB, IP, and IE represent the moments of inertia ($gm\text{-}cm^2$) of the balance, lever, and escape wheel. N is the number of steps per phase of the motion used in the solution. EPS2 and EPS8 are the escape wheel angles at the end of unlocking for the forward and reverse half-cycles, respectively. The iteration to determine the values of the catch-up angles (β_3 and β_9) is halted when the difference in successive values of one of the angles is less than the quantity DD. The remainder of the input has already been defined.

The computer output for the input data shown above, i.e. $\beta_m = \pi$, $\mu = 0.3$, and $L = 13.83$, follows on the succeeding pages.

T	BETA	$\dot{\beta}$	
0.00000000000	3.14159265	0.000000	free motion
.00126027690	3.08121121	-95.514353	
.00178518823	3.02082978	-134.420749	
.00218996789	2.96044834	-163.822583	
.00253291353	2.90006690	-188.227772	
.00283657224	2.83968547	-209.390793	
.00311249216	2.77930403	-228.215401	
.00336752528	2.71892259	-245.240674	
.00360613135	2.65854116	-260.819214	
.00383140534	2.59815972	-275.196822	
.00404559902	2.53777829	-288.553070	
.00425041132	2.47739685	-301.023939	
.00444716165	2.41701541	-312.715373	
.00463689910	2.35663398	-323.711834	
.00482047432	2.29625254	-334.081956	
.00499858858	2.23587110	-343.882407	
.00517182830	2.17548967	-353.160616	
.00534068996	2.11510823	-361.956746	
.00550559848	2.05472680	-370.305153	
.00566692107	1.99434536	-378.235484	
.00582497780	1.93396392	-385.773522	
.00598004986	1.87358249	-392.941846	
.00613238602	1.81320105	-399.760345	
.00628220778	1.75281961	-406.246633	
.00642971360	1.69243818	-412.416385	
.00657508221	1.63205674	-418.283608	
.00671847548	1.57167531	-423.860867	
.00686004066	1.51129387	-429.159465	
.00699991235	1.45091243	-434.189604	
.00713821411	1.39053100	-438.960515	
.00727505984	1.33014956	-443.480562	
.00741055496	1.26976812	-447.757344	
.00754479740	1.20938669	-451.797769	
.00767787846	1.14900525	-455.608125	
.00780988362	1.08862382	-459.194139	
.00794089311	1.02824238	-462.561030	
.00807098257	.96786094	-465.713549	
.00820022350	.90747951	-468.656023	
.00832868374	.84709807	-471.392385	
.00845642785	.78671663	-473.926205	
.00858351750	.72633520	-476.260716	
.00858351750	.72633520	-472.446825	impact
.00862193678	.70817682	-472.916603	
.00866031879	.69001844	-473.365573	
.00869866528	.67186006	-473.794012	
.00873697795	.65370168	-474.202202	
.00877525848	.63554330	-474.590430	
.00881350851	.61738492	-474.958986	
.00885172965	.59922654	-475.308167	

.00888992349	.58106816	-475.638268	
.00892809158	.56290978	-475.949592	
.00896623542	.54475140	-476.242442	
.00900435652	.52659302	-476.517121	
.00904245634	.50843464	-476.773938	
.00908053629	.49027626	-477.013198	
.00911859779	.47211788	-477.235208	
.00915664220	.45395950	-477.440274	
.00919467088	.43580112	-477.628701	
.00923268514	.41764274	-477.800792	
.00927068626	.39948436	-477.956846	
.00930867551	.38132598	-478.097160	
.00934665414	.36316760	-478.222025	unlocking
.00938462335	.34500922	-478.331729	
.00942258434	.32685084	-478.426554	
.00946053827	.30869246	-478.506775	
.00949848628	.29053408	-478.572659	
.00953642949	.27237570	-478.624467	
.00957436901	.25421732	-478.662451	
.00961230591	.23605894	-478.686852	
.00965024127	.21790056	-478.697904	
.00968817611	.19974218	-478.695829	
.00972611148	.18158380	-478.680838	
.00976404837	.16342542	-478.653130	
.00980198779	.14526704	-478.612892	
.00983993072	.12710866	-478.560299	
.00987787813	.10895028	-478.495512	
.00991583098	.09079190	-478.418680	
.00995379021	.07263352	-478.329935	
.00999175678	.05447514	-478.229398	
.01002973161	.03631676	-478.117173	
.01006771563	.01815838	-477.993352	
.01010570976	0.00000000	-477.858009	
.01014370933	-.01815838	-477.851874	
.01018170969	-.03631676	-477.833464	
.01021971182	-.05447514	-477.802757	
.01025771670	-.07263352	-477.759715	
.01029572531	-.09079190	-477.704288	
.01033373865	-.10895028	-477.636411	
.01037175772	-.12710866	-477.556006	
.01040978351	-.14526704	-477.462979	
.01044781705	-.16342542	-477.357225	
.01048585936	-.18158380	-477.238624	catch-up
.01052391148	-.19974218	-477.107045	
.01056197446	-.21790056	-476.962344	
.01060004937	-.23605894	-476.804366	
.01063813728	-.25421732	-476.632944	
.01067623930	-.27237570	-476.447901	
.01071435653	-.29053408	-476.249050	

.01075249011	-.30869246	-476.036194	
.01079064120	-.32685084	-475.809128	
.01082881095	-.34500922	-475.567637	
.01083080741	-.34595866	-475.554610	
.01083080741	-.34595866	-481.859709	impact
.01086837526	-.36407183	-482.271891	
.01090591186	-.38218499	-482.660308	
.01094341913	-.40029816	-483.024618	
.01098089901	-.41841133	-483.364476	
.01101835345	-.43652450	-483.679540	
.01105578444	-.45463767	-483.969468	
.01109319396	-.47275084	-484.233919	
.01113058404	-.49086401	-484.472558	
.01116795670	-.50897717	-484.685048	
.01120531400	-.52709034	-484.871061	
.01124265801	-.54520351	-485.030268	impulse
.01127999083	-.56331668	-485.162348	
.01131731458	-.58142985	-485.266986	
.01135463138	-.59954302	-485.343870	
.01139194339	-.61765619	-485.392697	
.01142925279	-.63576936	-485.413170	
.01146656179	-.65388252	-485.404998	
.01150387260	-.67199569	-485.367898	
.01154118746	-.69010886	-485.301597	
.01157850863	-.70822203	-485.205826	
.01161583842	-.72633520	-485.080328	
.01161583842	-.72633520	-485.080328	
.01174113160	-.78696584	-482.708321	
.01186706853	-.84759649	-480.133080	
.01199371000	-.90822714	-477.351316	
.01212111971	-.96885778	-474.359395	
.01224936456	-1.02948843	-471.153314	
.01237851506	-1.09011908	-467.728669	
.01250864578	-1.15074972	-464.080621	
.01263983584	-1.21138037	-460.203857	
.01277216951	-1.27201101	-456.092546	
.01290573681	-1.33264166	-451.740283	
.01304063430	-1.39327231	-447.140034	
.01317696588	-1.45390295	-442.284058	
.01331484384	-1.51453360	-437.163836	
.01345439000	-1.57516425	-431.769966	
.01359573702	-1.63579489	-426.092057	
.01373903006	-1.69642554	-420.118591	
.01388442867	-1.75705618	-413.836770	
.01403210903	-1.81768683	-407.232326	
.01418226673	-1.87831748	-400.289290	free
.01433512017	-1.93894812	-392.989715	motion
.01449091439	-1.99957877	-385.313339	
.01464992668	-2.06020942	-377.237160	
.01481247246	-2.12084006	-368.734910	
.01497891365	-2.18147071	-359.776382	

.01514966906	-2.24210136	-350.326575
.01532522801	-2.30273200	-340.344570
.01550616847	-2.36336265	-329.782042
.01569318160	-2.42399329	-318.581259
.01588710578	-2.48462394	-306.672290
.01608897497	-2.54525459	-293.969082
.01630008955	-2.60588523	-280.363696
.01652212395	-2.66651588	-265.717585
.01675729744	-2.72714653	-249.847796
.01700866034	-2.78777717	-232.503892
.01728060806	-2.84840782	-213.326631
.01757989371	-2.90903846	-191.766774
.01791789884	-2.96966911	-166.903543
.01831684526	-3.03029976	-136.949415
.01883418966	-3.09093040	-97.311586
.02007629230	-3.15156105	0.000000
.02007629230	-3.15156105	0.000000
.02133717038	-3.09093040	95.862541
.02186233489	-3.03029976	134.910133
.02226731173	-2.96966911	164.418220
.02261042609	-2.90903846	188.911219
.02291423571	-2.84840782	210.150033
.02319029415	-2.78777717	229.041730
.02344545662	-2.72714653	246.127369
.02368418495	-2.66651588	261.760845
.02390957559	-2.60588523	276.188864
.02412388135	-2.54525459	289.591655
.02432880197	-2.48462394	302.105703
.02452565748	-2.42399329	313.837338
.02471549748	-2.36336265	324.871334
.02489917300	-2.30273200	335.276577
.02507738568	-2.24210136	345.109942
.02525072220	-2.18147071	354.419034
.02541967929	-2.12084006	363.244162
.02558468209	-2.06020942	371.619808
.02574609799	-1.99957877	379.575726
.02590424722	-1.93894812	387.137794
.02605941112	-1.87831748	394.328673
.02621183859	-1.81768683	401.168323
.02636175126	-1.75705618	407.674421
.02650934770	-1.69642554	413.862700
.02665480674	-1.63579489	419.747217
.02679829034	-1.57516425	425.340578
.02693994585	-1.51453360	430.654129
.02707990796	-1.45390295	435.698107
.02721830031	-1.39327231	440.481773
.02735523689	-1.33264166	445.013522
.02749082317	-1.27201101	449.300976
.02762515718	-1.21138037	453.351066

β_6

free motion

.02775833029	-1.15074972	457.170102	
.02789042805	-1.09011908	460.763828	
.02802153077	-1.02948843	464.137477	
.02815171415	-.96885778	467.295817	
.02828104977	-.90822714	470.243186	
.02840960554	-.84759649	472.983528	
.02853744611	-.78696584	475.520422	
.02866463321	-.72633520	477.857108	
.02866463321	-.72633520	474.030433	impact
.02870292429	-.70817682	474.498029	
.02874117852	-.69001844	474.944886	
.02877939764	-.67186006	475.371278	
.02881758332	-.65370168	475.777489	
.02885573724	-.63554330	476.163804	
.02889386100	-.61738492	476.530514	
.02893195622	-.59922654	476.877914	
.02897002445	-.58106816	477.206302	
.02900806722	-.56290978	477.515978	
.02904608605	-.54475140	477.807245	
.02908408240	-.52659302	478.080409	
.02912205772	-.50843464	478.335775	
.02916001343	-.49027626	478.573651	
.02919795090	-.47211788	478.794342	
.02923587151	-.45395950	478.998155	
.02927377657	-.43580112	479.185396	
.02931166740	-.41764274	479.356365	
.02934954527	-.39948436	479.511364	
.02938741142	-.38132598	479.650689	
.02942526710	-.36316760	479.774632	unlocking
.02946311348	-.34500922	479.883480	
.02950095176	-.32685084	479.977516	
.02953878309	-.30869246	480.057013	
.02957660859	-.29053408	480.122241	
.02961442937	-.27237570	480.173460	
.02965224653	-.25421732	480.210921	
.02969006112	-.23605894	480.234867	
.02972787421	-.21790056	480.245530	
.02976568682	-.19974218	480.243134	
.02980349997	-.18158380	480.227889	
.02984131465	-.16342542	480.199994	
.02987913186	-.14526704	480.159638	
.02991695256	-.12710866	480.106993	
.02995477771	-.10895028	480.042223	
.02999260826	-.09079190	479.965474	
.03003044515	-.07263352	479.876881	
.03006828931	-.05447514	479.776563	
.03010614165	-.03631676	479.664625	
.03014400310	-.01815838	479.541158	
.03018187457	0.00000000	479.406237	
.03021975142	.01815838	479.400137	
.03025762905	.03631676	479.381832	

.03029550842	.05447514	479.351299	
.03033339051	.07263352	479.308501	
.03037127629	.09079190	479.253388	
.03040916673	.10895028	479.185895	
.03044706283	.12710866	479.105942	
.03048496558	.14526704	479.013438	
.03052287597	.16342542	478.908275	catch-up
.03056079504	.18158380	478.790335	
.03059872379	.19974218	478.659486	
.03063666327	.21790056	478.515583	
.03067461453	.23605894	478.358472	
.03071257865	.25421732	478.187986	
.03075055669	.27237570	478.003947	
.03078854978	.29053408	477.806168	
.03081205806	.30176547	477.676874	
.03081205806	.30176547	482.405834	impact
.03084871093	.31945587	482.747592	
.03088533870	.33714628	483.065630	
.03092194322	.35483668	483.359759	
.03095852635	.37252709	483.629791	
.03099508994	.39021749	483.875542	
.03103163586	.40790790	484.096829	
.03106816598	.42559830	484.293472	
.03110468221	.44328871	484.465295	
.03114118642	.46097912	484.612123	
.03117768052	.47866952	484.733786	
.03121416643	.49635993	484.830117	
.03125064606	.51405033	484.900951	impulse
.03128712136	.53174074	484.946129	
.03132359426	.54943114	484.965493	
.03136006671	.56712155	484.958893	
.03139654069	.58481195	484.926180	
.03143301816	.60250236	484.867210	
.03146950112	.62019277	484.781844	
.03150599156	.63788317	484.669945	
.03154249150	.65557358	484.531385	
.03157900296	.67326398	484.366036	
.03161552797	.69095439	484.173777	
.03165206860	.70864479	483.954491	
.03168862689	.72633520	483.708065	
.03168862689	.72633520	483.708065	
.03181383883	.78675481	481.337927	
.03193969532	.84717442	478.765327	
.03206625714	.90759403	475.986983	
.03219358790	.96801364	472.999270	
.03232175443	1.02843326	469.798192	
.03245082720	1.08885287	466.379356	
.03258088070	1.14927248	462.737937	
.03271199402	1.20969209	458.868634	

.03284425134	1.27011170	454.765631
.03297774262	1.33053131	450.422542
.03311256436	1.39095093	445.832350
.03324882041	1.45137054	440.987339
.03338662298	1.51179015	435.879012
.03352609381	1.57220976	430.497996
.03366736551	1.63262937	424.833928
.03381058316	1.69304898	418.875327
.03395590621	1.75346860	412.609432
.03410351077	1.81388821	406.022017
.03425359234	1.87430782	399.097162
.03440636915	1.93472743	391.816975
.03456208630	1.99514704	384.161255
.03472102079	2.05556665	376.107072
.03488348796	2.11598627	367.628236
.03504984958	2.17640588	358.694635
.03522052428	2.23682549	349.271375
.03539600117	2.29724510	339.317663
.03557685799	2.35766471	328.785326
.03576378562	2.41808432	317.616807
.03595762211	2.47850394	305.742396
.03615940098	2.53892355	293.076304
.03637042211	2.59934316	279.510927
.03659235925	2.65976277	264.908150
.03682743080	2.72018238	249.085584
.03707868585	2.78060199	231.793571
.03735051808	2.84102160	212.673981
.03764967791	2.90144122	191.179276
.03798754236	2.96186083	166.391527
.03838632438	3.02228044	136.528736
.03890345769	3.08270005	97.012279
.04014503909	3.14311966	.001572

free motion

END OF RUN. LOAD NEW DATA.

LIST OF REFERENCES

1. "Experimental Mechanical Timer with Detached Lever Escapement and Digital Readout System"; by D. L. Overman and D. S. Bettwy; Harry Diamond Laboratories TM-65-44, 31 August 1965.

2. "Cylinder Type Escapement Study"; by J. N. Shinkle; Sandia Laboratory Report SC-TM-65-399; October 1965.

3. "Environmental Sensitivity of Detached Lever Escapements"; by J. N. Shinkle; ASME paper number 66-WA/MD-11; 25 July 1966.

4. "Detached Lever Clock Mechanism Dynamics"; by William Clair Monday; Oklahoma State University, Mechanical Engineering Ph.D. Thesis, May 1965.

5. Numerical Methods and Fortran Programming; by Daniel D. McCracken and William S. Dorn, 1964; John Wiley and Sons, Inc., New York.

6. "Timers For Ordinance Symposium - Paper No. 49 - Cylinder Escapement Performance" by J. N. Shinkle; sponsored by Harry Diamond Laboratories, November 1966. AD 813 507

7. "Detached Lever Escapement Study"; by J. N. Shinkle; Sandia Laboratory Report SC-RR-65-57; May 1965.

8. Classical Mechanics; by Herbert Goldstein, 1953; Addison-Wesley Publishing Company, Inc., Reading, Massachusetts.